Light-Driven Heterogeneous Reduction of Carbon Dioxide: Photocatalysts and Photoelectrodes

James L. White,[1] Maor F. Baruch,[1] James E. Pander III,[1] Yuan Hu,[1] Ivy C. Fortmeyer,[1] James Eujin Park,[1] Tao Zhang,[1] Kuo Liao,[1] Jing Gu,[2] Yong Yan,[2] Travis W. Shaw,[1] Esta Abelev,[1] Andrew B. Bocarsly[1]*

[1]Department of Chemistry, Princeton University, Princeton, New Jersey 08544, United States

[2]Chemical and Materials Science Center, National Renewable Energy Laboratory, Golden, Colorado 80401, United States

1. INTRODUCTION

Although modern photoelectrochemistry is often traced back to 1972 and the report by Honda and Fujishima[1] that a TiO_2 photoanode in an electrochemical cell caused the splitting of water into O_2 and H_2 when illuminated, the first report of this type of phenomenon dates back to Becquerel's studies, published in 1839.[2] This makes photoelectrochemistry one of the oldest investigated techniques for the conversion of sunlight into usable energy. Over this time frame, two general types of photoelectrochemical cells have been developed. The first, typified by Honda's electrochemistry, is focused primarily on the storage of light energy as high energy chemical products. Initially, this was termed "artificial photosynthesis," and was focused for the most part on splitting water to generate H_2 as an environmentally benign fuel. The second type of photoelectrochemical cell utilizes a chemically reversible redox couple that undergoes a redox change of state at the photoelectrode, followed by conversion of the product species back to the reactant at the counter electrode. The net effect of this reaction is a chemically invariant system that generates electricity from light. The initial implementation of the Grätzel cell, which used a

reversible I_2/I_3^- couple and a dye-sensitized TiO_2 photoanode, is an example of this type of system.[3] The work under consideration in this paper focuses on the photosynthetic cells and related systems. However, an analysis of these systems, as is more obviously critical to electricity-generating systems, must take into account whether the system is merely catalytic for the reaction of interest or is a system that actually converts light energy into stored chemical energy. Thus, how one parameterizes and evaluates a heterogeneous photoinduced charge transfer process becomes a critical issue that is therefore reviewed in this work.

A second tension that is fundamental to synthetic photoelectrochemistry is the comparison between a pure photoelectrochemical process (i.e., a monolithic process based on a semiconductor-liquid junction) versus the use of an electrochemical cell (utilizing metal electrodes) that is driven by an external solid-state photovoltaic device to build a multicomponent system.[4] Though the latter process is not a photoelectrochemical process, there is a long-standing debate about which systems' approach is more efficient in terms of energy conversion. We will not enter that debate in this paper, other than to note that the answer is system-specific. In this paper, we consider both types of approaches so that the reader may evaluate the energy conversion efficiency and product selectivity of these two types of devices as applied to a well-specified chemistry.

In this review, we turn our attention from the well-studied water-splitting photoelectrochemical cells to heterogeneous processes that hold the promise of using insolation (incident sunlight) to drive both thermodynamically and kinetically the uphill conversion of CO_2 to organic products. Production of C1 species is the primary focus of this paper, since most work has been aimed at this class of reactions. Though a classical photoelectrochemical environment is the primary discussion topic presented, alternate heterogeneous environments ranging from metal-based

reactions to nanoparticle semiconductor systems to MOFs (metal organic frameworks) are also reviewed.

1.1. Solar Fuels from Carbon Dioxide Reduction

As noted already, the concept of generating a fuel using sunlight as the energy source began with work aimed at generating hydrogen, typically from water. The analogy, based solely on products, between this process and natural photosynthesis (if one considers sugars to be hydrogen carriers) led to the term "artificial photosynthesis." More recently, with an interest in the expanding diversity of energy-storing products. the term "solar fuels" has been adopted. Although the area of solar fuels dealing with the reduction of aqueous carbon dioxide and oxidation of water to form organic products and O_2 is a closer analogy (based on both reactants and products) to photosynthesis than water splitting, this term has already been used to describe the former processes. Thus, it has been suggested that the reduction of CO_2 been referred to as "reverse combustion."[5]

The production of H_2 from water as a fuel source is attractive in terms of minimizing environmental impact, given the reversible chemical cycle between water and hydrogen formation and combustion; however, hydrogen is ill-suited as a transportation fuel due to its gaseous state. As a result it suffers from both low volumetric energy density and low practical gravimetric energy density, since the mass of the device that contains the hydrogen must also be taken into account. Additionally, the introduction of hydrogen as a stored high pressure gas introduces safety concerns, and storage as an intercalate or via a molecular hydrogen carrier carries a severe energy penalty. All of these limitations are absent when using liquid fuels based on organic compounds. However, traditional organic fuels suffer from lack of sustainability, due to limited fossil fuel resources, and from potentially excessive environmental impact due to

greenhouse gas generation during combustion. These problems can be mitigated to some extent by using CO_2 as a feedstock to generate organic fuels. In this sense, the term "solar fuels based on reverse combustion" nicely captures the promise of carbon dioxide electrochemistry and its photo-driven analogs.

It is also interesting to note that one of the major concerns today with fossil fuels as chemical feedstocks in general is the large recent fluctuations in price. This causes an uncertainty in chemical manufacturing that is difficult to deal with. If CO_2 can be substituted as a feedstock, then given the impressive (and growing) supply of this material, feedstock prices will be lowered and stabilized. In this regard, given the highly oxidized state of carbon in CO_2 and the overall reduced state of carbon in fossil fuels, it makes some sense to base chemical manufacturing feedstocks on the oxidation state of the desired products.

In all cases, it must be realized that protons, which are always needed for reduction of CO_2 , are reduced thermodynamically at potentials that are similar to CO_2 reduction. Thus, these two processes are always in competition. Therefore, proton reduction must be considered to the extent that it affects the reduction of CO_2. In the work presented here the two reactions are therefore compared. The thermodynamics of both processes are considered, followed by an overall assessment of the kinetics of CO_2 reduction. This is followed by a review of heterogeneous systems by class that promote the light-driven reaction of CO_2 with water to generate reduced products.

1.2. Thermodynamics and Kinetics of CO_2 Reduction

1.2.1. Thermodynamics of CO_2 Reduction

The standard reduction potential (E_R^0) is a measure of the spontaneity of a given reaction relative to the hydrogen evolution reaction (HER), as given by Eq. 1.[6] Due to the relative

stability of gaseous CO_2 (ΔG_f^0 = -394.4 kJ mol^{-1}), energy must be introduced into the reaction mixture in order to drive its transformation to reduced products.[7] Ideally, energy for this process will be supplied by a renewable source such as wind, solar, or hydropower. Application of a potential more negative than E_R^0 to a suitable system, will generate a net negative ΔG, thus causing the reduction of CO_2 to become a spontaneous process.

$$\Delta G^0 = -nFE_{rxn}^0 \quad (1)$$

The formal redox potentials ($E^{0'}$) for various CO_2 reduction reactions can be obtained from thermodynamic data, and are tabulated below for reference.[8,9] Since many CO_2 reduction studies are conducted close to neutral pH, the potentials below are tabulated at pH 7 with all other species being at unit activity. All potentials are referenced to the standard hydrogen electrode (SHE). The reduction potential of the hydrogen evolution reaction is included since this reaction invariably competes with the electroreduction of CO_2 .

Table 1. List of formal electrochemical redox potentials (pH = 7) for the reduction of CO_2 and related compounds in aqueous media.

Eq.	Reaction	$E^{0'}$ vs. SHE
(2)	$CO_2 + e^- \rightarrow CO_2^{\bullet-}$	-1.85 V
(3)	$CO_{2\,(g)} + H_2O_{(l)} + 2e^- \rightarrow HCOO^-_{(aq)} + OH^-_{(aq)}$	-0.665 V
(4)	$CO_{2\,(g)} + H_2O_{(l)} + 2e^- \rightarrow CO_{(g)} + 2OH^-_{(aq)}$	-0.521 V
(5)	$CO_{2\,(g)} + 3H_2O_{(l)} + 4e^- \rightarrow HCOH_{(l)} + 4OH^-_{(aq)}$	-0.485 V
(6)	$CO_{2\,(g)} + 5H_2O_{(l)} + 6e^- \rightarrow CH_3OH_{(l)} + 6OH^-_{(aq)}$	-0.399 V
(7)	$CO_{2\,(g)} + 6H_2O_{(l)} + 8e^- \rightarrow CH_{4(g)} + 8OH^-_{(aq)}$	-0.246 V
(8)	$2H_2O_{(l)} + 2e^- \rightarrow H_{2(g)} + 2OH^-_{(aq)}$	-0.414 V

An ideal catalyst will allow the chemical transformation of interest to take place at potentials dictated by the Nernst equation (Eq. 9), which describes the relationship between the concentrations of oxidized and reduced species (C_O and C_R, respectively) and the potential. Thus, the reaction cannot proceed to completion until the electrode potential is several hundred millivolts beyond the equilibrium potential.[6] Catalysts that are able to reduce CO_2 at applied potentials close to the formal potential are said to have a low overpotential for the given transformation. Likewise, catalysts that are able to carry out CO_2 reduction only when the applied potential is significantly more negative than $E^{0'}$ are said to have a high overpotential for the reaction under consideration.

$$\frac{C_O}{C_R} = \exp\left(\frac{nF\left(E-E^{0'}\right)}{RT}\right) \tag{9}$$

More formally, the overpotential of a catalytic system is a measure of the energy (in addition to ΔG^0_{rxn}) required to drive a reaction due to inherent kinetic limitations. The overpotential is one figure of merit in the CO_2 reduction literature, and its mathematical definition is given in Eq. 10.[6] Generally, the overpotential for a reduction reaction is calculated using the most positive potential (E) at which the desired product can be detected using standard analytical techniques. Recently, Appel *et al.* suggested a standardized method with which to report overpotentials for molecular electrocatalysts.[10] Using this method, one analyzes a cyclic voltammetric curve of the electrocatalyst of interest. Ideally, the observed catalytic current will plateau as the potentials are scanned progressively more negative than the standard reduction potential of the couple of interest. Appel *et al*. suggest that the potential corresponding to $i_{cat}/2$ is the catalytic potential, E. However, this method has not yet been widely applied in the CO_2 reduction literature.

$$\eta = E - E^{0'} \tag{10}$$

Although the thermodynamics presented here suggest that only moderately negative potentials are needed to reduce CO_2 (*ca.* -0.52 V vs. SHE for the CO_2/CO couple), most catalytic systems undergo CO_2 reduction at significantly more negative potentials. This is often attributed to the rate limiting step involving the one electron reduction of CO_2 to $CO_2^{\bullet-}$.[11] The highly negative reduction potential of this electrochemical step can be understood in terms of the change of hybridization from sp^2 to sp^3 that occurs around the central carbon atom. Savéant and coworkers reported that the standard redox potential for the reduction CO_2 to $CO_2^{\bullet-}$ is -1.97 V vs. SHE in dimethylformamide.[12] A report by Schwarz *et al.* states that the $CO_2/CO_2^{\bullet-}$ redox couple lies at approximately -1.90 V vs. SHE in aqueous media.[13] This has been verified by Armstrong and coworkers who found that the redox couple lies at -1.85 V vs. SHE.[8]

One complicating factor that is prevalent in CO_2 reduction studies is that various competing electrochemical reactions can take place at the working potentials required to reduce CO_2. More specifically, the reduction of H_2O/H_3O^+ is highly prevalent in aqueous media. The formal thermodynamic reduction potential of the HER is -0.414 V vs. SHE at pH 7, and this potential is approximately a hundred millivolts more positive than the reduction potentials of CO_2 to many common reduction products (see Table 1). This unwanted side-reaction complicates standard voltammetric analysis, and careful examination of the gaseous hydrogen produced during electrolysis experiments is required. The Faradaic efficiency (Eq. 11) of a catalyst for a given product is a measure of the selectivity of the system for the product of interest. Due to the presence of the HER, as well as other side reactions, the Faradaic efficiencies of many CO_2 reduction catalysts are below 1.

$$\xi = \frac{Q_{product}}{Q_{total}} \tag{11}$$

Traditionally, CO_2 reduction has been carried out on metals that have a high overpotential for the hydrogen-evolution reaction.[11] Although metals such as Hg can reduce CO_2 to formate with essentially unit efficiencies, the potential at which this occurs is significantly more negative than the standard reduction potential for the CO_2 /$HCOO^-$ couple (see Table 1). Cathodes such as Bi, Sn, and In can reduce CO_2 to formate at more moderate potentials, but the efficiencies are often lower than unity due to the HER.[14–16] However, these systems still require a relatively large overpotential.

Other competing reactions include the electroreduction of heavy metal impurities present in trace amounts in the supporting electrolyte solution. The importance of using pre-electrolysis to rid the electrolyte solution of its heavy metal impurities has been strongly emphasized in a recent review.[11] Hori suggested that Fe or Pb impurities present in the supporting electrolyte in concentrations as little as 5 ppm can deactivate the catalytic behavior of copper electrodes in as little as 10 minutes.[11] In this case, the presence of an adlayer of foreign heavy metals on a surface can provide catalytic sites that facilitate the reduction of water, and thus, reduce the Faradaic efficiency of CO_2 reduction.

1.2.2. Figures of Merit

Two figures of merit are used in the CO_2 reduction literature as a basis of comparison between a given catalyst and those reported by others. As mentioned previously, the Faradaic efficiency of a catalyst is a measure of the extent to which the desirable reaction takes place during the course of catalysis. A high Faradaic efficiency means that the target reaction occurs predominantly over other possible reactions such as solvent decomposition, catalyst degradation, and even CO_2 reduction to a non-desired product.

A low overpotential means that a catalyst requires a relatively small electrochemical drive in order to convert a certain reactant to the desired product. It is an ongoing goal in the CO_2 reduction community to develop catalysts that have as small of an overpotential as possible while still producing products at an acceptable rate. In certain photocatalytic systems, light energy can be utilized in such a way as to allow the reduction of CO_2 to proceed at applied electric potentials more positive than the formal redox potential. One example of underpotential reduction, reported by Bocarsly *et al.*, involves the reduction of CO_2 to methanol at illuminated p-GaP electrodes.[17] In this particular study, the Faradaic efficiency of the reaction approached unity at underpotentials as high as 320 mV. An important consideration in assessing overpotential is the fact that various reference electrodes have been used in the CO_2 reduction literature. The two most common reference half-cells are the saturated calomel electrode (SCE, +0.242 V vs. the normal hydrogen electrode (NHE)) and the saturated Ag/AgCl electrode (+0.197 V vs. NHE).[6] Some authors report electrochemical potentials with respect to the reversible hydrogen electrode (RHE), which is dependent on the pH of the solution and converted from other reference electrodes using Eq. 12, which is valid at room temperature.[18]

$$E_{RHE} = E_{NHE} + 0.0591\ \text{V} \times \text{pH} \qquad (12)$$

Another desirable characteristic in an electrocatalyst is a high partial current density. The current density, j, is equal to the rate at which electrons cross the solution/electrode barrier in unit time per unit area of the catalytic surface. The partial current density, equal to the product of the current density and Faradaic efficiency for a particular product, is a measure of the rate of product formation. All else being equal, a high partial current density is desired in order to maximize the rate at which catalysis occurs. Figures of merit specific to photocathodes (quantum yield, overall thermodynamic efficiency) will be discussed in section 1.3.

1.2.3. Mechanism of CO_2 Reduction

Many studies have been dedicated to elucidating the mechanism of CO_2 reduction. However, most of these studies were conducted in systems utilizing metallic electrodes or homogeneous electrocatalysts. For this reason, the present discussion will be kept minimal, and mechanistic insights on specific CO_2 reduction photocathodes will be discussed in their respective sections. On metallic electrodes, it is generally proposed that the initial step involves the reduction of CO_2 to the $CO_2^{\bullet-}$ radical anion. Hori and coworkers claimed that the adsorption of this reduced species on metals such as Au, Ag, Cu, and Zn leads to the formation of carbon monoxide in aqueous media.[19] However, this conclusion is somewhat suspect, since the reduction of CO_2 on these surfaces occurs at potentials quite positive of the reported $CO_2/CO_2^{\bullet-}$ redox potential in solution. The proposed mechanism additionally involves a water-mediated proton transfer to an oxygen atom on $CO_2^{\bullet-}$, loss of a hydroxide group, and the subsequent second electron transfer to yield an adsorbed CO species. Further desorption leads to the presence of CO in detectable quantities.

It is further claimed that CO_2 reduction to formate on heavy p-block metals proceeds from a water-mediated proton transfer from a nonspecifically coordinated $CO_2^{\bullet-}$ radical anion. In this case, the nucleophilic carbon atom acts as the Lewis base. The addition of a second electron leads to the formation of the formate ion. The two mechanisms are shown in Scheme 1.

Scheme 1. A proposed mechanism for CO_2 reduction on various metallic electrodes leading to (a) the formation of CO (b) formate ion. Adapted from ref. 19 with permission from Elsevier, copyright 1994.

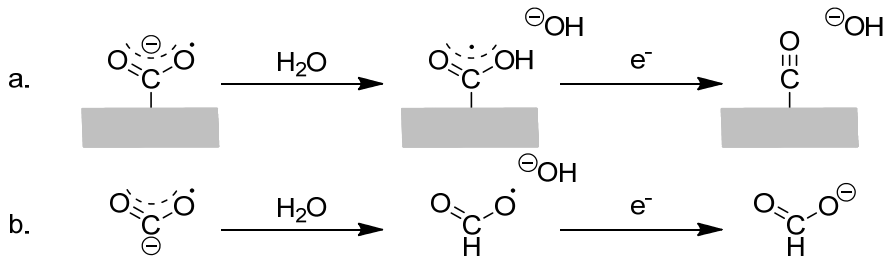

Recently, the validity of the two mechanisms shown in Scheme 1 has been questioned. Since products are often formed without attaining the highly negative potential required for the outer-sphere formation of $CO_2^{\bullet-}$, it is likely that an inner sphere mechanism takes place instead. It was discovered that metastable oxygen-containing moieties play a significant role in the reduction of CO_2 . Kanan *et al.* showed that Sn_xO_y based cathodes can reduce CO_2 to formate and CO with much greater yields than with pure metallic Sn.[15] For this reason, a nonspecific interaction between $CO_2^{\bullet-}$ and the catalytic surface is unlikely. The same phenomenon was found to be prevalent on lead electrodes.[20] Bocarsly and coworkers reported similar behavior on indium electrodes and claimed that $In(OH)_3$ was the active catalytic species. Additionally, they showed evidence for a surface-bound metal carbonate on both indium and tin.[16,21] Oxide-derived Cu and Au electrodes were also reported to possess higher catalytic activity than their smooth counterparts, but the increased catalytic behavior was explained in terms of morphological nanostructure rather than metastable oxide species.[22,23] These systems are further discussed in section 4.2.

Another mechanistic route by which to bypass the high-energy $CO_2^{\bullet-}$ radical is through a series of proton-coupled electron transfers (PCET). By transferring a proton with the electron, either from the same bond or two separate bonds, large activation barriers caused by significant reorganization energies as well as unstable intermediates can be more readily avoided.[24] PCET processes have a considerable kinetic dependence on the concentration of available protons in

solution, with the addition of acid greatly affecting the rate of catalysis.[25] Since the vast majority of CO_2 reduction studies take place at potentials more positive than -2.0 V vs. SCE, PCET is often implicated, though rarely proven.

1.3. Overview of Semiconductor Physics

The earliest reports of CO_2 reduction on semiconductors goes back to the late 1970s about the same time metal electrodes were discovered as electrodes for CO_2 reduction, though semiconductors have the ability to utilize light energy to supplement or even replace electrical energy inputs.[11,26,27] Semiconductor electrodes are different from metal electrodes as the applied potential does not directly govern the electrochemistry.[28] The differences between metallic electrodes and semiconducting electrodes result from the differences in band structure between metals and semiconductors.

1.3.1. Band Structure

Band theory utilizes delocalized orbitals that overlap to form a low energy band of mainly filled orbitals (the valence band, VB) and a set of higher energy band of mainly delocalized orbitals (the conduction band, CB) as illustrated in Figure 1. In metals, these two bands overlap forming a continuum of energy states for the electrons, while in semiconductors, the two bands are separated by a quantum mechanically forbidden energy zone, the band gap (E_g).

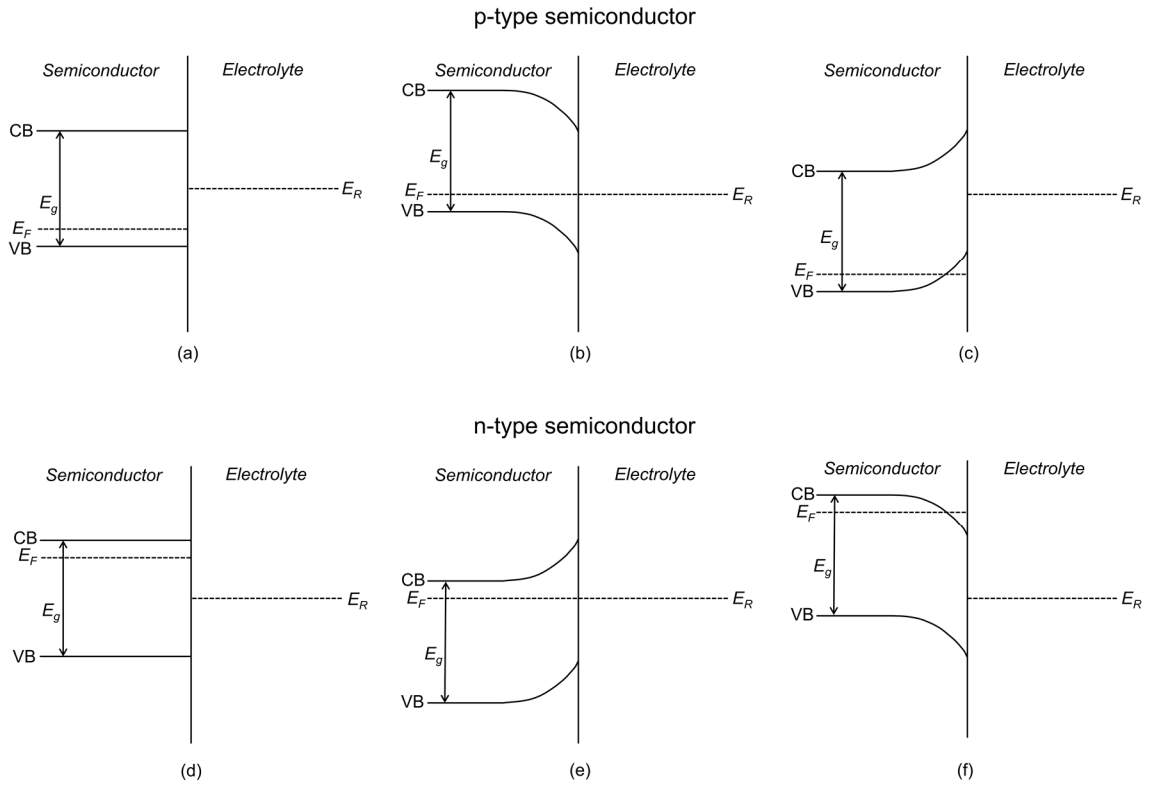

Figure 1. Band diagrams of p-type (a-c) and n-type (d-f) semiconductors immersed in an electrolyte with redox potential E_R before equilibrium (a,d), at equilibrium (b,e), with positive potential applied (c), and with negative potential applied (f).

Metals exhibit high electrical mobility due to the lack of a band gap which enables electrons to move to the available set of delocalized empty orbitals with small activation energy.[6,28] The transition between the filled and vacant electronic states can occur easily at room temperature, exhibiting high electrical mobility and thus conductivity in response to an electric field.[6] Semiconductors, on the other hand, have significant energy spacings between the two bands, which leads to the valence band being almost completely filled while the conduction band is almost vacant due to the higher energy required for the transition between the valence band and conduction band.[6] Because there are fewer empty states close in energy to the full states, it is considerably more difficult to redistribute the electrons with an applied electric field, which leads

to diminished electrical conductivity.[6] However, electrical mobility can be induced by exciting the electrons from the valence band to the conduction band. Upon illumination with photons of energy greater than or equal to E_g ($h\nu \geq E_g$), photogenerated electrons from the valence band are excited to the conduction band, leaving empty states in the valence band, which have the attributes of positively charged holes.[29] Both photogenerated electrons and holes can be utilized to perform electrochemical reactions.

1.3.2. Intrinsic and Extrinsic Semiconductors

Many different semiconductors have been utilized as electrodes for a wide variety of redox processes including CO_2 reduction.[30] Semiconductors are typically categorized depending on the charge densities of electrons and holes. For intrinsic semiconductors, the densities of electrons and holes are equal, and a controlled amount of impurities can be introduced through doping to produce extrinsic semiconductors with an excess of either electrons or holes.[29] Introduction of vacancies or impurities possessing a different electronegativity compared to the lattice elements alters the number of charge carriers. Semiconductors with donor impurities which provide electrons to the lattice are n-type semiconductors with electrons as the majority charge carrier. On the other hand, semiconductors with acceptor impurities that remove electrons from the lattice are p-type semiconductors, using positively charged holes as the majority charge carrier.[29] The electrical conductivity of the material can also be altered through doping with a sufficiently high population of impurities, which enables carrier migration in the dark under external bias.[29]

Doping normally does not result in a change of the band gap or band edge positions of the parental semiconductors. However, in some cases, band engineering can be achieved via doping, such as widening or narrowing band gaps and shifting band edges by altering the electronic band structure. Doping can enhance the light absorption range to longer wavelengths by introducing

shallow- or deep-level states while not changing the band gap.[31,32] Doping can also enhance the photocatalytic activity by narrowing the band gap without introducing any mid-gap states.[33]

1.3.3. Band Gap

Semiconductors exhibit band gaps having two different optical properties: direct band gaps and indirect band gaps. In a direct band gap material, transitions between the valence band and the conduction band involve transitions that preserve the angular momentum of the electron. As such, these transitions only require absorptions of an optical photon. On the other hand, an indirect band gap requires a change in the electron momentum and therefore necessitates the assistance of a phonon, or lattice vibration.[28,34] Therefore, an indirect transition requires the absorption or emission of a phonon, which is less likely to occur. As a result, the optical absorption coefficient for an indirect transition is much smaller than that of a direct transition.[28,34]

1.3.4. Fermi Level

The Fermi level (E_F) is defined as the energy level where the probability of finding an electron in a continuum of electronic states is 1/2 at 0 K, as indicated in Figure 1.[29] However, for semiconductors, a more useful working definition is the average energy of the electrons in the lattice, since the Fermi level typically lies within the band gap, where electron density is quantum mechanically forbidden. The Fermi level can be connected to the free energy of the semiconductor (ΔG_{semi}) as given in Eq. 13, where n is the number of electrons involved in the process (typically $n = 1$) and F is Faraday's constant.

$$\Delta G_{semi} = -nFE_F \tag{13}$$

In intrinsic semiconductors, where the number of electrons and holes are equal, the Fermi level is located at the midpoint of the band gap.[29] For doped semiconductors, the Fermi level is placed

slightly below the conduction band for n-type semiconductors and slightly above the valence band for p-type semiconductors.[29]

1.3.5. Band Bending

The free energy a semiconductor (ΔG_{semi}) of can be related to the free energy of an electrolyte ($\Delta G_{electrolyte}$) which is given by Eq. 14, where E_R is the redox potential of the electrolyte as given by the Nernst equation.

$$\Delta G_{electrolyte} = -nFE_R \quad (14)$$

When the Fermi level of a semiconductor placed in an electrolyte solution does not match the E_R, electron flow will occur at the semiconductor-electrolyte interface in order to minimize the difference in the Gibbs free energy of the two different phases (Figure 1a, 1d). Because of the much larger number of electroactive species in the electrolyte than the number of mobile electrons in the semiconductor, E_F changes significantly with electron flow at the interface, while E_R remains almost unchanged.[28] As the free energy of the semiconductor shifts, the valence and conduction band energies will shift near the semiconductor-electrolyte interface, with the spacing between the two bands (E_g) unchanged. The electron flow across the interface creates a space-charge region, also called the depletion layer since the majority charge carriers are depleted, near the junction inside the semiconductor.[6,28]

After establishing equilibrium, the valence band and the conduction band edges in the space-charge region are bent in the band diagram, indicating a different occupation of energy levels near the interface compared to the bulk, as illustrated in Figure 1b, 1e. The band bending is not simply the difference between E_F and E_R due to the Helmholtz layer formed at the semiconductor-electrolyte interface, which is formed by charged ions adsorbed on the semiconductor surface and reduces the band bending slightly due to the potential drop across this

layer.[35] The bending is indicative of an electric field that causes electrons and holes to migrate in opposite directions. The charge carrier moving toward the interface can then be utilized to perform electrochemical reactions. The opposite charge carrier, migrating toward the bulk, completes the photoelectrochemical redox cycle with the other half-cell reaction at another site for particles or on an auxiliary electrode connected via the external circuit for photoelectrochemical cells.

Since the minority charge carrier is directed toward the semiconductor-electrolyte interface, the nature of this species determines whether an oxidation or reduction reaction is observed at the semiconductor interface. For a p-type semiconductor, the Fermi level is located slightly above the valence band. Therefore, in attaining equilibrium, interfacial electrons flow towards the semiconductor, resulting in an increase in the Fermi level energy and a bandbending gradient that moves conduction band electrons toward the semiconductor interface (Figure 1b). The opposite occurs in an n-type semiconductor, with electrons flowing from the semiconductor to the solution lowering the Fermi level energy and forming a potential that moves valence band holes toward the semiconductor interface (Figure 1e). Photoreduction reactions typically utilize p-type semiconductors since electrons will flow down the potential gradient in the conduction band toward the interface, while n-type semiconductors are utilized in photooxidation reactions because holes in the valence band will migrate up to the interface.

While p-type semiconductors

serve as photocathodes, it is possible to perform CO_2 reduction with n-type semiconductors as dark cathodes. Conversely, p-type semiconductors can be used as dark anodes. When an external potential is applied to a semiconductor, the Fermi level of the semiconductor can move up or down and invert the band bending to form an accumulation region instead of an depletion region,

which changes the built-in electric field to the opposite direction (Figure 1c,f). For n-type semiconductors, applying a negative potential will invert the band bending to form an accumulation region of majority charge carrier electrons close to the interface, which can be utilized in cathodic reactions (Figure 1f).[28]

1.3.6. Electron-Hole Separation and Recombination

In order to utilize the photogenerated electrons and holes effectively in the reduction of CO_2 , which involves multiple steps, the electron-hole pair must be separated in a manner that precludes or at least slows recombination and thus promotes the transfer of the charge carrier to the redox active species at the semiconductor-electrolyte interface.[29] In the absence of an electric field, recombination of the electron-hole pair is a fast process which occurs on a nanosecond time scale by a nonradiative relaxation of excited electrons to the ground state.[28] It is commonly known that the electron-hole recombination limits the electron transfer process at the semiconductor interface for subsequent oxidation or reduction reactions as the time scale for electron-hole recombination is typically two or three orders of magnitude faster than the interfacial electron transfer processes.[36] The band bending provides the interfacial electric field that separates the electron-hole pair by directing these charges in opposite directions.[29] The separation of an electron-hole pair formed beyond the depletion layer occurs if the minority carrier diffuses to the depletion layer before recombination occurs.[35] Applying an external potential to the semiconductor electrode controls the Fermi level, which can further increase the band bending and enhance the electron-hole pair separation which drives effective interfacial charge transfer.[28]

1.3.7. Fill Factor

Fill factor, a term typically used for photovoltaics, is a measure of the carrier kinetics and how quickly photocurrent is obtained at different potentials. The fill factor provides mechanistic information on charge separation and recombination.[4,14,15] The fill factor can be interpreted as a measurement of the "squareness" of the current response with different applied potentials.[28] The short circuit current (i_{SC}) is the current flow when the Fermi level of the semiconductor (E_F) and redox potential of the electrolyte (E_R) are equal in energy.[28] The open circuit voltage (V_{OC}) is the voltage at which photocurrent is observed and is the difference between the photocurrent onset potential and short-circuit potential.[28,35] For an ideal situation, the photocurrent is instantaneously increased from zero to maximum (i_{SC}) at the open circuit voltage, resulting in a rectangular shape in an *i-V* plot and a fill factor of 1 (Figure 2).[28] The fill factor in real systems is obtained by measuring the ratio of the area enclosed by the current and voltage to the area of the ideal rectangle.[28] This definition is slightly different from the one utilized in photovoltaics in which the area of the maximum power point (i_{mp} and V_{mp}) is employed from the obtained data. Fill factor is dependent on the intensity of the light source illuminating the electrode, as the surface recombination is dependent on the light intensity.[37] In most cases, the ideal current-potential relation is not obtained due to the kinetics of charge separation, recombination, and transport.[28]

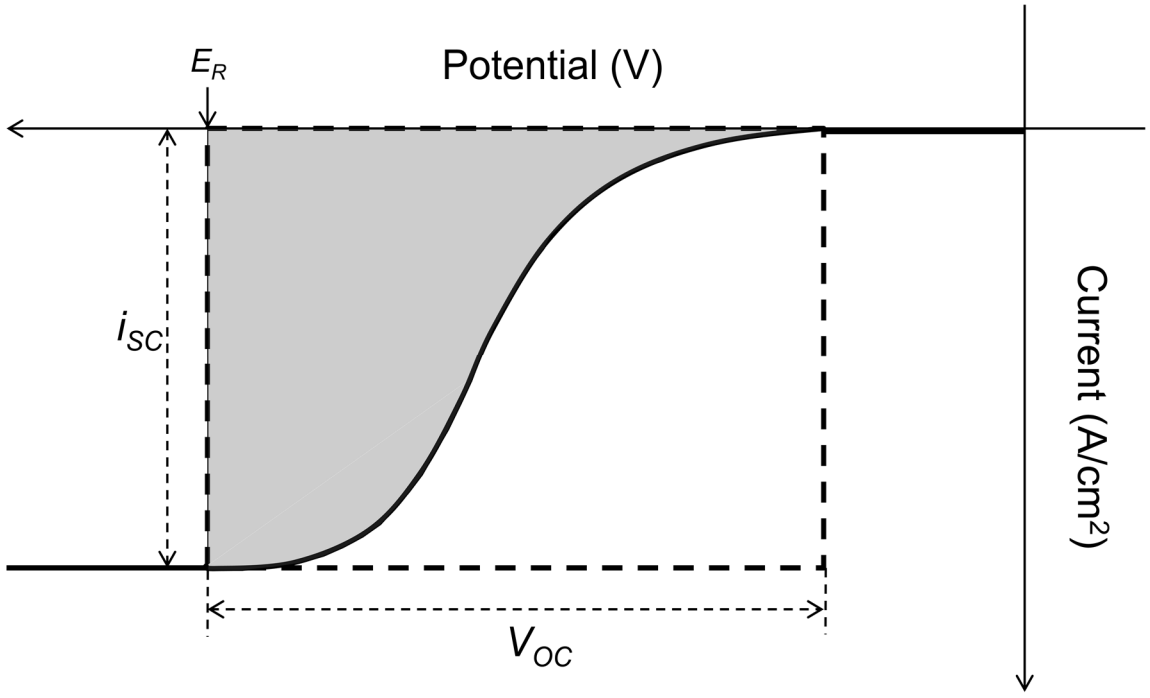

Figure 2. The fill factor in a photoreduction *i*-*V* curve on a semiconductor, with the short circuit current (i_{SC}) and open circuit voltage (V_{OC}). The dashed rectangle indicates the ideal photocurrent response while the shaded area represents the fill factor in the area above the observed photocurrent response.

1.3.8. Quantum Efficiency

For semiconductor-based photoelectrochemistry, the quantum efficiency represents the conversion efficiency of the incident light to the desired product. Quantum efficiency is defined as the ratio of the number of photogenerated electrons that react to the number of incident photons that strike the semiconductor. In photovoltaics, the definition of quantum efficiency differs slightly, in that quantum efficiency is the percentage of electron-hole pairs produced from absorbed photons rather than all incident photons.[38] With band bending, the quantum efficiency increases as the band bending aids the electron-hole separation.[28] The quantum efficiency is often reported as the incident photon-to-current efficiency (IPCE) as a function of wavelength

(Eq. 15), which is derived from the photocurrent density obtained (j_{ph}), the power intensity of monochromated illumination (P_{mono}) at a particular wavelength (λ). The value of 1239.8 V·nm is the product of Planck's constant (h) and the speed of light (c).[39]

$$\mathrm{IPCE}(\lambda) = \frac{j_{ph}(\mathrm{mA{\cdot}cm^{-2}}) \times 1239.8\ (\mathrm{V{\cdot}nm})}{P_{mono}(\mathrm{mW{\cdot}cm^{-2}}) \times \lambda\ (\mathrm{nm})} \quad (15)$$

1.3.9. Effect of pH

The band edge positions of a semiconductor are good indicators if a given electrochemical reaction is thermodynamically feasible at the interface, since the energies of the electrons and holes remain constant at the band edge potential even with different degrees of band bending and applied potentials. For photoreduction reactions, it is required for the standard reduction potential to be below the conduction band edge, while photooxidation reactions can occur only when the redox potentials are above the valence band edge. The band edge position can, however, shift -59 mV per pH by obeying the Nernst equation.[34] This is due to the surface hydroxylation that occurs with the continuous adsorption and desorption of H^+ and OH^- ions from the aqueous electrolyte, which varies according to changes in pH.[34] The Fermi level of the electrolyte can also change with pH if the standard reduction potential involves H^+ or OH^- in the reaction, which is the case in water splitting and CO_2 reduction reactions.[34]

The change in the Fermi level of the semiconductor is typically identical to the change in the redox potential in solution, yielding no thermodynamic advantage to changes in pH. However, the band edge positions can remain unchanged by coating the semiconductor with a pH-insensitive organic group.[40] Moreover, the band edges can be directly tuned without altering the semiconductor by forming a dipolar structure at the interface which is caused by the specific adsorption of ions from the electrolyte.[41]

1.3.10. Schottky Barrier and Ohmic Contact

Unlike particles, in which the majority charge carrier is transferred to the opposite interface on the particle to perform the other half-cell reaction, photoelectrochemical cells require the semiconductor electrodes to be connected to an auxiliary electrode via an external circuit. The advantage of photoelectrochemical cell is that a controlled external potential bias can be applied which can enhance the band bending by controlling the Fermi level of the semiconductor. However, when semiconductors are fabricated into electrodes by connecting them to conductive wires, band bending occurs at the semiconductor-metal interface, also known as the Schottky barrier.[29] The Schottky barrier causes the electron transfer between the metal wire and semiconductor not to follow Ohm's Law, often accompanied by a rectifying effect.[39] In order to overcome this issue, ohmic contact needs to be achieved between the metal wire and semiconductor.

Ohmic contact establishes optimal charge carrier transfer at the semiconductor-metal interface without reflecting the majority charge carrier back to the semiconductor.[39] Ohmic contact yields negligible junction resistance, which provides uninhibited current flow with sufficiently small voltage drops and ensures that the device performance is not perturbed.[34,42]

Ohmic contact is formed by depositing a thin layer of conductive material between the conductive wire and semiconductor. To form an accumulation at the semiconductor-metal interface which causes the semiconductor to behave like a metal, the conductive material needs to have the appropriate work function (ϕ_M) compared to that of the semiconductor (ϕ_S).[39] For p-type photocathodes, (ϕ_M) has to be larger than (ϕ_S), while n-type photoanodes requires the opposite.[39] For p-type photocathodes, metals with high work functions such as gold and platinum are used, while aluminum, which has a small work function, can be used for n-type

photoanodes.[34,39,42] Other than pure metals, the conductive material may also be metal alloy eutectics.[40,42] However, it is important to verify the formation of the ohmic contact experimentally as the work function difference does not always correctly predict this, and the substrate may alloy with the semiconductor which can alter the work functions.[34,39,42]

1.3.11. Surface states

Electron transfer at the semiconductor-electrolyte interface can be affected by surface states. Surface states form a set of energy levels that exist only at the surface of semiconductor electrodes and not in the bulk. The ones of interest in this context reside in the band gap between the conduction band and valence band. Surface states are caused by the termination of the crystal lattice at the electrode surface. The dangling bonds, which are free radicals, at the semiconductor surface will interact with solution species, creating surface states with energy levels between the band edges.[1] Dangling bonds present in grain boundaries are also responsible for interband surface states.[43,44]

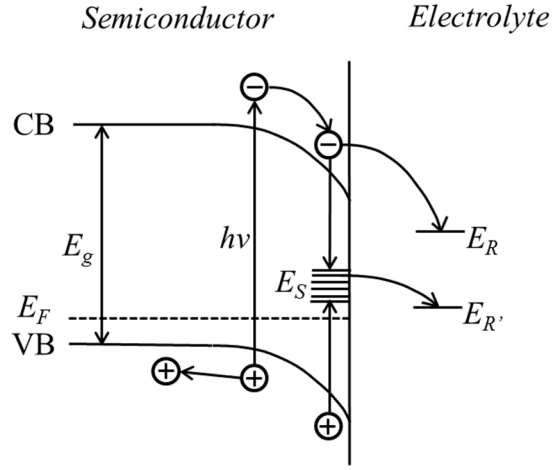

Figure 3. Model for recombination and charge transfer reactions involving surface states (E_S). Adapted with permission from ref. 45. Copyright 1982 The Electrochemical Society.

Surface states usually behave as the recombination centers for the photogenerated electrons and holes, which is a competitive process with the electron transfer processes from the conduction band to solution species (Figure 3).[45,46] Surface states can also work as trapping sites for charge carriers from the conduction band or valence band, which can be further transferred to redox couples in solution with proper potentials.[47] For metal oxide semiconductors, for example, oxygen vacancies at the semiconductor surface have been suggested to be the active sites for CO_2 activation. CO_2 molecules are likely to adsorb at the oxygen vacancies at the surface of electrodes.[48] A missing O^{2-} in the TiO_2 lattice can reduce two adjacent Ti^{4+} to Ti^{3+}, which may act as electron rich spots to interact with anti-bonding orbitals of CO_2 molecules.[49]

1.3.12. Effect of Co-Catalysts

Incorporation of co-catalysts could greatly improve the performance of semiconductor electrodes for CO_2 reduction. The co-catalysts can function as trapping sites for the electrons, thus promoting the charge separation and altering the selectivity of the products.[49,50]

The co-catalysts that have been investigated can be classified into two categories based on their phases. Nanoparticles of metals or oxides can be deposited on the surface of semiconductor photoelectrodes. When the Fermi level of the deposited metal lies below the conduction band of the semiconductor and above the redox potential of desired reaction, the particles can act as electron shuttles.[49] Metal oxide co-catalysts can function as trapping sites for holes. Co-deposition of metals is usually performed so that electrons and holes can be trapped by metal and metal oxide separately.[49] Another major category of co-catalysts are molecular species that are present in the electrolyte. Metal complexes of rhenium,[51,52] ruthenium,[53] iron,[54] and copper[55] are among the most well-investigated examples.

1.3.13. Nanostructured Semiconductors

Besides the material, their dimensionality, architecture, and exposed crystal faces can also influence the performance of photoelectrodes. Making materials into nanostructures is a well-established way to increase the surface area to volume ratio, which results in a great enhancement of the population of surface-active sites. Secondly, arrays of nanostructures can enhance the light absorption by suppressing the reflection of the incident light while facilitating the scattering and secondary absorption between the nanostructures. Thirdly, reducing the size of the crystals decreases the distance between minority carrier photo-formation and the charge transfer interface, minimizing the opportunity for electron-hole recombination.[56]

Moreover, tailoring the size of the semiconductor on the nanometer scale is a facile measure to engineer the band structure by virtue of quantum confinement. The band electronic properties of a semiconductor undergo dramatic changes as its dimensions enters the nanometer regime, resulting in discrete energy levels and increase in band gap energy.[57,58] Wang *et al.* reported CO_2 reduction on CdSe quantum dot-sensitized TiO_2 heterostructures. The conduction band of CdSe quantum dot rises 0.7 V compared to bulk CdSe, promoting the electron transfer from the conduction band of CdSe to the conduction band of TiO_2.[59]

Besides these general factors, some delicately engineered nanostructures can enhance the photocatalytic activity for other reasons. In some cases, the semiconductor prepared in a reduced size also exhibited an enlarged population of a desired crystal facet possessing catalytic activity, due to its characteristic surface energy and surface atomic structure. Yu *et al.* synthesized nanoplates of anatase TiO_2 possessing different ratios of {001} and {101} facets. Among the series of samples, the one with 58% of exposed {001} facets exhibited the maximum productivity of CO_2 reduction to CH_4. Density functional theory (DFT) calculation results

showed that these two different sets of facets have different conduction band and valence band energy levels, facilitating the flow of electrons from the {001} facet to the {101} facet, while holes flow from the {101} facet to the {001} facet . Here, the ratio of different facets plays a key role in regulating the CO_2 reduction productivity.[60]

Nanostructures of different dimensionalities may behave differently. For a suspension of nanoparticles (zero dimension), the nanoparticles are isolated from each other. Short travelling distances for charge carriers on all three dimensions are allowed.[32] For electrodes assembled from nanoparticles, the charge carriers have to transfer through the grain boundaries, where a great amount of trapping and detrapping events occur and leads to a low diffusion rate and hence enhance the possibility of recombination.[61]

One dimensional (1-D) nanostructures include nanowires, nanorods, nanotubes, nanofibers, and nanobelts.[32] The non-nanoscale dimension acts as a "highway" for the majority charge carriers to diffuse away from the surface, while the minority carriers migrating in the transverse direction can readily reach the semiconductor-electrolyte interfaces.[56] The fast diffusion of majority carriers and short travelling distance for minority carriers can enhance the charge separation process. The scattering of incident light among nanostructures is particularly significant in well assembled 1-D nanostructures leading to enhanced absorption of light.[62] Spurgeon *et al*. compared the fill factors of electrodes assembled from nanorod arrays of $CdSe_{0.67}Te_{0.33}$ with that of a planar electrode of the same composition. The fill factor for the nanorod array electrode was 0.428, while the fill factor for the planar electrode was 0.288.[63]

Two dimensional (2-D) nanomaterials possess two dimensions larger than the nanoscale. In 2-D nanostructures the charge carriers are less localized compared to 1-D systems. Nanosheets can

be fabricated into electrodes in one of two ways. They may form assemblies in a similar way as the 1-D nanostructures, or they can be deposited as thin films.[32]

Three dimensional (3-D) nanostructures are constructed from assembles of nanostructures of lower dimensions. A template may be required, or they can self-assemble. 3-D ordered structures can show unique optical effects that are absent in disordered ones, like the slow-light effect.[64] A photonic crystal is a nanostructure assembled by two or more materials of different permittivities periodically. Upon illumination, the light undergoes multiple scattering events in the photonic crystal, therefore slowing down the group velocity of light. The slow-light effect enhances the absorption of incident photons.[32]

1.3.14. Photodecomposition of Semiconductors

Most semiconductors (especially narrow band gap semiconductors) in contact with an electrolyte are subject to decomposition caused by the reduction or oxidation of the semiconductor by photogenerated electrons or holes, respectively.[65] This has been one of the most critical problems restricting their application. The criteria for a semiconductor to be stable against anodic decomposition is that ${}_pE_{decomp} > E_{VB}$,where ${}_pE_{decomp}$ is the redox potential of anodic decomposition reactions and E_{VB} is the potential of the valence band edge. Similarly, when ${}_nE_{decomp} < E_{CB}$, in which ${}_nE_{decomp}$ is the redox potential of cathodic decomposition reactions and E_{CB} is the conduction band edge, the material is stable against cathodic decomposition.[66]

Upon illumination, the populations of electrons in both the conduction band and valence band are altered. Thermal equilibrium of electrons in the bands no longer holds. Since the recombination rate is relatively slow compared to the relaxation rate within each band, both the conduction band and valence band can relax to a state of quasi-thermal equilibrium. Thus, the Fermi level does not provide sufficient energy information with regard to specific charge

carriers. Quasi-Fermi levels, ${}_nE_F$* and ${}_pE_F$*, are introduced to represent the energy levels of electrons in the conduction band and valence band respectively. When the reduction reaction is slow, ${}_nE_F$* is of higher energy than ${}_nE_{decomp}$. Thermodynamically, the decomposition processes are possible. If the reduction is fast, the quasi-Fermi levels of both bands will be closer to the redox potential of reaction. The decomposition Fermi level will be above the ${}_nE_F$*, making the semiconductor stable against the cathodic photodecomposition (Figure 4).

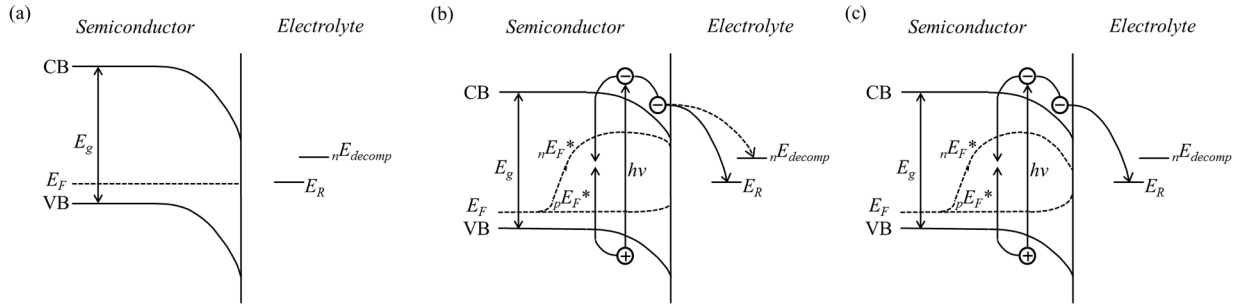

Figure 4. Behavior of the Fermi level (E_F) and quasi-Fermi levels for electrons (${}_nE_F{}^*$) and holes (${}_pE_F{}^*$) for a p-type semiconductor in contact with a redox system: (a) dark; (b) under illumination with a slow redox reaction; (c) under illumination with a fast redox reaction. Adapted from ref. [67] with permission from The Royal Society of Chemistry, copyright 1980.

For example, the n-type semiconductor CdS undergoes anodic photodecomposition by photogenerated holes, producing Cd^{2+} and S^0.[66] Gerischer *et al.* reported stabilization of CdS in the presence of the $[Fe(CN)_6]^{4-/3-}$ redox couple. The mechanism was ascribed to the moderately fast one-electron transfer process associated with this redox couple.[68] Rubin *et al.* demonstrated that photogenerated Cd^{2+} formed a surface film with $[Fe(CN)_6]^{4-/3-.}$ The generated $[CdFe(CN)_6]^{2-/1-}$ film possessed a surface localized highest occupied molecular orbital (HOMO) that is in good communication with the valence band of n-CdS. Electron transfer from the surface species to the valence band was fast compared to a surface without the $[CdFe(CN)_6]^{2-/1-}$ layer stabilization.[69]

P-type semiconductors are susceptible to cathodic decomposition. P-GaP and p-GaAs undergo three-electron reduction reactions, producing Ga metal.[70,71] Introduction of co-catalysts enhances interfacial charge transfer, which is expected to suppress the decomposition processes. In the work of Barton *et al.*, pyridine was used as a co-catalyst for CO_2 reduction on p-GaP. When there was no pyridine, the photocurrent decreased rapidly under illumination. This was attributed to the photodecomposition of p-GaP. While the photocurrent in the presence of pyridine was significantly larger than the situation without pyridine, one of the possible explanations is that the fast electron transfer from p-GaP to pyridine greatly reduced the photodecomposition.[17]

2. CO_2 REDUCTION ON SEMICONDUCTORS

The heterogeneous chemical reduction of CO_2 at the interface of a light-absorbing semiconducting material and liquid electrolyte is considered a direct avenue to realizing "artificial photosynthesis", and has been studied extensively since the late 1970s.[32,72–80] The primary goal of photo-assisted CO_2 reduction is to find a stable, highly efficient, and scalable semiconductor-based system to produce organic fuels solely driven by solar energy. If realized, this system would be a promising way of creating a sustainable cycle of consuming/recycling carbon-based fuels with zero net CO_2 emission.

In general, there are two configurations of semiconductor-based systems for photo-assisted CO_2 reduction. A photoelectrochemical cell (PEC) is composed of a semiconducting photoelectrode and a counter electrode, as Fig. 5a shows. The photoelectrode harvests light to promote charge separation and carries out a half-cell chemical reaction, normally using energized electrons to reduce CO_2 . The second configuration utilizes a suspension of semiconductor particles as a photocatalyst in a solvent that contains dissolved CO_2 . In this kind of system (Fig. 5b), both the photo-driven reduction and oxidation take place on the same

semiconducting particle, but on different sites. Photocatalysts range in size from micron sized particles to nanoparticles.

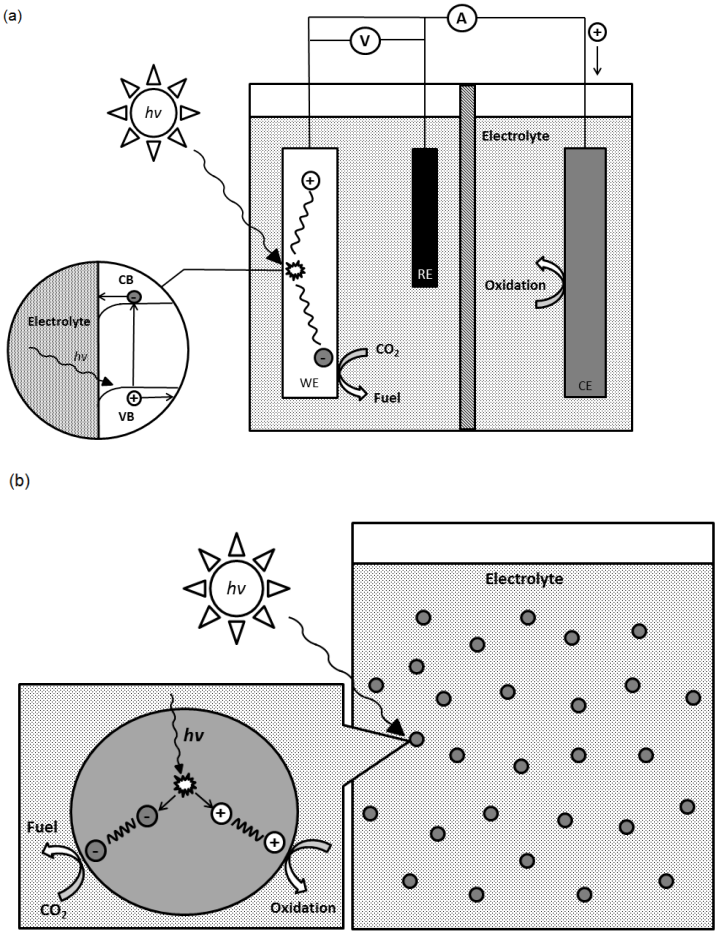

Figure 5. (a) Photoelectrochemical cell (PEC) under illumination, with a p-type semiconductor working electrode (WE) cathode, a reference electrode (RE), and a counter electrode (CE) anode immersed in an electrolyte containing CO_2 . The inset shows the bent semiconductor bands at the electrolyte interface and the separation of the photogenerated electron and hole. (b) Photocatalytic particles suspended in a CO_2 -containing electrolyte performing both oxidation and reduction reactions, though on different sites.

Based on the theory provided in section 1.3, one criterion for a solar-driven CO_2 -PEC is a photoelectrode having a bandgap overlapping the visible solar spectrum(E_g ~ 1.75 – 3.0 eV). Additionally, the conduction band edge of the semiconductor must lie at a potential that is more negative than the proton-assisted multi-electron reduction potentials of CO_2 (Fig 6).[32,49] When kinetics are taken into account, one anticipates that the conduction and edge may have to lie up to 1 V negative of the CO_2 reduction potential in order to supply the necessary overpotential to overcome slow kinetics and thus to drive the reaction at a meaningful rate. Theoretically, this kinetic barrier could be drastically reduced by the choice of an appropriate semiconducting material that possesses sufficient catalytic activity. Although many believe that the semiconductor surface-related catalytic process involves the formation of an adsorbed surface species of CO_2 , which is governed by the chemical constituents, surface microstructure, electronic band structure, and crystal phase, no universally recognized mechanism has been established to explain the catalysis on semiconductor surfaces.[49]

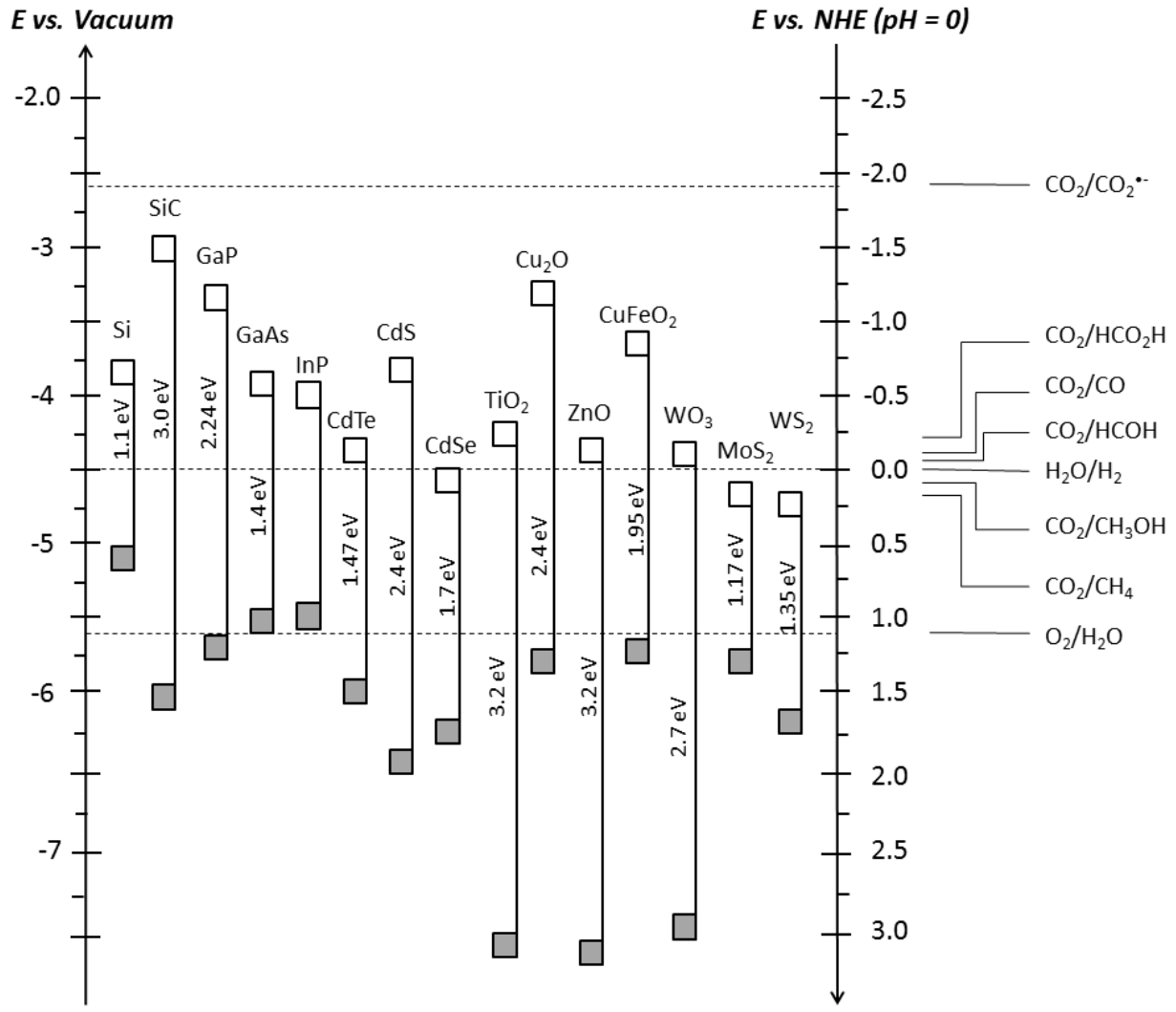

Figure 6. Conduction band (white squares) and valence band (gray squares) potentials of some commonly used semiconductors, with the potentials of several CO_2 and water redox couples at pH = 0, plotted vs. vacuum (left) and NHE (right).[32,49,77,81,82]

Typically, illuminated p-type semiconductors are chosen to perform solar-driven CO_2 reduction since they act as photocathodes when immersed in supporting electrolytes. The majority of this section will focus on p-type semiconductors, including Si, III-V, II-VI, and oxide materials. Catalytic semiconducting materials that do not fall into one of these categories, although rare, will also be discussed. Although n-type semiconductors typically are photoanodes,

they can be employed as particulate photocatalysts, performing oxidation on an illuminated face and reduction of CO_2 on a dark face with the photogenerated electrons.

The modification of semiconductor surfaces with molecular catalysts or metals has long been a technique employed to increase catalytic activity and stability. Semiconductors modified with molecular catalysts take advantage of the selectivity and tunability of molecular catalyst systems as well as the advantages of heterogeneous catalysts including utilization of lower amounts of expensive catalysts, high concentrations of the catalysts at the reaction site, and easy separation of the catalyst from the reaction mixture. In some cases, surface confinement of a catalyst improves the rate of heterogeneous charge transfer from the electrode to the catalyst; however, due to orientation effects, the rate of heterogeneous electron transfer has been observed to be decreased in certain cases. Likewise, surface confinement can lead to higher catalyst stability, but this is not assured, and in cases where the surface species has a limited lifetime, replacement of a surface-attached species is more difficult than continuous addition of a molecular catalyst to solution. There has been a significant amount of research into methods of attaching catalysts to electrodes, yielding a large variety of attachment methods to choose from. These techniques vary from utilizing a covalent linker to adsorbing polymer films to the surface, which represent two of the most common techniques. A second class of modified semiconductors is comprised of materials on which deposition of metallic particles or thin films occurs directly onto the photoactive surface. This method takes advantage of the high catalytic activity of many metal nanoparticles for CO_2 reduction, which typically behave in similar ways to the bulk metal electrodes.[11] The metal typically acts as an electron trap, aiding in the separation of photogenerated charge carriers. Several semiconducting materials modified with a variety metal particles have shown very promising CO_2 reduction results. Another trend in photo-assisted CO_2

reduction research is to combine chemical and physical properties of multiple semiconducting materials into one integrated system. Different approaches have been developed to realize this idea, including heterostructure, Z-schemes, solid solutions, and micro/mesoporous composites.[49] Such novel photo-driven CO_2 reduction systems are normally designed and engineered to incorporate different functions from each component material to achieve a higher light-to-energy conversion efficiency and a more controlled product selectivity. The Z-scheme is designed to mimic the natural photosynthesis of converting *CO_2* .[35,49] In a typical Z-scheme, shown in Figure 7, two different semiconductors are mediated by a reversible redox couple. The two photocatalysts are excited simultaneously to generate electron-hole pairs, and an electron from one semiconductor and a hole from another are consumed by the bridging redox couple, leaving the un-recombined electron and hole with strong reduction and oxidation abilities on different active sites. These and other integrated schemes are also included in this chapter as they open a new pathway for scientists to explore more advanced "artificial photosynthesis" systems.

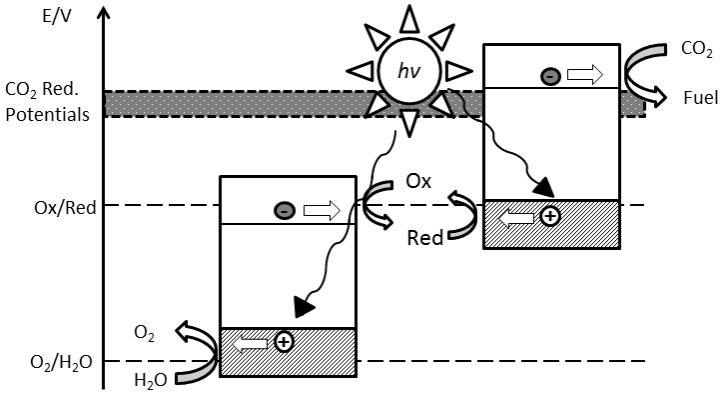

Figure 7. Z-scheme system, employing two semiconductors which together bridge the water oxidation potential and CO_2 reduction potentials. Both semiconductors absorb light, generating photoelectrons, and the transfer of charge carriers is mediated by a reversible redox couple in solution.

2.1. Group IV Materials

Si has a narrow indirect bandgap of 1.1 eV, which allows its photoabsorption to span from the UV region to the near-IR region. Due to its simplicity and abundance, many early studies of photoelectrochemical reduction of CO_2 have been performed on Si photoelectrodes. Although a light-induced photovoltage is established on the semiconductor electrode upon illumination, in nearly all the studies, an external electrical bias has been applied to drive the CO_2 reduction reaction.

In the early 1980s, Bockris *et al*. reported using boron doped p-Si to reduce CO_2 to CO in a non-aqueous electrolyte under 600 nm illumination at potentials equal to or more negative than -2.0 V vs. SCE.[83] The water content in the non-aqueous electrolyte, DMF, was believed to negatively influence the efficiency of CO_2 reduction, as increased water content led to increased hydrogen evolution. Both the (100) and (111) crystal faces of Si were examined in this study, but no significant variation on the product distribution was observed, and only the ratio between light-induced current and dark current were observed different on the two different faces. The p-Si electrode demonstrated high quantum efficiency, 85-95%, as a function of wavelength in the visible light range 400 - 800 nm, as well as high Faradaic efficiency for CO production. However, the *i-V* characteristics indicated that potentials as negative as -2.5 V vs. SCE are required to drive the reaction. Since these potentials are more negative than the CO_2 reduction potentials (see Table 1), the system does not convert light energy to stored chemical energy.

In 1992, Junfu *et al*. reported their study of photo-assisted CO_2 reduction on a p^+/p-Si photocathode in an aqueous electrolyte.[84] The material was monocrystalline p^+-Si with a 10 μm epitaxial layer of p-Si on the (111) crystal face. The current efficiency for converting CO_2 to formic acid was reported to be constant for the first 6 hours at -1.6 V vs. SCE but subsequently

decreased. A potential of -1.2 V vs. SCE was found to yield the highest Faradaic yield on this electrode. Junfu *et al*. also concluded that the optimal electrolyte pH for photoelectrolysis of CO_2 was neutral or slightly basic, and they suggested that the reduced current density in *CO_2* -saturated electrolyte compared to N_2-saturated electrolyte is possibly due to the adsorption of CO_2 molecules on the electrode surface.

In a later study, Hirota *et al.* studied p-Si at elevated CO_2 concentrations by varying the pressure up to 40 atm.[85] The experiment was performed in a methanol medium saturated with *CO_2* . At -1.8 V vs. Ag QRE (a silver wire quasi reference electrode with a potential ~80 mV vs. SCE), p-Si was reported to produce CO and methyl formate with Faradaic yields of 75% and 10%, respectively. The formyl group of methyl formate was produced via CO_2 reduction to formate and then reacted with methanol to form the ester. Since the study revealed that the CO_2 pressure is the most critical factor influencing the product distribution, Hirota *et al.* proposed that at high CO_2 pressures, the adsorbed $(CO_2)_2^{\bullet-}$ radical reached high coverages, which resulted in both a high current efficiency for CO production, low production of H_2, and a stabilizing effect on the semiconductor electrode. This radical, however, is highly unstable and would not be able to remain adsorbed at the surface. Aurian-Blajeni *et al*. investigated the effect of coating silicon with polyaniline, a conductive organic polymer.[86] The polyaniline-coated p-Si had a much lower overpotential than bare p-Si, with onset close to -1.0 V vs. SCE under illumination from a xenon lamp. This system produced predominantly formic acid and some formaldehyde, with combined Faradaic efficiencies of 20-30%, though the efficiency dropped as more charge was passed.

P-Si photoelectrodes modified with either Cu, Au, or Ag particles have been shown to produce CO, CH_4, and C_2H_4 in aqueous media.[87,88] It was determined that obtaining fine control of the surface structure of the particles on the surface was very important in order to decrease surface

carrier recombination and to control the barrier height and energy-level matching between the semiconductor and solution.[87] Additionally, it was determined that the theoretical optimum yield would occur with particles 5 nm in size, though particles of 20-200 nm in size were employed experimentally.[88]

A diamond substrate has also been employed to reduce CO_2 to CO with greater than 90% product selectivity.[89] Diamond has a band gap of 5.5 eV, which requires high energy UV excitation. The conduction band edge of diamond is well above the reduction potential of $CO_2/CO_2^{\bullet-}$, and the excited electrons in the conduction band are readily ejected into the adjacent aqueous phase and then relaxed to form solvated electrons. The actual reduction of CO_2 to $CO_2^{\bullet-}$ is via the reaction with the solvated electrons, which is followed by photodissociation of $CO_2^{\bullet-}$ to produce the final product CO.

Gondal *et al*. investigated granular α6H-SiC (band gap = 3.17 eV) as a photocatalyst for CO_2 reduction.[90] Using a 355 nm laser, the reduction was selective for methanol production with a 1.95% maximum quantum yield. A broad band light source (Xe-Hg lamp) was found to produce other hydrocarbons as well, with methanol accounting for roughly 50% of the products formed. The maximum quantum yield for methanol production under the Xe-Hg lamp was only 1.16%.

Cook *et al*. demonstrated the use of copper loading on p-SiC dispersions for CO_2 photoreduction.[91] In the presence of Cu, it was shown that methane and oxygen were the gaseous products of this reaction, but no attempt was made to identify liquid products. Methane production decayed over the course of 2 hours, and oxygen production was relatively low. This observation was ascribed to surface oxide growth. The diminished methane production was attributed to Cu deposition on the photoactive sites of the p-SiC. A pH dependence study showed

that methane production maximized at pH 5, with detectable ethane and ethylene appearing only at this pH. Methane could only be produced in a temperature range of 30-60˚C.

Dzhabiev *et al*. attempted CO_2 photoreduction on SiC under various conditions, including the addition of Na_2S, rhodium, and/or copper to the suspension.[92] Only with the rhodium and the copper were trace amounts of methane detected, suggesting that impurities in the SiC may be a key factor in the reduction of CO_2 .

Zhang *et al.* used spin-polarized density functional theory (DFT) to explore the adsorption and reduction capabilities of silicon carbide (SiC) nanotubes and nanosheets.[93] Three different structure types were explored: a variety of (n, 0) zigzag SiC nanotubes ($3 \leq n \leq 12$), multiple (n, n) armchair SiC nanotubes ($2 \leq n \leq 10$), and a single SiC layer comprised of a 5 x 5 supercell. It was discovered that, upon adsorption, CO_2 bends and forms a four-membered ring resulting from the attack of the C-O bond in CO_2 with the Si-C bond in SiC. CO_2 adsorbs to armchair SiC nanotubes in a direction perpendicular to the tube axis. A parallel direction is preferred for zigzag SiC nanotubes. The adsorption energy (E_{ad}) of CO_2 decreased with decreasing surface curvature, which implies that SiC nanotubes with smaller diameters are able to bind CO_2 more tightly than nanotubes with larger diameters. The chirality of the SiC nanotube had a negligible effect on the calculated adsorption energies. A single-layer of SiC cannot adsorb CO_2 stably, as evidenced by a positive ΔG of 0.41 eV. It was asserted that nanotubes with higher curvatures cause increased electron density to exist outside of the tube, and this aided in adsorption. It is concluded that SiC nanostructures may reduce CO_2 to formic acid in a three step process: the hydrogenation of the starting material to formate, protonation to formic acid, and ultimately desorption.

2.2. III-V Semiconductors

Great efforts have been made on the investigation of CO_2 reduction on III-V semiconductors.[77] Among all the III-V family members, GaP (2.24 eV), GaAs (1.4 eV) and InP (1.34 eV) are the most commonly studied. Halmann *et al.* pioneered photoelectrochemical CO_2 reduction on III-V semiconductor surfaces.[26] In aqueous media, he reported that HCOOH, HCHO and CH_3OH were produced from CO_2 on an illuminated Zn doped p-GaP surface. The optical conversion efficiency was reported to be a function of the applied potential, and when a 365 nm illumination source was used, the maximum optical conversion efficiency was calculated to be 5.6% at -0.8 V vs. SCE. However, this conclusion is fundamentally flawed, since when an overpotential is needed to drive the reaction (as was the case here), there is no net solar energy stored.[17] Only a few years later, Taniguchi *et al*. attempted to study the mechanism of conversion of CO_2 to small molecules on p-GaP in a Li_2CO_3 electrolyte.[94] The addition of 15-crown-5 enhanced the current efficiency of formation of HCOOH, HCHO and CH_3OH. In the potential window from -0.6 to -1.4 V vs. SCE, the current efficiency of every product decreased when the cathodic polarization was increased. As the crown ether facilitated the deposition of Li onto the p-GaP surface, Taniguchi *et al.* suggested that the electrodeposited lithium reduced CO_2 to its one-electron reduced radical form.[94] In a study under elevated CO_2 pressure of 8.5 atm, the highest observed Faradaic efficiency on p-GaP was a total of 80% for HCOOH, HCHO and CH_3OH production, at -1.00 V vs. standard Ag electrode in Na_2CO_3 electrolyte.[95] Although nearly all the literature studies of CO_2 reduction on p-GaP reported HCOOH, HCHO and CH_3OH as the products, in 1984, Ito *et al*. claimed that formic acid was the only experimentally confirmed product of CO_2 reduction, and the rest of the organics could be ascribed to the photolysis of epoxy resin used to fabricate the cell.[96] Ito *et al.* also suggested in a later paper that the incident light intensity

strongly influences the Faradaic efficiency of $HCOO^-$ formation from CO_2 on p-GaP. Altering the light intensity led to the change of the photocurrent, and this resulted in the variation of the ratio between the partial current for $HCOO^-$ production and that of H_2 evolution.[97] Ito *et al.* also studied the effect of surface treatment of p-GaP towards the product distribution obtained from CO_2 reduction.[98] Varying etchants would affect the population of crystal defects, surface morphology, and predominant crystal phases exposed on the surface, which would lead to different activity of the surface for CO_2 reduction. Halmann *et al.* suggested that on an illuminated GaP electrode, the observation of a 15% enhancement in photocathodic current in a pH = 7 phosphate buffer between CO_2 bubbling and Ar bubbling was due to the first step in the reduction of CO_2 , producing the formate radical with a one-electron reduced surface-adsorbed proton.[99]

In non-aqueous solutions, specifically, in an aprotic DMF solution, a cell consisting of a p-GaP photocathode and a TiO-$LaCrO_3$ photoanode was employed to produce oxalate from CO_2 .[100] This work is one of the earliest reports that a C-C bond can be formed from CO_2 reduction on a semiconductor. Taniguchi *et al.* reported that, in a DMF solution containing 5% H_2O, CO is the major CO_2 reduction product on both p-GaP (100) and (111) surfaces.[83]

Theoretical studies have also been conducted on the way in which p-GaP interacts and reduces CO_2 .[101–103] Using DFT calculations, Carter *et al.* suggested that the structural and electronic properties of the GaP(110)/H_2O interface is capable of forming hydride-like H atoms as a consequence of the dissociation of water. This H radical may be a key intermediate in the mechanistic pathway for CO_2 reduction on GaP(110) surfaces.

In 1978, Halmann *et al.* reported that photo-assisted CO_2 reduction has been achieved on p-GaAs, but they indicated that no net gain of energy conversion was achieved due to an highly

cathodic applied bias.[26] After this early attempt, extensive research on GaAs ensued in the early '80s. It was discovered by Aurian-Blajeni and coworkers that p-GaAs and p-GaP exhibit a similar dependence on CO_2 pressure.[95] The GaAs electrode also displayed better Faradaic efficiency for CO_2 reduction compared to GaP at -1.0 V vs. SCE; however, it was much less stable under illumination.

Seven-fold higher CO_2 concentration (~210 mM) can be obtained in methanol compared to water at room temperature. This solvent has been employed as the electrolyte in work conducted by Hirota *et al.* and Kaneco *et al*.[85, 104] At a high CO_2 pressure of 40 atm, p-GaAs demonstrated an 88% overall CO_2 reduction current efficiency at -1.9 V vs. Ag QRE. The electrode also exhibited a high selectivity for CO production. A white film was observed on the surface of p-GaAs after an electrolysis in aqueous media, which was ascribed to the reductive decomposition of GaAs to Ga and As in the presence of a proton source. However, this film was absent on the p-GaAs surface when electrolysis took place in a methanol medium, and this was suggested to indicate enhanced stability of p-GaAs in this electrolyte.[85] It was suggested that under high CO_2 pressure, an adsorbed layer of $(CO_2)_2^{\bullet-}$ is instrumental in protecting the semiconductor surface by blocking the attack of methanol, and by sinking the photogenerated electrons. However, given the known instability of the oxalate radical anion, this is unlikely. However, this mechanism was supported by Kaneco and coworkers, who claimed that the reaction proceeded via a similar route.[104] In that study, due to the detection of HCOOH in the reduced products, a proton was suggested to be involved in part of the reaction coupled with a second electron transfer to account for the formation of formate.

p-InP is another example of a III-V semiconductor that possesses a bandgap matching the solar spectrum, and has thus been studied extensively. In the study carried out by Kuwabata *et al.* on

p-InP, it was discovered that using a carbonate-based electrolyte favored the production of formic acid from CO_2 , while other electrolytes such as sulfates, perchlorates and tetraethylammonium perchlorate (TEAP) favored the production of CO.[105] This finding was ascribed to the presence of abundant carbonates suppressing the reaction between a $CO_2^{\bullet-}$ radical and a CO_2 molecule coupled with an electron to form a CO and a carbonate anion. A maximum current efficiency of 73.5% for CO_2 reduction was achieved in 0.1 M TEAP electrolyte at -1.2 V vs. SCE.

CO_2 reduction on p-InP in non-aqueous media was also preformed, and these studies focused primarily on methanol as the solvent. At a high current density of 100 mA cm^{-2}, a current efficiency of 93% for CO production was achieved, with $HCOOCH_3$ as the secondary product.[106] This current efficiency stabilized at approximately 94% at potentials more negative than -1.4 V vs. Ag QRE, which indicated that the CO_2 reduction rate was limited by light intensity. The tetrabutylammonium perchlorate (TBAP)-methanol solution had the distinct advantage of stabilizing the electrode surface, even at potentials significantly more negative than -1.1 V vs. Ag QRE. At CO_2 pressures up to 40 atm, the partial current density for CO production increased steadily as the potential became more negative, and the current efficiency for CO production exceeded 90%.[85] However, in a study conducted by Ohta *et al.* using a CO_2 saturated LiOH/methanol medium in the cathodic range from -2.2 to -2.5 V vs. Ag/AgCl, formate was observed as a reduction product generated through a proton coupled electron transfer to a surface adsorbed $CO_2^{\bullet-}$.[104]

InP electrodes have been modified by a variety of metals and shown to reduce CO_2 to CO and formic acid in a LiOH/MeOH solution.[107] It was shown that Pb produced formate with efficiencies up to 30%, while Au and Ag modified electrodes produced CO with efficiencies of

70% and 80% respectively. Ni-modified electrodes produced primarily H_2 with very small amounts of CH_4 and C_2H_4, while Cu-modified electrodes produced CO and formate at 40% and 15% Faradaic efficiencies, respectively, and Pd-modified electrodes produced CO with 55% efficiency. Hydrocarbons were observed from CO_2 reduction on p-InP when Cu particles were suspended in a methanol solution.[108] Small Faradaic efficiencies for methane and ethylene were reported at 0.56% and 0.8%, respectively, but without the copper only formic acid and CO were formed. The maximum efficiencies for the production of all four products required potentials in the range of -2.5 to -2.7 V vs. Ag/AgCl. The addition of Cu particles created new adsorption sites for CO_2 , and the formation of hydrocarbons was suggested to be from CO_2 adsorbed on metal particles or at the semiconductor/particle junctions. In the proposed mechanism, a multielectron-reduced carbene species was suggested as the intermediate leading to the production of methane and ethylene. In an earlier study using 5% H_2O in a DMF solution, the current efficiency for CO_2 reduction was fairly low due to dominant hydrogen evolution, and photodecomposition was observed on p-InP.[83]

2.3. Oxide Semiconductors

2.3.1. Titanium Dioxide

Titanium dioxide (TiO_2) is by far the most popular of the oxide semiconductors, since it is highly stable under photocatalytic conditions, inexpensive to use, and able to perform a variety of photocatalytic reactions, including water splitting,[1] degradation of various organic species,[109,110] and carbon dioxide reduction.[111] As such, this material has been extensively researched and reviewed for the past few decades.[76,78,112–125] Various types of TiO_2 photocatalysts have been studied, including particle suspensions and nanostructured materials. Furthermore, numerous modifications to these catalysts, such as the addition of co-catalysts or

photosensitizers have been investigated. These different variations will be discussed in a representative fashion in the following sections; however, many aspects have been covered already in greater depth in previous reviews cited above.

2.3.1.1. TiO_2 Photocatalysis: Structure and Mechanism

TiO_2 has three main crystal structures, rutile, anatase, and brookite. Anatase is the most utilized given its abundance and ease of synthesis compared to brookite and its improved photocatalytic abilities compared to rutile. Even though rutile has a band gap of 3.0 eV and anatase has a larger band gap of 3.2 eV, the former more readily promotes electron-hole pair recombination.[126–130] Several reports have shown that mixed-phase TiO_2, especially P25, which contains ~70% anatase and ~30% rutile, has photocatalytic properties that exceed either pure phase.[117,129,131–135]

The mechanism of CO_2 reduction on illuminated TiO_2 catalysts has been studied using a variety of spectroscopic and quantum mechanical methods.[136] An *in situ* IR spectroscopy study showed the presence of bent CO_2 on the titania surface, with greater concentrations appearing under illumination.[137] Electron paramagnetic resonance (EPR) spectroscopy observed Ti^{3+} ions at the surface as well as carbon, CH_3, and hydrogen radicals at 77 K under UV light.[127,132,138] Hurum *et al.* suggested that, in P25, a rutile structure absorbs the photon and transfers the photoelectron to an anatase trap state, with a subsequent transfer to a surface state, which can react with CO_2.[132] Due to oxygen vacancies in the intrinsically n-type TiO_2, numerous Ti^{3+} states are present, though more are generated by doping[139–146] and by reduction of Ti^{4+} with photoelectrons under illumination.[127] At the surface, these Ti^{3+} species can reduce adsorbed CO_2 to a bent $CO_2^{\bullet-}$ species,[147] reforming Ti^{4+}, and again serve as electron trap states for further reduction (Scheme 2). Oxygen vacancies can also induce dissociation of CO_2 to adsorbed CO

and a healed vacancy.[148] Adsorbed hydrogen atoms are also formed, which can further reduce the bound $CO_2^{\bullet-}$ radical.[138] Many different CO_2 reduction products can be formed on TiO_2 in the presence of water, which acts as the source for both protons and electrons. CO and CH_4 predominate when gaseous H_2O is used, whereas typically methanol is formed when photocatalysis takes place in solution.[136] This difference may result from the hydrogen-bonding network available in the aqueous phase, which more readily stabilizes polar surface intermediates.

Scheme 2. Formation of surface Ti^{3+} with a photogenerated electron, leading to binding and bending of CO_2 and the formation of $CO_2^{\bullet-}$.

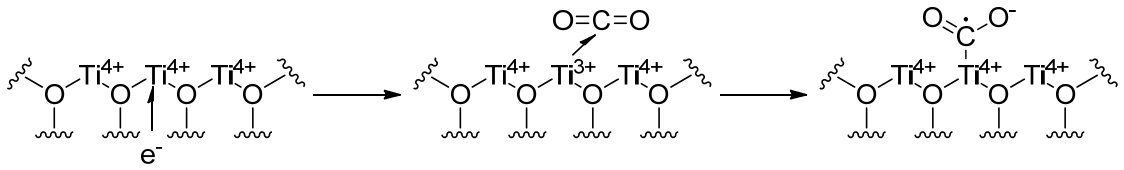

2.3.1.2. Nanostructured TiO_2

A variety of different morphologies of TiO_2 have been tested for their CO_2 reduction abilities, including powder dispersions, thin films, nanosheets, nanotubes, and nanorods. Some titania catalysts have also been incorporated into zeolites and other mesoporous structures, but these catalysts will be discussed in section 3.2. Simple powder dispersions and thin films had seen much interest in the past,[111,127,149–154] but have not attracted as much focus lately. Instead, studies utilizing nanostructured materials have seen a surge of interest. The effect of TiO_2 nanoparticle (NP) size on their aqueous CO_2 reduction properties was recently investigated by Kočí *et al.* under UV light.[155] Particles 14 nm in diameter outperformed NPs as small as 4.5 nm and as large as 29 nm in the production of CH_4 and CH_3OH on both a mass and surface area basis. The

smallest NPs had larger band gaps due to quantum confinement[156] and had less ability to separate charges effectively.

Nanosheets, like single crystals, preferentially show a particular facet, which can have vastly differing photocatalytic reactivities (Figure 8). Yamashita *et al.* studied CO_2 reduction on TiO_2(100) and (110) single crystals and found the former to yield methane and methanol whereas the latter produced only methanol and in much lower quantities, possibly due to a higher concentration of Ti species on the (100) surface.[157] Pan and coworkers determined that the {010} facet, which is geometrically equivalent to the {100} facet, had more favorable surface electronic and atomic structure for photocatalysis than either the {101} or {001} facets.[158] Consequently, Xu *et al.* synthesized titania nanosheets with 95% {100} facets exposed and found that they produced CH_4 at about 6 times the rate as cuboids with only 53% {100} facets.[159] Yu *et al.* studied the effects of varying ratios of {001} to {101} facets, since the slightly different band structures of the two planes can lead to the formation of a heterojunction that more readily separates the photogenerated charge carriers.[60] The optimal catalyst tested had 58% {001} facets and produced CH_4 at 1.35 μmol g^{-1} h^{-1}. Nanosheets with percentages of {001} facets of 72% were synthesized, generating CO, formaldehyde, methanol, and methane from an alkaline CO_2 solution.[145]

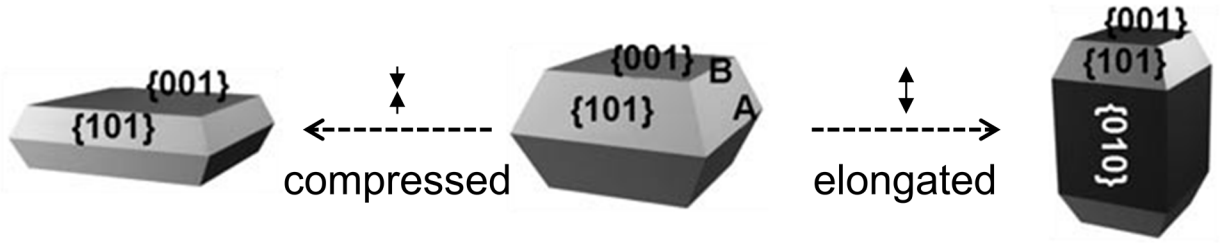

Figure 8. {001}, {101}, and {010} facets on TiO_2 crystals. Adapted with permission from ref. [158]. Copyright 2011 Wiley-VCH Verlag GmbH & Co. KGaA, Weinheim.

Titania nanotubes (TNTs) and nanorods (TNRs) have lately seen significant interest due to their high surface area and their extended length in a single direction, which allows for increased charge separation.[117,118,125] These nanostructures have lengths several to hundreds of times their diameters and are generally prepared by oxidation of titanium at high voltages in fluoride electrolytes, though hydrothermal methods are also employed.[118] Schulte *et al*. found that 90% anatase TNTs made methane at a rate of 3.4 μmol m^{-2} h^{-1}, while TNTs annealed at higher temperatures and thus with higher concentrations of the rutile phase performed more poorly.[129] Vijayan *et al*. prepared 8 nm diameter anatase TNTs that collapsed into TNRs upon calcination above 500 °C, resulting in a sharp decrease in surface area.[160] The TNTs calcined at 400 °C yielded 0.50 μmol g^{-1} h^{-1} of methane, whereas TNRs produced only 0.33 μmol g^{-1} h^{-1}; the authors attributed this difference to the greater surface polarity and acidity present on the inner curvature of the tubes that was not accessible in the collapsed tubes. 11 nm diameter TNTs were synthesized by He *et al*. and generated CO, formaldehyde, methanol, and methane in basic solution.[145] The quantum efficiency of these TNTs were about the same as the nanoparticles, on a surface area basis. Wang *et al*. modified anatase TNRs with rutile NPs and found an increase in activity from 1.29 μmol g^{-1} h^{-1} to 2.36 μmol g^{-1} h^{-1} of methane under UV light.[134] As noted above, the mixed-phase catalysts were implicated in better charge separation, leading to higher photocatalytic activity.

2.3.1.3. Metallic Co-Catalysts on TiO_2

Titania is infrequently used on its own and is instead typically modified with metallic particles or thin films, which function as co-catalysts and aid in the reduction of CO_2 .[112,161–163] The addition of metal particles, often incorrectly called "doping" since the metals do not incorporate into the crystal structure, encourages electron-hole charge separation since the metals act as

electron traps. Both the metal and the TiO_2 can act as catalytic surfaces; the decrease in electron density in the latter from the formation of the Schottky barrier increases the acidity of the surface hydroxyl groups and can enhance photocatalysis.[161] As noted previously, the metallic co-catalysts typically lead to nearly identical product distributions in the reduction of CO_2 as with the bulk metal electrodes when in aqueous conditions.

There have been numerous studies with a variety of transition metals as well as recent reports utilizing carbon, in the forms of graphene and nanotubes, and indium, summarized in Table 2. The most commonly employed metals with TiO_2 have been the coinage metals, particularly copper, which, as an electrode in aqueous solution, yields several different hydrocarbons.[19] Typically, the metals are photoreduced onto the TiO_2 substrate prior to CO_2 photocatalysis, but some sol-gel methods have also been employed, which incorporate the metals into the macrostructure of the titania as it is synthesized.

A few particularly interesting investigations into metal-modified TiO_2 photocatalysts have recently been published. Hou *et al.* used gold nanoparticles on anatase thin films and employed a 532 nm laser to excite the plasmon resonance of the gold.[164] This plasmon generated localized electric fields strong enough to excite electron-hole pairs in the TiO_2 to a much greater extent than possible with just the incident light, even though no electrons actually transferred from the gold particles to the TiO_2. A recent study by Wang *et al*. claimed the highest quantum yield, at 2.41%, for CO_2 photoreduction, by using a nanostructured columnar thin film of TiO_2 with Pt nanoparticle co-catalysts.[135] The maximum rate of CH_4 production was an incredibly large 1361 $\mu mol\ g^{-1}\ h^{-1}$ after 5 hours, which the authors attributed to both optimal Pt NP sizes, which greatly enhanced the charge separation, and the pointed columnar structure of the TiO_2, which had a high density of (112) planes that possess high electron mobility. Xie *et al*. tested Pt-TiO_2

photocatalysts in both aqueous and vapor conditions, and compared the platinum catalysts with other noble metals.[165] Under both phases of water, the photelectrons were utilized at about the same rate; however, in the liquid phase, the selectivity for CO_2 reduction products was much lower than in the vapor phase, due to the high rate of hydrogen formation. The other metal catalysts tested (Pd, Rh, Au, and Ag) all had comparable CO_2 reduction selectivities to Pt, but the rates were typically much lower. In addition, the product distributions between CO and CH_4 varied from metal to metal.

Table 2. Summary of various metal-modified TiO_2 photocatalytic systems.

Photocatalyst	Structure[a]	Reductant	Light	Products	Yields (μmol g^{-1} h^{-1})	Year
Cu + TiO_2	Powders	H_2O liquid	Xe lamp	CO HCHO CH_3OH	0.27 0.28 0.55	1992[166]
5%Cu-TiO_2	Powder	H_2O liquid	Xe lamp	CH_4 C_2H_4 C_2H_6	0.65 0.92 0.13	1994[167]
0.1%Cu-TiO_2	Powder	H_2O vapor	Hg lamp ($\lambda > 290$ nm)	CH_4	0.08	1994[126]
2.0%Cu-TiO_2	Powder	0.2 N $NaOH_{(aq)}$	Hg lamp	CH_3OH	19.8	2002[131]
1.2%Cu-TiO_2	Film in optical fiber	H_2O vapor	Hg lamp	CH_3OH	0.45	2005[168]
Cu-TiO_2	NP on Nanorods	H_2O liquid	UV lamp	CH_4	0.18	2012[169]
Cu-TiO_2	NP on Permeable Wafer	H_2O vapor	AM1.5 lamp	CO CH_4	24[b] 36[b]	2014[170]
$Cu_{0.33}Pt_{0.67}$-TiO_2	Internally-coated NT	H_2O vapor	AM1.5 lamp	CH_4 C_2H_4 C_2H_6	134 12.0 24.1	2012[171]
Pt@Cu_2O-TiO_2	Core-Shell NP on Powder	H_2O vapor	Xe lamp	CO CH_4	8.3 33	2013[172]
Au_1Cu_2-TiO_2	Film	H_2O vapor	AM1.5 lamp	CH_4	2200	2014[173]
Au-TiO_2	NP on Film	H_2O vapor	UV lamp (254 nm)	HCHO CH_3OH CH_4 C_2H_6	1.36 0.86 2.31 1.63	2011[164]
0.2%Au-TiO_2	Mesoporous Powder	H_2O vapor	Xe lamp	CH_4	1.50	2012[143]
0.5%Au-TiO_2	NP on Powder	H_2O vapor	Xe lamp	CO CH_4	1.5 3.1	2014[165]
0.15%Pt-TiO_2	NP on NT	H_2O vapor	Hg lamp	CH_4	0.66	2009[174]
Pt-TiO_2	NP in NT	H_2O vapor	AM1.5 lamp	CH_4	25[b]	2011[175]
0.2%Pt-TiO_2	Mesoporous Powder	H_2O vapor	Xe lamp	CH_4	2.81	2012[143]

Photocatalyst	Structure[a]	Reductant	Light	Products	Yields (μmol g^{-1} h^{-1})	Year
Pt-TiO_2	NP on Columnar Thin Film	H_2O vapor	Xe lamp	CO CH_4	190 1361	2012[135]
0.5%Pt-TiO_2	NP on Powder	H_2O vapor	Xe lamp	CO CH_4	1.1 5.2	2014[165]
0.5%Pt-TiO_2	NP on Powder	H_2O liquid	Xe lamp	CO CH_4	0.76 1.4	2014[165]
Pt-TiO_2	NP on Permeable Wafer	H_2O vapor	AM1.5 lamp	CH_4	28[b]	2014[170]
Pt-TiO_2	NP on NP	H_2O vapor	Xe lamp	CH_4 C_2H_6	60.1 2.8	2014[176]
2.0%Ag-TiO_2	Powder	0.2 N $NaOH_{(aq)}$	Hg lamp	CH_3OH	14.2	2004[162]
0.1%Ag-TiO_2	Mesoporous Powder	H_2O vapor	Xe lamp	CH_4	0.80	2012[143]
0.5%Ag-TiO_2	NP on Powder	H_2O vapor	Xe lamp	CO CH_4	1.7 2.1	2014[165]
1%Pd-TiO_2	NP on Powder	H_2O liquid	Hg lamp ($\lambda > 310$ nm)	CO CH_4 C_2H_6	0.04 0.38 0.06	2011[177]
0.5%Pd-TiO_2	NP on Powder	H_2O vapor	Xe lamp	CO CH_4	1.1 4.3	2014[165]
0.5%Rh-TiO_2	NP on Powder	H_2O vapor	Xe lamp	CO CH_4	0.62 3.5	2014[165]
0.5%Ru-TiO_2	NP	1 M 2-propanol$_{(aq)}$	Hg lamp	CH_3OH CH_4	2.91 35.2	2006[178]
10%In-TiO_2	NP	H_2O vapor	Hg lamp	CO CH_4	230 675	2015[179]
MWCNT-TiO_2	NP on NT	H_2O vapor	UV lamp	HCOOH CH_4	18.7 11.7	2007[180]
0.27%Graphene-TiO_2	Film	H_2O vapor	Hg lamp	C_2H_5OH CH_4	29.9 500	2011[181]

[a] Abbreviations used are NP (nanoparticles) and NT (nanotubes) [b] Units are: ppm cm^{-2} h^{-1}

2.3.1.4. Doped TiO_2

Doping of TiO_2 with other elements has been employed to alter the band gap and increase catalytic activity for CO_2 reduction. These dopants, which include nitrogen,[140,143,144] fluorine,[145] iodine,[141] cerium,[142] and rhodium,[146] were incorporated into the structure of TiO_2. Nitrogen and fluorine typically substitute onto the anionic oxygen sites,[139] whereas cerium, rhodium, and even iodine are thought to replace some of the Ti^{4+} species in the titania lattice.[141]

Nitrogen-doping mixes the N 2*p* orbitals with the O 2*p* orbitals, raising the level of the valence band and decreasing the band gap from 3.2 eV, which allows for the increased absorption of visible light.[182] Varghese and coworkers synthesized 0.4 atom% N-doped titania nanotubes, which had a band gap of only 2.3 eV.[140] They subsequently decorated them with Pt or Cu nanoparticles and exposed them to natural sunlight under humidified *CO_2* . The Pt-N-TiO_2 yielded predominantly H_2 (190 ppm cm^{-2} h^{-1}), while the Cu-N-TiO_2 produced mostly CH_4 (75 ppm cm^{-2} h^{-1}) as well as H_2 and CO. Though the authors claimed to obtain extended hydrocarbons, they may be derived from an adhesive in the cell instead of from the photocatalytic reaction, especially since comparable systems yield no such products.[121] Li *et al.* prepared 0.84 atom% N-doped mesoporous structures, which had a band gap of 2.72 eV, and photodeposited them with 0.2 wt% Pt to serve as co-catalyst. These authors detected no H_2 or CO; instead only CH_4 was formed at a rate of 0.52 μmol g^{-1} h^{-1}. Michalkiewicz and coworkers synthesized a N-doped TiO_2 nanopowder, without any metal co-catalyst, with an overall nitrogen content of 0.45 atom% but a surface concentration of 0.85 atom%.[144] This material exhibited no change in the band gap, unlike the other two N-doped TiO_2 systems, indicating a different mode of incorporation into the TiO_2 lattice. The discrepancy may be due to the high content of amorphous TiO_2, almost 70%, due to the low calcination temperature of 100 °C.[183] The N-TiO_2

photocatalyst produced only methanol, at an overall rate of 10 μmol g^{-1} h^{-1}, when exposed to UV-vis light in an aqueous solution of *CO_2* . Nitrogen and vanadium co-doped nanotube arrays, in which vanadium replaced titanium atoms, were also prepared for CO_2 reduction.[184] These catalysts generated methane at rates of 64.5 ppm h^{-1} cm^{-2}, even in aqueous media, and were stable over multiple experiments.

The synthesis of surface fluorinated TiO_2 nanosheets was recently reported by He *et al*., with fluorine replacing surface hydroxyl groups and forming Ti-F bonds.[145] The fluorine increased the number of Ti^{3+} defects present at the surface by adding electrons into the 3*d* orbitals of Ti^{4+}. These Ti^{3+} species, bonded to highly electronegative fluorine, served as electron trap states and promote the photoreduction of CO_2 more readily than their hydroxylated counterparts. When conducting the photoreaction in aqueous solution, He and coworkers detected primarily methane and methanol, as well as some formaldehyde, CO, and H_2.

Zhang *et al*. prepared iodine-doped TiO_2, using HIO_3, for visible light CO_2 reduction.[141] Even though it is a nonmetal, the iodine was found to replace titanium as I^{5+}, which also caused some Ti^{4+} to be reduced to Ti^{3+} to maintain neutrality. The band gap decreased slightly to 3.0 eV, though there was significant absorption of visibly light beyond 500 nm. CO was the only reduction product from visible light photolysis of humidified CO_2 on a nominally 10% I-doped catalyst, at a yield of 2.4 μmol g^{-1} h^{-1}.

Zhao and coworkers synthesized cerium-doped titania, both unsupported and on mesoporous silica.[142] The cerium promoted the formation of the anatase phase and shifted the absorption edge from 400 nm to 500 nm; however, when supported on SBA-15, a silica with one-dimensional pores, the absorption edge was shifted to shorter wavelengths due to the formation of smaller Ce-TiO_2 nanoparticles in the size-constraining pores. Under UV-vis irradiation in the presence of

humidified CO_2 , 3 atom% Ce-TiO_2 generated CO and CH_4 at rates of 0.25 and 0.02 μmol g^{-1} h^{-1}, but the supported photocatalysts were substantially better, with rates of 1.88 and 1.98 μmol g^{-1} h^{-1}, possibly due to both the confinement in the 1D pores and the abundance of proximal silicon hydroxide groups for proton donation. Xiong *et al*. also prepared Ce-TiO_2 nanoparticles, finding optimal yields of CO_2 reduction products at 1% doping.[185] From aqueous CO_2 , predominantly methanol was produced, at a rate of 23.5 μmol g^{-1} h^{-1}. In both cases, the Ce atoms were found to be partly in the +4 oxidation state and partly in the +3 oxidation state, the latter of which, like Ti^{3+}, was implicated in aiding the reduction of CO_2 .[142,185]

Recently, Lee *et al.* made 0.02 wt% Rh-doped TiO_2 for CO_2 photoreduction.[146] The band gap of this material was 2.95 eV, but the authors sought to increase the visible light photoresponse and so adsorbed the light-harvesting complex II (LHCII) from the photosynthetic pathway onto some of the Rh-TiO_2 particles. As with many of the other doped catalysts, the addition of the dopant reduced some of the Ti^{4+} to Ti^{3+}, which improved electron trapping and CO_2 reduction. Photocatalysis of CO_2 in an aqueous suspension of Rh-TiO_2 produced CO, acetaldehyde, and methyl formate with moderate yields, though the LHCII-modified catalyst was considerably better at forming acetaldehyde and methyl formate. However, the LHCII either degraded or desorbed during the photoreaction, leading to a lack of stability, though controls without CO_2 showed that the products were primarily from CO_2 reduction with minimal contributions from decomposition of the protein complex.

2.3.1.5. Organic and Organometallic Modifications to TiO_2 Surfaces

The organic and organometallic species adsorbed to TiO_2 surfaces can be classified as either CO_2 reduction catalysts or as visible light-absorbing moieties that extend the operational spectral range of the photocatalyst. Interestingly, though the use of dyes has been well-established in the

solar cell literature by Grätzel,[3,81,186] it has not seen as much application in the field of carbon dioxide photoreduction.[123] Molecular surface modifications have also been with known homogeneous CO_2 reduction electrocatalysts that have been altered for heterogeneous binding. Localization of these homogeneous species on the electrocatalytic surface greatly increases their effective concentration and reduces the absolute quantity used when compared to solution-phase reactions, which is a significant boon especially when rare and expensive transition metals such as Ru and Re are required. Due to the directionality of electron flow for these types of modifications, a single molecule cannot serve as both photosensitizer and CO_2 reduction catalyst, since the former transfers an electron to the conduction band of the semiconductor and the latter receives an electron and transfers it to carbon dioxide (Figure 9).

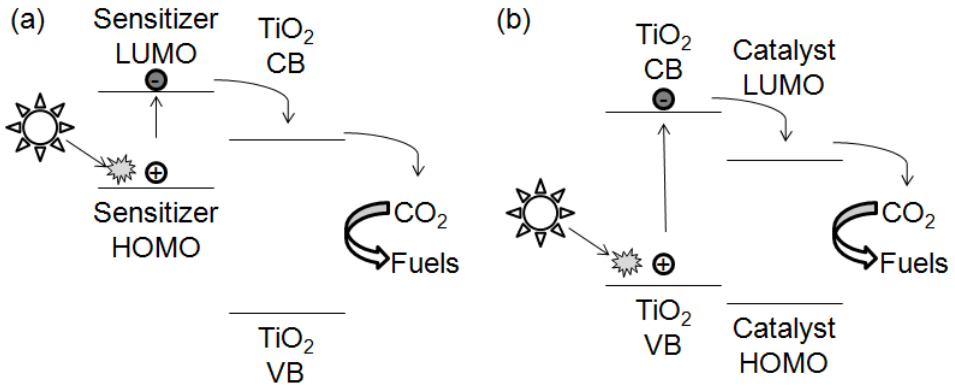

Figure 9. Schematic showing the electron flow in the use of (a) a sensitizer and (b) a CO_2 reduction catalyst on TiO_2.

Very few purely organic dyes have been used, with most researchers relying on more common transition metal complexes. However, Finkelstein-Shapiro *et al.* recently studied the influence of aminosalicylic acid on CO_2 photoreduction.[187] The carboxylic acid bound strongly to the TiO_2 surface, increasing the visible light photoresponse. When the catalyst was exposed to aqueous

CO_2 , the absorption edge was further red-shifted due to formation of a hydrogen-bound species that is also coordinated to the nanoparticle surface, leading to an electron trapping defect site.

$Ru(bpy)_3^{2+}$-based photosensitizers have been employed in both homogeneous and heterogeneous photoreactions. Nguyen *et al*. and Ozcan *et al.* have studied their use with TiO_2 in the context of CO_2 reduction.[188–190] The first group used the Ru^{2+}-containing N3 dye (Figure 10a), which has carboxylate groups to allow attachment to oxide surfaces. This dye was chemisorbed onto P25 TiO_2 that had been modified by 0.5 wt% each of Cu and Fe oxides and coated onto optical fibers.[188] This catalyst had strong absorbance in the visible region of the spectrum, and under concentrated sunlight produced methane at a rate of 0.62 μmol g^{-1} h^{-1}, though under intense artificial light, ethylene was also generated. Ozcan and coworkers incorporated $Ru(bpy)_3^{2+}$, as well as two dibromo-perylene diimides (called BrAsp and BrGly), into TiO_2 films by wet impregnation, though the BrAsp and BrGly dyes contained carboxylate moieties to aid in binding.[189,190] All three dyes improved visible light absorption, and led to the formation of methane from CO_2 and water vapor at rates of 0.16, 0.10, and 0.20 μmol g^{-1} h^{-1} for $Ru(bpy)_3^{2+}$, BrGly, and BrAsp, respectively. The presence of Pt as a co-catalyst on the TiO_2 improved yields for all of the photosensitizers, and, while thick films performed better than thin films based on the amount of CH_4, the latter had the advantage on a catalyst mass basis.

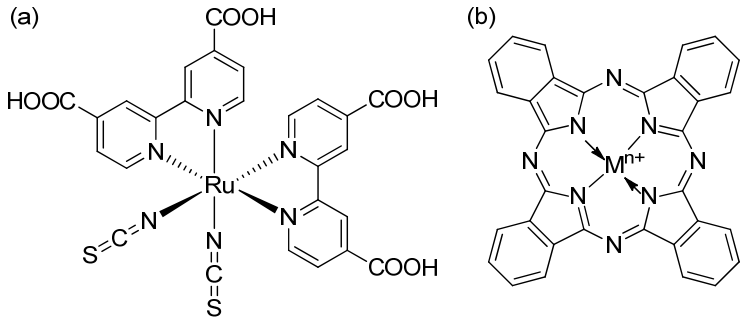

Figure 10. Organometallic TiO_2 photosensitizers (a) N3, employed by Nguyen *et al.*[188] and (b) metallophthalocyanine, used by Zhao *et al*.[191–193]

Zhao and coworkers utilized metal phthalocyanine complexes (MPc), as depicted in Figure 10b, to photosensitize TiO_2 as well.[191–193] Cobalt and zinc phthalocyanines led to strong light absorption in the visible region, accompanied by electron transfer from the MPc to the conduction band of the semiconductor particle. In *CO_2* -saturated aqueous NaOH, 0.5 wt% CoPc-TiO_2 produced incredibly large amounts of formate, at a rate of 28.99 μmol g^{-1} h^{-1}, as well as formaldehyde (2.63 μmol g^{-1} h^{-1}) and small amounts of methanol and methane (0.21 and 0.63 μmol g^{-1} h^{-1}, respectively).[191] The quantity of methane did not change substantially when CH_3OH or HCHO were added to the initial suspension, indicating a different route than the two- or four-electron reductions from those species. Synthesizing the CoPc in the TiO_2 sol from dicyanobenzene and $CoCl_2$ greatly enhanced the yields of the first three products substantially, possibly due to localization in TiO_2 pores, keeping CoPc molecules from aggregating.[193] Similar behavior was observed with the zinc phthalocyanine, with the *in situ* synthesized Pc performing better, but methane yields were over an order of magnitude greater than with either CoPc.[192]

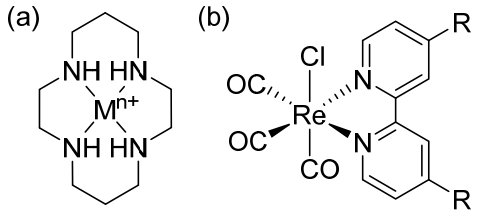

Figure 11. Carbon dioxide reduction catalysts (a) metal cyclam[194,195] and (b) rhenium bipyridine tricarbonyl,[196–200] which have both been adapted for covalent binding to TiO_2.

Metal cyclam catalysts (Figure 11a) have been studied for homogeneous CO_2 reduction for over thirty years.[201–203] However, only in the past few years have these complexes been attached to semiconductor particles for heterogeneous CO_2 photocatalysis. Neri *et al*. chemisorbed a [Ni(cyclam-*CO_2* H)]$^{2+}$ to TiO_2 nanoparticles and, though the organometallic catalyst was selective for CO formation in aqueous solution, it was not stably bound to the TiO_2 under

electrochemical conditions. Transfer of photoelectrons from the semiconductor particle to the Ni(cyclam) was improved by covalent adhesion, but effective CO_2 reduction was not achieved.[195] Cobalt cyclam was also chemisorbed to TiO_2 by Jin *et al.*, with a surface hydroxyl group binding the Co^{III} center, and was found to have decent CO production capabilities under UV light on P25 and anatase nanoparticles.[194]

Similarly, $Re(bpy)(CO)_3Cl$ and its substituted bipyridine analogues (Figure 11b), which can electrochemically generate CO with high selectivity, have seen a great deal of interest lately.[204–209] Cecchet *et al.* electropolymerized a vinyl derivative of the $Re(bpy)(CO)_3Cl$ complex onto a TiO_2 thin film to produce a polymeric layer of catalyst centers.[196] The rhenium polymer showed increased current under CO_2 in an electrochemical setup, but no bulk electro- or photocatalytic reactions were performed. Batista, Lian, and coworkers have determined the vibrational spectra of carboxylate-bound rhenium bipyridine catalysts on (001) TiO_2 single crystal surfaces using calculations to study their conformations, but did no CO_2 reduction studies.[197,198]

2.3.2. Other Binary Metal Oxides

Both electrochemical and photoelectrochemical studies have been conducting using Cu_2O. Handoko and Tang showed that Cu_2O powders can reduce CO_2 to CO under illumination from visible light ($\lambda > 420$ nm).[210] Yields as high as 400 ppm CO g^{-1} h^{-1} were achieved in the first 30 minutes of the reaction using small amounts of RuO_x as a cocatalyst and Na_2SO_3 as a sacrificial hole scavenger. However, the yields quickly decayed within the first hour. An earlier study by Tennakone and coworkers found that methanol is produced from Cu_2O powders and CO_2 if a full-spectrum mercury lamp is used as a light source.[211] An optimum yield of 24.0 μmol MeOH L^{-1} was measured. However, the reaction is believed to proceed via the oxidation of Cu_2O to CuO, and thus, is not catalytic in the classical sense. Additionally, thin films of electrodeposited

Cu_2O were used as CO_2 reduction catalysts under illumination from a blue LED (435-450 nm).[212] Methane and ethane were found to be the major products, with the current efficiency of ethane approaching 33% for a p-type sample of Cu_2O. Nonetheless, an extremely negative potential had to be applied (-2.0 V vs. Ag/AgCl) to obtain such yields.

WO_3 was reported to reduce CO_2 to methanol and formaldehyde, with 5.04 and 0.21 μmol h^{-1} as typical yields for the two products, respectively, in the presence of a 70 W high-pressure Hg lamp.[111] Recently, WO_3 was used as a photocatalyst in the presence of visible light ($\lambda > 420$ nm).[213] Methane yields around 1.0 μmol g^{-1} h^{-1} were observed for thin WO_3 nanosheets. Bulk WO_3 was found to be significantly less reactive, as reported previously.[111] Recently, composites made from graphene oxide and 10% wt Cu nanoparticles were reported to produce 2.94 μmol g^{-1} h^{-1} methanol and 3.88 μmol g^{-1} h^{-1} acetaldehyde under illumination from a halogen lamp.[214]

Yahaya *et al*. have shown that NiO and ZnO produce methanol in high yields (388 and 325 μmol g^{-1} h^{-1} over 1.5 hours, respectively) using a 355 nm UV-laser.[215] Another interesting NiO system was recently reported by Kou *et al.* and utilized a covalently linked zinc porphyrin light-harvesting sensitizer and rhenium bipyridine CO_2 reduction catalyst on a p-NiO semiconductor, though with low Faradaic yields of only ~6.2%.[52] Another interesting system utilized a p-NiO electrode modified with the visible-light-responsive organic dye P1 (4-[bis(4-{5-[2,2-dicyanovinyl]-thiophene-2-yl}phenyl)amino]benzoic acid) and the carbon monoxide dehydrogenase enzyme.[216] Interestingly, using this system, it was possible to reduce CO_2 or oxidize CO efficiently simply by switching from an n-type to a p-type NiO semiconductor. The catalytic behavior of ZnO to yield methanol and formaldehyde have been reported.[149,215] A separate publication reports yields of 764 ppm g^{-1} h^{-1} of CO and 205 ppm g^{-1} h^{-1} of CH_4 upon illumination of porous ZnO with a xenon arc lamp.[217]

Sato *et al.* demonstrated hotochemical CO_2 reduction to formic acid at a rate of up to 70 μmol g^{-1} h^{-1} on p-Ta_2O_5 modified with a series of adsorbed ruthenium bipyridine catalysts ($[Ru(bpy)_2(CO)_2]^{2+}(PF_6^-)_2$, $[Ru(dcbpy)(bpy)(CO)_2]^{2+}(Cl^-)_2$, and $[Ru(dcbpy)_2(CO)_2]^{2+}(Cl^-)_2$) in an acetonitrile/triethanolamine mixture with high quantum yields.[218,219] Akimov *et al*. performed a computational comparative study of the anchors for Ru catalysts on Ta_2O_5.[220] The phosphonate (PO_3H_2) anchor was found to possess greater electron transfer rates than both COOH and OH in terms of more favorable electron transfer energetics and tilting angles as well as localization of acceptor states on the catalytic Ru center.

Liu *et al.* have recently reported attaching a rhenium bipyridyl compound to silica nanoparticles through an amide linker (Figure 12a), studying the system using *in situ* Fourier transform infrared spectroscopy (FTIR) and electron paramagnetic resonance (EPR) spectroscopy to show that the rhenium center behaved as it did in homogenous solution.[221] The group also reported that when the amide linker was modified so as to withdraw electron density from the rhenium by changing which atom of the amide is attached to the bipyridine ligand (Figure 12b), the catalytic activity was significantly lower, and anchoring the complex onto silica nanoparticles showed little effect on the catalytic activity.[221]

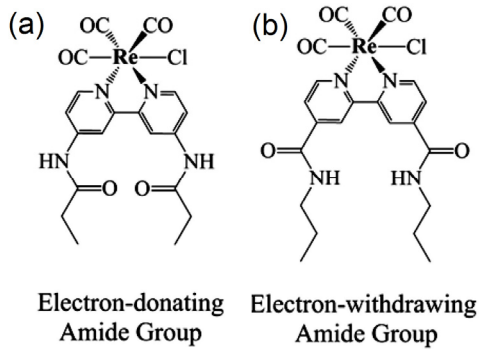

Figure 12. Rhenium bipyridyl CO_2 reduction catalysts with amide linkers attached so to be (a) electron-donating and (b) electron-withdrawing. Adapted with permission from ref. [221]. Copyright 2013 American Chemical Society.

Other binary oxides have been used to reduce CO_2 . For instance, MgO was shown to form CO with a yield of approximately 1.6 μmol g^{-1} h^{-1} over the course of 6 hours in the presence of H_2 as a reductant.[222] However, only UV light with $\lambda < 290$ nm could drive the reaction. Ag-loaded Ga_2O_3 produced 10.5 μmol CO g^{-1} h^{-1} in the presence of CO_2 and UV-light.[223] Mesoporous Ga_2O_3 yielded 1.46 μmol CO g^{-1} h^{-1} and 0.21 μmol CH_4 g^{-1} h^{-1} under visible light.[224] Indium oxyhydroxide nanoparticles ($In_2O_{3-x}(OH)_y$), with a band gap of 2.9 eV, yielded 15 μmol CO g^{-1} h^{-1} from CO_2 and H_2 at 150 °C in a pressurized flow cell under illumination from a xenon lamp.[225] This fairly high reactivity was ascribed to the reaction of hydrogen with lattice oxygen to form plentiful surface oxide vacancies, which subsequently reduced CO_2 to CO.

ZrO_2 is also catalytically active, and produces CO from CO_2 and H_2. [226–229] In one publication by Lo *et al.*, a CO production rate of 0.51 μmol g^{-1} h^{-1} was measured upon illumination from a mercury lamp ($\lambda = 254$ nm).[226]

2.3.3. Ternary Metal Oxides

Liu *et al*. reported the photocatalytic reduction of CO_2 to ethanol in the presence of bismuth vanadate.[230] Two crystal structures were obtained: monoclinic and tetragonal zircon-type, with the former having higher visible light photoactivity for the production of ethanol. Further work by Mao[231] and coworkers produced a lamellar monoclinic $BiVO_4$ catalyst capable of CO_2 reduction under irradiation by a Xe lamp. Methanol was detected as the major product, with trace amounts of ethanol that could not be quantified. The lack of quantifiable ethanol is ascribed to the gas-tight nature of their setup, as it limits the carbon source. Methanol production plateaus after six hours of irradiation, due to methanol oxidation by the $BiVO_4$.

In recent years, various delafossite compounds having the general formula ABO_2 have been studied as CO_2 reduction catalysts. Lekse and coworkers used broadband illuminated $CuGaO_2$ to

reduce CO_2 to CO and trace CH_4.[232] In the course of a 24 hour experiment, a maximum yield of 9 ppm CO g^{-1} h^{-1} was observed. Iron was substituted into the structure in the form of $CuGa_{1-x}Fe_xO_2$ in amounts up to x = 0.20, but the yields did not change appreciably with these substitutions. Gu *et al.* reported that the Mg-doped delafossite $CuFeO_2$ can act as a photoelectrocatalyst under illumination of < 800 nm light.[233] Although this system can be used to reduce CO_2 to formate at an underpotential of approximately 400 mV, the Faradaic efficiencies are generally poor, with a maximum efficiency of 10% at -0.9 V vs. SCE.

Matsumoto *et al*. demonstrated the use of p-$CaFe_2O_4$ powder as a photocatalyst for CO_2 reduction.[234] Irradiation by a mercury lamp with Fe^{2+} and $Na_2H_2PO_2$ as reducing agents led to the production of methanol and formaldehyde, with trace CO and formic acid. Increasing the concentration of the reducing agents increased the yield of methanol. The addition of $BaCO_3$ was also found to increase methanol yield.

Liu and coworkers used Zn_2GeO_4 nanoribbons illuminated with a 300 W Xe lamp to reduce humidified CO_2 to methane at a rate of 1.5 μmol g^{-1} h^{-1}.[235] It was noted that bulk Zn_2GeO_4 does not reduce *CO_2* , and this was explained in terms of the increased surface area and crystal quality of the nanobelts. In a follow-up study, Zn_2GeO_4 nanorods were used to reduce aqueous CO_2 to methanol with yields of approximately 0.143 μmol g^{-1} h^{-1}.[236] The methanol yield approximately doubled upon the addition of the metal-organic framework ZIF-8 to Zn_2GeO_4, and is likely due to the increased adsorptive properties associated with ZIF-8. In contrast to the previous study, no methane was formed with either the Zn_2GeO_4 nanorods or the Zn_2GeO_4/ZIF hybrid, though this difference was likely due to the different phases of CO_2 employed.

Shi and coworkers used $NaNbO_3$ to reduce CO_2 to methane upon irradiation from a Xe arc lamp.[237] It was discovered that platinum loaded $NaNbO_3$ nanowires are significantly more active

for CO_2 reduction than bulk $NaNbO_3$, and this was explained in terms of the superior crystallinity and the large surface-to-volume ratio of the nanowires in comparison to the bulk $NaNbO_3$ ($E_g \approx 3.4$ eV). Methane yields approaching 653 ppm g^{-1} h^{-1} were reported for the Pt-$NaNbO_3$ nanowires. HNb_3O_8 nanobelts ($E_g \approx 3.7$ eV) were shown to reduce CO_2 to methane with illumination from a Xe lamp.[238,239] The yield changed when SiO_2 was intercalated into the structure, reaching about 2.90 μmol g^{-1} h^{-1} when Pt is used as a co-catalyst. Another niobium oxide-based material, $InNbO_4$, photocatalytically reduced CO_2 to methanol using light whose wavelength ranges from 500 to 900 nm.[240] Yields averaging 1.5 μmol g^{-1} h^{-1} were achieved, and it was shown that the addition of either NiO or Co_3O_4 as co-catalysts marginally increased these yields.

Other In-containing ternary oxides have also been used for CO_2 reduction, with much of the effort focusing on $InTaO_4$, often with a NiO co-catalyst. The first study, by Pan and Chen, found that doing a reduction-oxidation pretreatment led to marginally increased methanol production, to about 1.4 μmol g^{-1} h^{-1}.[241] $InTaO_4$ samples of varying particle sizes and degrees of crystallinity, with bandgaps ranging from 2.60 eV to 3.01 eV, were also used to reduce CO_2 to methanol.[242] It was shown that the addition of 1 wt% NiO as a catalyst significantly increased the yields, with a maximum of around 2.7 μmol g^{-1} h^{-1}. The production of methanol was later enhanced by Tsai and coworkers, who used a reduction-oxidation process to produce Ni@NiO core-shell nanoparticles on nitrogen-doped $InTaO_4$ powder to achieve significantly higher yields of methanol.[243] Yields as high as 160 μmol g^{-1} h^{-1} were achieved using light with wavelengths ranging from 390-770 nm.

Li *et al.* used $KTaO_3$ (irradiated with a 300 W Xe lamp) to reduce CO_2 to CO in the absence of an applied potential.[244] The bandgaps of three samples synthesized via different routes varied

between 3.5 and 3.7 eV. CO yields of approximately 62 ppm g^{-1} h^{-1} were reported, although, admittedly, the H_2 yields were approximately 21 times larger. An experiment in which Pt was used as a co-catalyst produced H_2 exclusively, while the use of Ag as a co-catalyst increased the CO yields to approximately 153 ppm g^{-1} h^{-1}. In the latter case, the H_2 yields were still approximately 7.5 times larger than the CO yields. Notably, the validity of these results was confirmed by reducing $^{13}CO_2$ to labeled CO.

Barium zirconate, which has a perovskite structure, was prepared with various noble metal co-catalysts.[245] $BaZrO_3$ has a band gap of 4.8 eV, which only allowed for the absorbance of UV light. However, with a silver co-catalyst at 0.3 wt% loading, yields of methane up to 0.52 μmol g^{-1} h^{-1} were obtained. Lower amounts of Ag had fewer active sites for reduction, whereas high loading levels hindered light absorption.

Several pervoskite titanates have been explored for their ability to reduce CO_2 to formic acid, formaldehyde, methanol, and other C-C coupled products, initially by Halmann and coworkers.[111,150,246] Among the semiconductor materials used were TiO_2 as a control, $SrTiO_3$, $BaTiO_3$, and $CaTiO_3$. The latter two semiconductors performed poorly in comparison to $SrTiO_3$, and will not be discussed further. However, in this system, the overall energy efficiencies, calculated as the ratio of the heat of combustion of the products to the incident light energy, were poor (<0.011% for $SrTiO_3$), and the system was only stable for a few days before generation of reduction products ceased. Other attempts at using $SrTiO_3$ as a CO_2 reduction catalyst have been made more recently. In one particular study, Xie *et al.* used oxygen-deficient $SrTiO_{3-x}$ as a means of making the material more responsive to visible light irradiation.[247] It was shown that 600 nm light was sufficient to photochemically reduce CO_2 to methane, with maximum yields of approximately 0.30 μmol g^{-1} h^{-1}.

Other examples of ternary titanium oxides include $K_2Ti_6O_{13}$, which formed methane, formaldehyde, and formic acid from reduced CO_2 under light from either a Xe or Hg lamp.[248] Various additives were examined, and maximum yields of 0.27, 0.57, and 3.04 μmol g^{-1} h^{-1} for methane, formaldehyde, and formic acid, respectively, were obtained with a composite Pt/Cu/ZnO-$K_2Ti_6O_{13}$ catalyst. Interestingly, although methanol was not detected when Xe or Hg lamps were used for illumination, yields ranging from 13.60 to 32.03 μmol g^{-1} were obtained upon illumination from concentrated sunlight, and this phenomenon was explained by the change in the system's temperature (to 583 K). In another study, Pt-loaded $K_2Ti_6O_{13}$was used to reduce water to H_2, which then combined with CO_2 to form reduced products on a Fe-Cu-K/DAY zeolite.[249] In the absence of the zeolite, methane, formic acid, and formaldehyde were formed, in agreement with the photolysis results discussed above for $K_2Ti_6O_{13}$.[248] Likewise, methanol was detected when the reaction temperature was increased to 562 K or above. Finally, small amounts of ethanol were also detected at elevated temperatures, with a maximum yield of approximately 1.2 μmol g^{-1} h^{-1}. In the present study, however, the yields were quite small unless concentrated sunlight was used for illumination, and the bandgap of the catalysts are such that only wavelengths < 420 nm are utilized.

More complex titanium oxides have also been reported to be catalytically active, with $ALa_4Ti_4O_{15}$(A = Ca, Sr, or Ba) being a prime example.[250] $BaLa_4Ti_4O_{15}$, $SrLa_4Ti_4O_{15}$, and $CaLa_4Ti_4O_{15}$, all loaded with 1 wt% Ag catalyst, produced CO with typical yields of 63, 23.7, and 31 μmol g^{-1} h^{-1} upon irradiation from a 400 W Hg lamp. Out of all co-catalysts tested (NiO_x, Cu, Ru, Au, and Ag), Ag had the highest catalytic behavior for increased CO yields. Formic acid was detected in small amounts throughout, and in general, the competing HER was largely suppressed. Additionally, $KCaSrTa_5O_{15}$ has been used as both a water splitting and CO_2

reduction photocatalyst.[251] Optimized yields of 16.2 μmol g^{-1} h^{-1} were achieved upon the addition of Ag as a co-catalyst. However, the bandgap of the material, 4.1 eV, is too large to utilize visible light effectively, and the catalyst was nonetheless more active for water splitting than CO_2 reduction.

Another ternary oxide-containing system is a $ZrOCo^{II}/IrO_x$ couple assembled onto a mesoporous SBA-15 surface.[252] Labeled studies show that, upon irradiation from 355 nm light, CO_2 and water are converted to ^{13}CO and $^{18}O_2$, respectively. Moderate yields of CO, approximately 1.75 μmol g^{-1} h^{-1}, were obtained.

Recently, layered double hydroxides (LDHs) Zn-Al LDH, Mg-In LDH and Zn-Cu-Ga LDH have been prepared as CO_2 photocatalysts for the purpose of utilizing their anisotropic properties caused by a 2-dimensional structure.[253–255] The main products from the first two systems are CO, while the last LDH produced CH_3OH primarily. CO_2 is suggested to bond to the surface hydroxyl in the form of CO_3^{2-}, and then being converted to CO. the layered structure create an ideal architecture to trap CO_2 molecules, and the 2-dimensionality allows engineer surface with active sites ratio approaching 100%.

2.4. Chalcogenide Semiconductors

CdTe, with a band gap of 1.5 eV, has been the most extensively studied II-VI semiconductor for photo-assisted CO_2 reduction due to the availability of its p-type form. Bockris *et al.* demonstrated that CO_2 can be reduced to CO on a p-CdTe photocathode in a 0.1 M tetrabutylammonium tetrafluoroborate (TBAF)/MeCN solution.[256] A Faradaic efficiency of 60% in the potential range of -0.9 to -2.4 V vs. Ag/AgCl was determined. When the photo-assisted reduction of CO_2 was performed on a p-CdTe surface in a 0.1 M TBAP/DMF solution containing 5% water, CO production reached 70% at a controlled potential of -1.6 V vs. SCE.[257] A further

study of the *i-V* relation on p-CdTe showed that introducing CO_2 into the same DMF solution with 5% H_2O shifts the photocurrent onset by nearly 700 mV more positive, which was indicative of an CO_2 reduction taking place at less negative potential on p-CdTe. All tetraalkylammonium supporting electrolytes stabilized the photocurrent in the course of a 24-hour photoelectrolysis. However, when the electrolyte was replaced by either $LiClO_4$ or $NaClO_4$, the photocurrent dropped by 90% under the same experimental conditions. Taniguchi *et al.* suggested that tetraalkylammonium ions play an important role in providing a suitable environment for CO_2 reduction at the electrode surface due to their hydrophobic nature.[83] Using NH_4ClO_4 instead of TBAP as the supporting electrolyte led to a further anodic shift of the photocurrent onset by approximately 500 mV, which suggests a different CO_2 reduction pathway was established in the presence of NH_4^+.[258] Taniguchi et al. suggested the NH_4^+ cation acted as a mediator and receives an electron to form a $NH_4^{\bullet}$ radical, and that the radical then transferred an electron to a nearby CO_2 molecule to form the $CO_2^{\bullet-}$ radical. Yet, this mechanism sounds problematic due to the energetically unfavorable formation of $NH_4^{\bullet}$. The addition of a catalytic crown ether to an electrochemical cell utilizing p-CdTe as the working electrode increased the current efficiency and shifted the onset potential anodically.[259] The proposed mechanism suggested that the crown ether formed an adsorbed layer on the electrode surface, which eliminated adsorbed solvent molecules and coordinated with tetraalkylammonium cations to increase the production of $CO_2^{\bullet-}$. Crown ethers also affected the product distribution, as CH_3OH was observed as another reduced product in addition to CO.

In aqueous solutions, the choice of electrolyte is significantly more important on p-CdTe surfaces in comparison to p-InP.[105] Carbonate-containing electrolytes favor the formation of formic acid, while other salts such as sulfates and perchlorates favor the production of CO. The

highest reported current efficiency was nearly 80% for CO production, and was achieved in 0.1 M TEAP aqueous solution at -1.2 V vs. SCE.

Photoreduction of CO_2 by a CdS suspension in water was studied by Eggins *et al*., employing tetramethylammonium chloride (TMACl) as an electron donor.[260] This work was extended to study the effect of pH on the photoreduction of CO_2 by quantum crystallite ZnS suspensions in the presence of TMACl.[261] With the TMACl significant amounts of oxalate (≥400 μM) were produced across a broad range of pH from 2 to 14, for irradiation times spanning 1-2 days. Other products observed during these reactions include formate, formaldehyde, methanol, glyoxylate, glycolate, and tartrate in lower amounts. Exceptions include pH=6, where the major product was formate, and pH=10, where the catalyst was relatively inactive, producing less than 10 μM products in 60 hours. In the absence of the TMACl, the yield of oxalate from ZnS catalysis was very close to the detection limit of 10^{-7} μM. Using CdS, it was found that the addition of TMACl led to greatly increased production of glyoxylate at pH 4 and 6, in addition to acetate, formate, formaldehyde, and methanol. The authors offer three possible explanations for this drastic enhancement by TMACl addition, focusing on the TMA^+, were proposed: (a) the TMA^+ ions adsorb to the surface of the semiconductor, forming a nearly aprotic layer; (b) low charge density on the TMA^+ give it a negligible Lewis acid effect; and (c) CO_2 molecules and radical anions adsorb at the surface, where a large concentration of both species can lead to dimerization. The presence of water then allows for further reduction of the dimerized product (oxalate), leading to the multicarbon products observed. A screen of several other hole scavengers (iodide, ferricyanide, hydroquinone, sulfite, and ruthenium(IV) oxide) in the CdS catalytic system showed that the quantum yield for formaldehyde and formate increases with an increase in redox potential of the scavenger. Considering this trend, it seems likely that the Cl^- from TMACl plays

a significant role as an electron donor. However, this study did not test other chloride salts nor other TMA^+ salts, providing no conclusive evidence of the significance of one ionic species over the other. Recent studies by Berto *et al.* have found that the anion in tetraalkylammonium salts do not alter the electrochemistry of CO_2 reduction at platinum, boron-doped conductive diamond, thin-layer diamond on molybdenum, and glassy carbon electrodes.[262] This study also concluded that tetraalkylammonium ions are not catalytic for CO_2 reduction.

Kisch and Twardzik investigated the difference in CO_2 reduction by ZnS powder and previously reported ZnS colloids.[263] It was found that if 2-propanol was added as a reducing agent in water, no product was formed using the ZnS powder. However, replacing the 2-propanol with 2,5-dihydrofuran yielded formate for a quantum yield of 0.001 at λ=300 nm. A mechanism is proposed, whereby photogenerated electrons are trapped at Zn^{2+} surface sites. These surface electrons are then able to reduce adsorbed HCO_3^- to formate, while the holes oxidize 2,5-dihydrofuran to a dimer. The failure of 2-propanol to act as a hole acceptor in the presence of a ZnS powder suggests that the valence band of ZnS is shifted cathodically compared to the colloid.

Combining computational and experimental methods, Kanemoto and coworkers investigated the surface chemistry of CO_2 reduction at ZnS nanocrystals.[264] Synthesis of the nanocrystals in different organic solvents yielded different crystal structures. Photoreduction of CO_2 by the the ZnS nanocrystals synthesized in methanol and DMF produced formate, CO, and H_2, while acetonitrile-synthesized ZnS yielded only small quantities of CO and H_2. Photoreduction by bulk ZnS powders yielded only CO and H_2. Addition of excess Zn^{2+} was found to enhance conversion to formate at low levels, but above 1.25 mM decreased formate yields. Addition of Zn^{2+} in excess of 5 mM led to the competitive formation of CO, with increased H_2 production as well. It

was also found that changing the Zn precursor altered the activity of the catalyst, which is suggested to be due to consumption of photo-generated electrons by anions adsorbed on the ZnS surface. Photoemission studies on the ZnS-DMF system suggested that the catalyst has shallow surface states that act as a reservoir for excited electrons, leading to a relatively long lifetime of the exciton pair. Addition of CO_2 to the system further increased the emission lifetime from 36 ns to 50 ns, due to the reduction of a surface-adsorbed CO_2 to $CO_2^{\bullet-}$. This intermediate can be further reduced via electron-transfer to produce formate and CO. DFT computation methods were used to evaluate CO_2 activation on the ZnS, and the effect of surface sulfur vacancies on this process. A mechanism was proposed whereby CO_2 adsorbs onto the ZnS via a Zn-O interaction and is reduced to $CO_2^{\bullet-}$. If sulfur vacancies are low, then the radical is attacked by adsorbed hydrogen atoms, leading to formate. If sulfur vacancies are high, the $CO_2^{\bullet-}$ must accept additional electrons from the surface or by reaction with another CO_2 molecule to form a Zn^{2+}-$OCOCO_2$ complex. Reduction of this complex leads to CO elimination. Further work by this group employed FTIR, UV-Vis, and EXAFS to explore the surface chemistry of the ZnS particles in the presence of excess Zn^{2+}, confirming the role of surface sulfur vacancies in the product distribution of CO_2 photoreduction.[265]

ZnTe, which was formed directly on a Zn/ZnO nanowire substrate, has demonstrated stable photocatalytic activity toward the reduction of CO_2 to CO.[266] ZnTe possesses a 2.26 eV bandgap and a conduction band position located at -1.63 V vs. RHE at pH=7.5, which is more negative than the standard reduction potentials of the common CO_2 reduction reactions. The as-prepared ZnO/ZnTe core-shell nanowires exhibited p-type conductivity and great photoresponse. At -0.7 V vs. RHE at pH = 7.5 in 0.5 M $KHCO_3$ solution, the system reduced CO_2 to CO with a 22.9% Faradaic efficiency and an 85% incident-photo-to-current-conversion efficiency (IPCE).

Transition metal chalcogenides have also received significant attention in their photoelectrochemical application. Most of the chalcogenides having been investigated with respect to CO_2 reduction were metal sulfides. The earliest study using a chalcogenide was conducted by Cabrera *et al*.[267] They used a polycrystalline thin film of p-WSe_2, possessing a surface modified by electropolymerized films of $[Re(CO)_3$(v-bpy)Cl](v-bpy is 4-vinyl,4'-methyl-2,2'-bipyridine), which was capable of reducing CO_2 to CO at an onset potential of -0.65 V vs. SSCE in an 0.1 M TBAP/MeCN electrolyte. CO was the predominant product, with Faradaic efficiencies approaching unity.

The lamellar chalcogenide MoS_2 possesses highly active sites for electrocatalytic H_2 evolution.[268] Because the redox potential of H^+/H_2 is located close to many of the standard reduction potential of CO_2 , MoS_2 offers special interest in employing its active sites to carry out CO_2 reduction. In addition, this layered semiconductor has a band gap (1.17 eV) matching the solar spectrum, exists in high abundance, and is environmentally friendly, which means that it may be harnessed as a scalable photocatalyst for CO_2 reduction. $MoSe_2$, another 2-D semiconductor strongly resembling the properties of MoS_2, is also a promising candidate. Nørskov *et al.* used DFT calculations to demonstrate how the key reaction intermediates, COOH, CHO and CO, bind to different sites on MoS_2 edges, and predicted improved activity of MoS_2 and $MoSe_2$ over the transition-metal catalysts for CO_2 reduction.[269] To the best of our knowledge, these theoretical findings have not yet been validated experimentally.

Aliwi *et al*. tested the photoreduction of CO_2 in the presence of several different metal sulfide colloids with band gaps ranging from 0.37 to 3.5 eV, finding formaldehyde and formic acid as products.[270] The most efficient metal sulfides for this process were determined to be V_2S_3, SnS_2, and CdS, with a band gap range of 2.07 to 2.40 eV. The other semiconductors tested were PbS,

Ag_2S, MoS_2, Bi_2S_3, and ZnS. Ideal pH conditions were determined for all of the semiconductors in the study, with the highest quantum efficiencies occurring in a range from pH = 3 for CdS to pH=6 for MoS_2 and SnS_2. Time dependence showed that the amount of formaldehyde produced plateaued around 1 hour of irradiation. A temperature dependence study showed that production rates increased with temperature up to 30˚C. A subsequent decrease in production is attributed to lower solubility of CO_2 in water at higher temperatures. It is also shown that increased light intensity led to a proportionally higher production of formate and formaldehyde, but no quantum yield was provided. The lower yields of formic acid than formaldehyde are explained by its reoxidation in the presence of the illuminated metal sulfides. An observed change in pH from 3.3 to 3.9 after irradiation in the absence of a buffer is consistent with this explanation.

2.5. CO_2 Reduction on Multi-Semiconductor Systems

As the research on photo-assisted CO_2 , reduction keeps progressing, new trends and new directions emerge. The most recent studies sharing several common perspectives that can be summarized as designing and fabricating multi-semiconductor composite systems to promote high photo to energy conversion efficiency and high product selectivity.

2.5.1. Heterostructured Semiconductors

The semiconducting heterostructure consisting of two semiconducting materials are designed to broaden the light absorption range, promote spatial separation of electron-hole pairs to prolong the lifetime of photo-carriers in photocatalysts, abate recombination to enhance IPCE and enhance the stability of a narrow band semiconductor against photocorrosion.[32] In order to prevent the corrosion of a p-type GaP photocathode, Zeng *et al.* passivated the GaP surface by depositing a thin film of n-type TiO_2.[271] This chemically robust oxide layer not only prevented the GaP surface from photocorrosion, but also enhanced the photoconversion efficiency through

passivation of surface states. In addition, a p-n junction was formed which created a build-in field to assist the photo-induced charge separation, as well as provided extra driving force for electron transfer to CO_2 . Measured in a 3-elctrode electrochemical setup, under a 532 nm illumination, the Faradaic efficiency of CH_3OH production on this TiO_2-passivated GaP was reported to be 55% at a controlled potential of -0.5 V vs. NHE.

According to Xin Li *et al.*, a Cu_2O/SiC heterostructured photocatalyst can reduce CO_2 to CH_3OH under visible light illumination.[272] Although Cu_2O has been known as being very unstable under illumination, the Cu_2O/SiC particulate photocatalyst was able to undergo at least 5 hours of photo-assisted CO_2 reduction with a nearly constant reactivity. There was no explanation about this improved stability of Cu_2O provided by the authors. The Cu_2O modification enhanced the photocatalytic performance of SiC nanoparticles. The heterostructure consisting of Bi_2S_3/CdS was also reported to reduce CO_2 to CH_3OH, and this provides validation to the idea that the heterojunction can bring about a greater separation of electron-hole pairs.[273]

Using heterostructures to sensitize wide-bandgap semiconductors with narrow-bandgap semiconductors has been mostly applied to TiO_2 systems. With this approach, visible light can induce electron-hole separation while the catalytic activity of TiO_2 remains unchanged. Given a higher conduction band position in the modifying semiconductor than that in TiO_2, photoexcited electrons in the former can transfer to TiO_2 and subsequently to CO_2 (Figure 13). The junction between the two particles aids in preventing charge recombination and helps reduce photodegradation of the typically less stable sensitizer.

Chalcogenides are the most common class of semiconductor photosensitizers used with TiO_2 for CO_2 reduction, due to both their favorable band positions and their ease of synthesis as small nanoparticles.[59] Quantum confinement in the quantum dots (QDs) raises the conduction band

position, promoting transfer of excited electrons to TiO_2 (Figure 13). In 2010, the heterostructure $CdSe/Pt/TiO_2$ was prepared by depositing CdSe quantum dots on to Pt/TiO_2 followed by annealing in an Ar atmosphere..[59] The photocatalyst reduced CO_2 to CH_4, CH_3OH, and CO under illumination of $\lambda > 420$ nm. This light absorbance is a selective absorbance corresponding to the CdSe decoration, since the maximum wavelength can be utilized by TiO_2 is ca. 420 nm. Pt particles were specified as a co-catalyst in the $CdSe/Pt/TiO_2$ system; however, no particular discussion was included to elucidate the role of Pt particles, and there were no control experiments performed by author to verify if the same products would be produced without incorporating Pt. CdS particles in a TiO_2 nanocomposite at a loading of 45 wt% performed better than either semiconductor alone in forming CO (1.95 μmol g^{-1} h^{-1}) and CH_4 (0.38 μmol g^{-1} h^{-1}).[274] CdSeTe nanosheets were loaded onto a titania nanotube electrode by Li *et al.* and used to reduce CO_2 photoelectrochemically to methanol at -0.8 V under visible light, with a Faradaic efficiency of 88%.[275] Li *et al.* deposited CdS onto TiO_2 nanotubes and found that, from an aqueous solution of Na_2SO_3, only methanol was generated, at a rate of 31.9 μmol g^{-1} h^{-1}. However, when Bi_2S_3 was loaded onto the nanotubes, the methanol production increased to 44.9 μmol g^{-1} h^{-1}, which was attributed to greater visible light absorption and CO_2 adsorption than the $CdS\text{-}TiO_2$ nanotube system.[276] PbS QDs were also used, in conjunction with a Cu co-catalyst, to reduce CO_2 to CO, CH_4, and C_2H_6.[277] Park *et al.* prepared sodium trititanate nanotubes with CdS QDs as light absorbers and Cu particles as CO_2 reduction co-catalysts.[278] These composite photocatalysts formed mostly methane as well as C2 and C3 hydrocarbons, which were confirmed with $^{13}CO_2$. The chalcogenide nanoparticles, even when attached to the photostable TiO_2, were subject to photocorrosion due to their inability to oxidize water.[277]

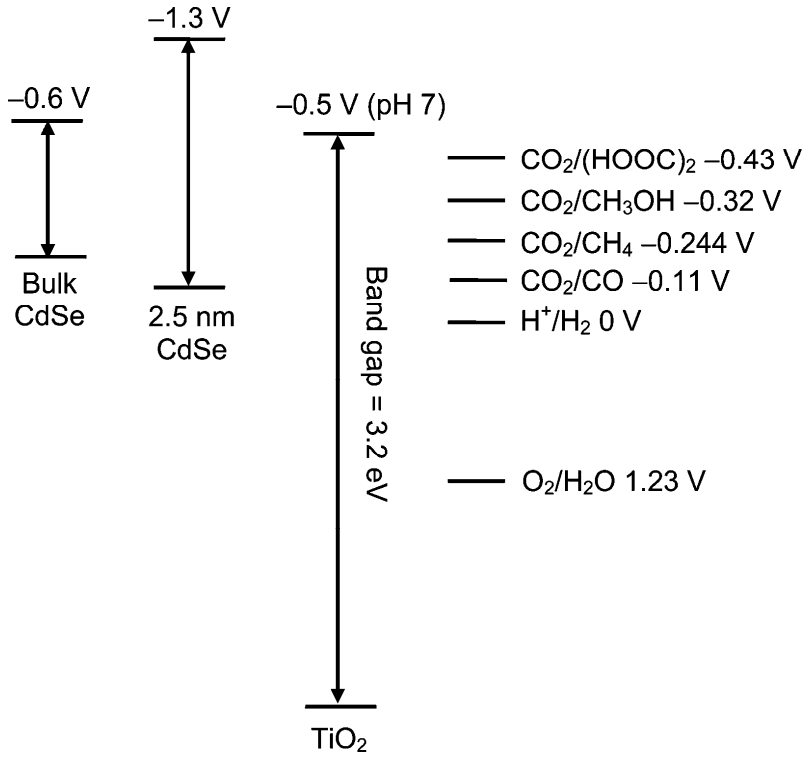

Figure 13. Band positions of both bulk and 2.5 nm QD CdSe relative to those of TiO_2 and redox potentials of H_2O and CO_2 . Reprinted with permission from ref. [59]. Copyright 2010 American Chemical Society.

Other kinds of semiconductors have also been employed for TiO_2 sensitization. Abou Asi *et al.* deposited AgBr particles, which have an indirect band gap of 2.64 eV, to P25 TiO_2, forming a variety of reduced products including CO, methanol, methane, and ethanol in aqueous solution.[279] Various parameters, such as the loading, sintering temperature, and pH, were optimized to maximize the yields. Worm-like InP structures on titania nanotubes were synthesized and tested photoelectrochemically by Li *et al.*[280] The photoelectrode, with a band gap of only 1.52 eV, made methanol with a Faradaic efficiency of up to 85%. Tan *et al*. modified anatase TiO_2 with reduced graphene oxide (rGO) to form a composite with a smaller band gap of 2.90 eV.[281] Using a low intensity power-saving light, the composite catalyst demonstrated a higher yield of 0.135 μmol g^{-1} h^{-1} for CH_4 production than either of the separate materials.

Cuprous oxide-TiO_2 composite hollow nanospheres generated 0.16 μmol g^{-1} h^{-1} of CH_4 from aqueous suspension under visible light, an improvement over pure Cu_2O, which was attributed to the formation of a p-n junction.[282] Slamet *et al*. tested Cu_2O- and CuO-impregnated TiO_2 particles and found the latter to have a much higher yield of methanol (433 μmol g^{-1} h^{-1} compared to 225 μmol g^{-1} h^{-1}) after 6 hours of UV illumination.[283]

2.5.2. Z-Scheme Photocatalysts

The Z-scheme photocatalytic setup utilizes two different semiconductors in order to carry out a dual excitation and more efficaciously separate the charge carriers. In the study carried out by Sato *et al.*, a p-InP photocathode with various anchored Ru metal complex polymer electrocatalyst was coupled with a TiO_2 photoanode.[53] This Z-scheme was capable of driving CO_2 reduction under illumination without electrical bias, and the best performance in terms of product selectivity was achieved by tethering two different Ru electrocatalysts ([Ru(4,4'-diphosphate ethyl-2,2'-bipyridine)$(CO)_2Cl_2$] and [Ru{4,4'-di(1*H*-pyrrolyl-3-propyl carbonate)-2,2'-bipyridine}$(CO)(MeCN)Cl_2$] together onto p-InP, which yielded a 70% selectivity for $HCOO^-$. However, this p-InP/Ru MCE coupled with n-TiO_2 Z-scheme possessed a poor solar to chemical energy conversion efficiency of 0.03-0.04%. A later study using $SrTiO_3$ photoanodes with the same InP photocathode and Ru catalysts saw much higher currents than with TiO_2 and an increase in conversion efficiency up to 0.14%.[284]

A highly active Z-scheme consisting of Si/TiO_2 was composed of porous Si nanospheres and TiO_2 nanosheets, and was capable of harvesting visible light for the reduction of CO_2 to CH_3OH with a maximum photonic efficiency exceeding 18%.[285] The Z-scheme composite using graphitic carbon nitride (g-C_3N_4) as a photocathode reduced CO_2 to CH_3OH, HCOOH and CH_4, while the counterpart composed of a WO_3 photoanode carried out H_2O oxidation.[286] The Z-scheme

constructed using a Ru(II) dinuclear complex for CO_2 reduction, and using a Ag-loaded TaON for methanol oxidation, was capable of reducing CO_2 to HCOOH under illumination with wavelengths over 400 nm.[287] According to Zhou *et al.*, a novel design of a Z-scheme array using all solid-state materials was constructed from FeV_4O_{13} nanoribbons and reduced graphene oxide/CdS nanoparticles grown on a stainless steel scaffold.[288] This Z-scheme array has been demonstrated to produce CH_4 from gaseous CO_2 on the oxide sites.

2.5.3. Semiconductor Solid Solutions

Semiconductor-based solid solutions are achieved by incorporating one or more semiconducting component into a similarly structured parent semiconductor, such as $ZnAl_2O_4$-modified ZnGaNO, Zinc gallogermanate ($4.5(ZnGa_2O_4):(Zn_2GeO_4)$), etc.[289,290] Forming solid solution has been often applied as an approach of engineering the band gap width and band edge positions. The Zn_2AlO_4-modified mesoporous ZnGaNO solid solution was synthesized by nitriding a mesoporous $Zn(Ga_{1-x}Al_x)_2O_4$ template. The solid solution demonstrated a narrowed bandgap of 2.35 eV, which is equal to a 40 nm red shift from that of a pristine ZnGaNO.[289] This effect is attributed to the increased Zn content enhancing Zn 3*d* and N 2*p* *p*-*d* repulsion and resulted in a rise of the valence band position. This Zn_2AlO_4-modified mesoporous ZnGaNO solid solution had been applied as a photocatalyst, which was capable of reducing CO_2 to CH_4 at the rate of 9.2 μmol g^{-1} h^{-1} under visible light illumination ($\lambda \geq 420$ nm). The solid solution formed by introducing $ZnGeO_4$ into $ZnGa_2O_4$ took advantage of the enhanced *p*-*d* repulsion too, but this time the effect occurred between O 2*p* and Zn 3*d*, which again raised the valence band.[290] The incorporation of the Ge *s* orbital led to downshift of the conduction band edge. The mole ratio between $ZnGa_2O_4$ and $ZnGeO_4$ was determined to be 4.5:1, and a band gap narrowing effect was observed too. This system reduced CO_2 to CH_4 owing to the enhanced proton

production facilitated by the accelerated hole mobility. Furthermore, Zinc germanium oxynitride ZGeON was reportedly to reduce CO_2 to CH_4, and $Cu_xAg_yIn_zZn_kS_m$ solid solution exhibited catalytic reduction of CO_2 to CH_3OH under visible light.[291,292]

2.6. Heterogeneous CO_2 Reduction on Semiconductor Dark Cathodes

Although one purpose of employing semiconducting materials for CO_2 reduction is to take advantage of their photo-generated current and voltage, it is undeniable that the catalytic activity associated with semiconductor surface is of equal importance. Hence, there have been studies on using n-type semiconductors as dark cathode driven by an external bias to reduce CO_2 . In fact, most of the research performed with TiO_2 electrodes used the n-type form of TiO_2. This section will cover a few other n-type semiconductors that have been employed as dark cathodes to reduce CO_2 .

Frese *et al*. were the first ones to use an n-type GaAs electrode to perform selective CH_3OH synthesis.[293] The applied potential was in the range of -1.2 to -1.4 V vs. SCE, and CH_3OH was produced from CO_2 with a nearly 100% selectivity. Frese *et al.* proposed that CO_{ads} is an important intermediate on the n-GaAs surface. These results contrast the work carried out on an illuminated p-GaAs, in which other reduction products were observed.[294]

Reported by Hara *et al.*, a conductive n-Si electrode was employed to reduce CO_2 in aqueous solution under 30 atm of CO_2 .[295] At a fairly negative potential of -2.04 V vs. Ag/AgCl, HCOOH and CO were produced as the primary products at nearly equal Faradaic efficiency (~ 40%).

2.7. Reduction at Semiconductors Using Homogeneous Catalysts

The photoelectrochemical reduction of CO_2 with a light-absorbing material is appealing since a significant amount of the energy input could come from light rather than solely from electrical energy. As noted above, many studies have been devoted to the direct utilization of p-type

photocathodes to convert CO_2 to value-added fuels. However, an unavoidable concern is the competition from H_2O or proton reduction, which is, in general, a much more kinetically favored process than CO_2 reduction.[233,296,297] It is a promising strategy to combine semiconductor electrodes with molecular CO_2 reduction catalysts, which can selectively reduce the activation barrier for this process and outcompete proton reduction in aqueous electrolytes. With the assistance of such homogenous molecular catalysts, particularly with high catalytic selectivity and efficiency, an improved overall cell performance for CO_2 photoelectrocatalytic reduction may be achieved.

2.7.1. Metal Complexes

In 1982, Bradley *et al.* briefly reported photoelectrochemical reduction via a series of tetraazomacrocyclic Ni^{II} and Co^{II} complexes (Figure 14) at p-Si photocathodes in 0.1 M TBAP/MeCN.[298] The investigations showed that the reduction of the complex at the p-Si surface can be achieved at potentials more positive than those at a metal electrode such as Pt or Hg. The efficient photoreduction of other complexes with redox potentials more negative than the E_{CB} of p-Si was also observed. This result was theorized to derive from Fermi level pinning originating from surface states or surface electronic levels, which raised the band edge positions.[299,300] More detailed studies followed in 1983 and an improved system employed $[Me_6[14]aneN_4Ni^{II}]^{2+}$ as the electron transfer mediator in 1:1 acetonitrile-water solution. CO and H_2 (syngas) were produced in a 2:1 ratio at -1.0 vs. SCE with 95 ± 5% total Faradaic efficiency in electrolyses lasting from 2 h to over 24 h.[301] The reaction conversion efficiency was highly dependent on the solvent. In aqueous dimethyl sulfoxide and dimethylformamide solutions, low CO conversion efficiency of less than 5-50% was observed. In dry solvents, equal amounts of CO and CO_3^{2-} were formed, but only at potentials lower than -1.3 V vs. SCE, . Similarly, hydrogen-terminated Si (H-Si) in the

presence of a [Re(bpy-^{t}Bu)(CO)$_3$Cl] (bpy-Bu^t=4,4'-di-*t*-butyl-2,2'-bipyridine) electrocatalyst was used for CO_2 reduction to CO.[302] At a potential 600 mV more positive than at a Pt electrode, Faradaic efficiencies of 97 ± 3% were achieved. Fermi-level pinning, or the unpinning of the band edges also occurred in this case.

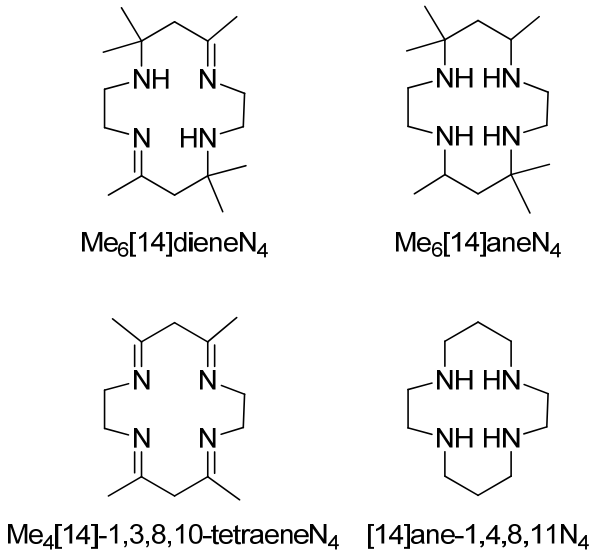

Figure 14. The macrocyclic ligands used in conjunction with Ni^{II} or Co^{II} for CO_2 reduction on illuminated p-Si from the work of Bradley *et al*.[298,301]

Photoelectrochemical systems utilizing the III-V semiconductors p-GaAs and p-GaP in conjunction with a Ni(cyclam)$^{2+}$ (cyclam=1,4,8,11-tetraazacyclotetradecane) catalyst were comprehensively studied by Petit *et al.*[303–305] With p-GaP and Ni(cyclam)$^{2+}$, although the electrolyte is aqueous, CO was the primary reduction product with efficiencies exceeding 80% under applied potentials of only -0.2 V vs. SHE. Ni(cyclam)$^{2+}$ greatly improved the selectivity of this system by suppressing H_2O reduction. The CO/H_2 production ratio is 50:1 at the beginning of the experiment, though the product ratio decreases to an average of 5:1 to 10:1 over the course of the whole experiment. The difference in charge separation efficiency between p-GaAs and p-GaP is due to the amplitude of the band bending, which is only 0.4 V for p-GaAs at a bias of -

0.95 V vs. SHE, whereas a bias of only -0.2 V vs. SHE on p-GaP yields band bending of 0.8 V. The decreased efficiency and CO selectivity over the course of the hours of electrolysis was attributed to the deposition of carbon from $Ni(cyclam)^{2+}$, which limited light absorption and exposure of catalytic sites to the electrolyte and CO_2 .

Another integrated system, studied by Zafrir et al., consisted of a p-GaAs photocathode as light absorber under an applied bias of -0.5 V vs. SCE, V^{3+}/V^{2+} in aqueous HCl as charge transfer mediator, and carbon as the counter electrode to convert CO_2 into formic acid, formaldehyde, and methanol. However, the Faradaic efficiencies were only 0.14%, 0.3% and 1.5%, respectively, and the optical to chemical energy conversion efficiency was marginal. The authors hypothesized that the catalytically active V^{3+}/V^{2+} system may exist as chloride complexes rather than hydrated vanadium ions.[294]

2.7.2. Enzymatic CO_2 Reduction Catalysts

Reversible electrochemical interconversions of carbon dioxide and formate (or other CO_2 reduced products) by an electroactive enzyme, which usually contains a molybdenum, nickel, or tungsten dithiolene active center, have been extensively investigated and reviewed.[306–312] The use of such CO_2 -active enzymes as electron transfer mediators with semiconductor electrodes was first reported in 1984. Parkinson *et al.* have discovered that the fixation of CO_2 to formate can be achieved by coupling a p-InP photoelectrode with a formate dehydrogenase enzyme (FDH).[313] Photogenerated electrons in the semiconductor transfer from methyl viologen to the enzyme, and subsequently to CO_2 at a potential of +0.05 V vs. NHE in 0.5 M pH 6.8 phosphate buffer/0.5 M $NaHCO_3$. The system resulted in a current efficiency of 80-93% for the formate conversion and

product turnover number up to 21,000. However, this system suffered from loss of enzymatic activity due to the denaturation of the protein under prolonged electrolysis.

Armstrong and coworkers have reported the use of both a chemisorbed ruthenium tris(bipyridine) photosensitizer and an enzymatic CO_2 reduction catalyst adsorbed onto P25 TiO_2 nanoparticles (Figure 15).[199,200] Under visible light and in the presence of 2-(N-morpholino)ethanesulfonic acid (MES) as sacrificial electron donor, this combined system generated 250 μmol g^{-1} h^{-1} of CO, though production was unstable over time. The nickel-containing carbon monoxide dehydrogenase (CODH) enzymes, which utilize a two-electron pathway for CO_2 reduction, may have been weakly adsorbed or have few positioned in such a fashion to accept electrons from the conduction band of the TiO_2.[199] Changing the sacrificial electron donor to EDTA led to 40% greater yields, implying that regeneration of the photosensitizer after it transferred the photoexcited electron to the TiO_2 was a limiting factor.[200]

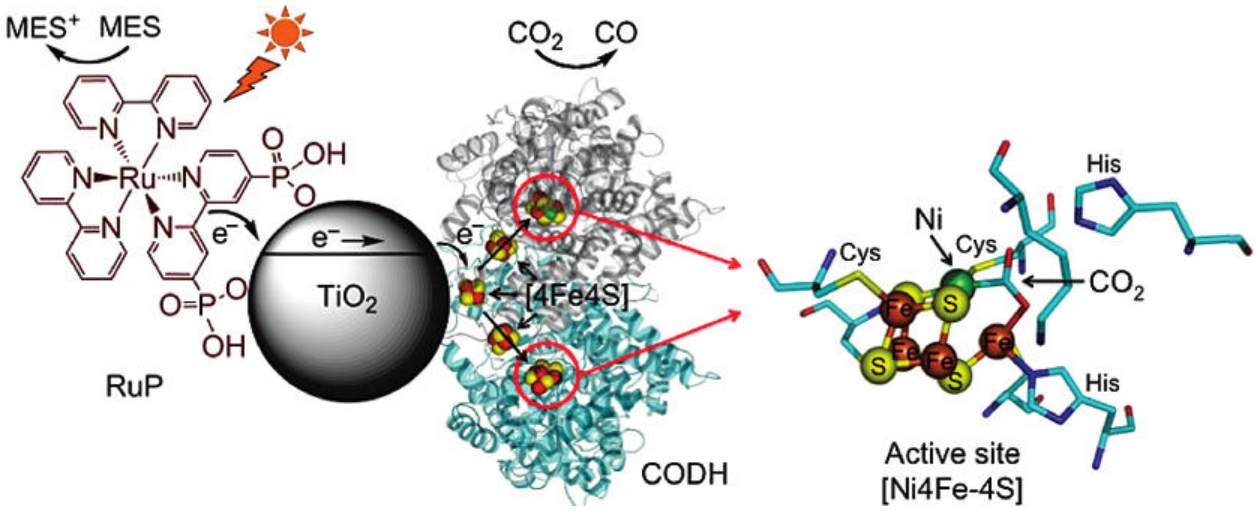

Figure 15. Schematic of the ruthenium dye-sensitized TiO_2 nanoparticles with adsorbed CODH enzyme, which catalyzes the reduction of CO_2 to CO. Reprinted with permission from ref. [199]. Copyright 2010 American Chemical Society.

The Armstrong group also examined the use of CODH-modified CdS to photoreduce CO_2 under visible irradiation, testing different electron donors in the process.[314] Variations in MES concentration were not found to effect the CO production, but the presence of ascorbate or KI as sacrificial electron donors, led to no CO generation. Use of triethanolamine (TEOA) decreases CO production by 80%. It is postulated that these differences in activity are related to the differing degrees of interaction of these sacrificial agents with the surface of the CdS. TEM shows that calcination led to agglomerates that were on the order of 20x larger than the QDs. The authors propose that the increased number of grain boundaries in the calcined particles lowered the activity of the CdS, due to their role as recombination sites. CODH-attached nanorods led to a significant production of CO, even though the amount of CODH attachment was very low. This increased yield was attributed to lower probability of recombination due to lower dimensionality of the catalyst.

Kuwabata and coworkers also investigated the use of enzymes to aid in photochemical reduction of CO_2 at metal sulfide particles.[315] Using SiO_2-supported ZnS microcrystallites in the presence of methanol dehydrogenase and a phyrroloquinoline quinone electron mediator, a formate-containing solution was reduced to methanol under UV irradiation. The use of CO_2 instead of formate as the starting material led to immediate detectable formation of both formate and methanol under the UV illumination.

2.7.3. Organic Electrocatalysts

Barton *et al*. reported a non-transition metal based molecular catalyst, a simple protonated pyridine in aqueous solution, as the electrocatalyst for very highly efficient CO_2 reduction to produce methanol when this catalyst was combined with a p-GaP(111) photocathode.[17] Interestingly, very high selectivity (>92%) for solar-driven reduction of aqueous CO_2 to

methanol could be obtained at an applied potential that was less than the thermodynamic potential of CO_2 reduction to methanol (-0.52 V vs. SCE at pH 5.2). For instance, at -0.20 V vs. SCE, 320 mV of underpotential, with irradiation of 365 nm light, the Faradaic efficiency for methanol production was reported to be 96%, and the quantum efficiency for electron flow was observed to be 13% while the value of the quantum efficiency for methanol production was up to 12.5%. Hence, optical conversion efficiency, η, defined as the ratio of power output to incident light power, was calculated to be up to 4.8% under these conditions. While under less energetic illumination of 465 nm, the photoelectrochemical cell performance was decreased; the quantum yield for methanol production was only 1.35%, and optical conversion efficiency was reported to be only 0.84% at an applied potential of -0.30V vs. SCE. Nevertheless, no other photoelectrodes, as discussed in this review, have been reported to generate methanol at an underpotential (lower than the thermodynamic potential). Therefore, this is the first example of highly selective solar-driven reduction of CO_2 to methanol using a catalyzed p-GaP based photoelectrochemical cell.

Several other semiconductors have been tested with pyridine for their CO_2 reduction capabilities. A thin film of the ternary chalcogenide $CuInS_2$ was used as a photocathode for the reduction of CO_2 to methanol in the presence of pyridine at -0.59 V vs. SCE under visible light illumination.[316] An enhancement in catalytic current upon the introduction of pyridine as a co-catalyst was also reported by Woo *et al.* on a CdTe/FTO electrode.[317] The primary product formed in this case was formic acid with a Faradaic efficiency exceeding 60%. The authors further elucidated that the mass transfer resistance, resulting from a saturated pyridine adsorption layer on the electrode surface, decreased the Faradaic and catalytic efficiencies for CO_2 reduction. de Tacconi *et al*. employed a Pt-TiO_2 composite supported on carbon black as a dark electrode with aqueous pyridinium for CO_2 reduction to methanol and isopropanol.[318] Though no

Faradaic yields are reported, the production of methanol per gram of Pt was almost 10^5 times greater than on a bulk electrode, and 350 mmol g_{Pt}^{-1} isopropanol, which was not detected on bulk Pt, was generated.

Bocarsly and coworkers have further reported the chemistry of the electrocatalytic reduction of CO_2 using nitrogen-containing heteroaromatics by the direct comparison of imidazole and pyridine as electrocatalysts at illuminated iron pyrite (FeS_2) electrodes.[319] Under similar electrochemical conditions (pH 5.3) as with the p-GaP electrode, the iron pyrite photocathode with electrocatalyst pyridinium or imidazolium was reported to only produce formic acid with Faradaic efficiencies of 2.7% and 4.9%, respectively, at -1.1 V vs. SCE. It is also noteworthy that the imidazolium catalyst was observed to generate carbon monoxide with a Faradaic efficiency of 2.4% while no such product was observed when pyridinium was utilized with the iron pyrite photoelectrode. The mechanism of imidazole-based catalysts of CO_2 reduction was also investigated by analyzing the catalytic activity of a series of imidazole derivatives using cyclic voltammetry. While the formation of formic acid and carbon monoxide by the aromatic amines was initially thought to proceed through the formation of a carbamate radical, as proposed for pyridinium,[320] the results obtained for 2-methylimidazole and 1-ethyl-3-methylimidazolium bromide suggest a much different mechanism for imidazole and its derivatives. Imidazole more likely proceeds through an imidazolium 2-ylidene, which forms a carbon−carbon bond with CO_2 to form an imidazolium 2-carboxylate. However, it is important to point out that the mechanisms, particularly the involvement of the pyridinyl radical in the pyridinium catalytic cycle, were subsequently re-investigated and ruled out by Yan *et al*., and instead they proposed and demonstrated an interfacial platinum hydride mechanism for CO_2 reduction when Pt was used as the working electrode.[321]

The report that pyridinium serves as a highly selective electrocatalyst for methanol with an illuminated p-GaP electrode for CO_2 reduction to methanol with high Faradaic efficiency and quantum yield at an underpotential has sparked enormous curiosity and debate as to the mechanism by which this process occurs.[17] Bocarsly and coworkers further reported an experimental mechanistic investigation of pyridinium's role as electrocatalyst in 2010.[320] In this study, the aqueous multiple-electron, multiple-proton reduction of carbon dioxide to products such as formic acid, formaldehyde was reported. At metal electrodes, particularly platinum, formic acid and formaldehyde were observed to be intermediate products along the pathway to the 6 e^- reduced product of methanol. This simple organic molecule was found to be capable of reducing several different chemical species (CO_2 , formic acid, and formaldehyde) to methanol through sequential electron transfers.

The mechanism for the pyridinium-catalyzed reduction of carbon dioxide was also investigated by theoretical quantum calculations. Keith and Carter applied first-principles density functional theory and continuum solvation models to calculate acidity constants for pyridinium cations and their corresponding pyridinyl radicals, as well as their electrochemical redox potentials.[322–325] Contrary to experimental observations, their quantum mechanics calculations showed two important results: 1) the redox potential of pyridinum to pyridinyl radical was predicted to occur at about −1.4 V vs. SCE (at pH = 5.3), nearly 900 mV more negative than the observed the quasi-reversible redox potential of this species in aqueous solution on a platinum electrode; 2) the pK_a of the pyridinyl radical was calculated to be ~27. On the basis of these calculations, they concluded that pyridinyl should not form in the experimental conditions, and deprotonations should not be facile at all due to the high acid dissociation constant of this radical species, indicating that the proton-CO_2 exchange to form a carbamate is not favored. Instead, they

proposed that 4,4-bipyridine, formed from coupling of two pyridinyl radicals, might be the active catalyst.[325] The proton-coupled-electron-transfer (PCET) process from singly protonated bipyridine (monocation) to form the doubly protonated bipyridine mono-cation radical was calculated to be the exactly the same as the redox experimental potential, and the latter's calculated pK_a (12.8) may be low enough to facilitate proton−CO_2 exchange in water to form a carbamate.

Lim *et al.* provided another creative quantum mechanistic approach to this mechanism, and, in contrast to Keith and Carter, predicted a very low barrier, reasonably close to the experimental observations, for the carbamate species formation.[326,327] The predicted enthalpic barrier for the PCET reaction proposed by Barton *et al*. was 45.7 kcal mol^{-1}. However, when the proton transfer (PT) was mediated by one, two, or three water molecules acting as a proton relay, the barrier decreases to 29.5, 20.4, and 18.5 kcal mol^{-1}, respectively. The water proton relay reduced strain in the transition state (TS) and facilitates more complete electron transfer. For PT mediated by a three water molecule proton relay, adding water molecules to explicitly solvate the core reaction system further reduced the barrier to 13.6−16.5 kcal mol^{-1}, depending on the number and configuration of the solvating waters, which correlated well with the experimentally determined barrier of 16.5 ± 2.4 kcal mol^{-1}. These results suggested that pyridinium could catalyze the homogeneous reductions of formic acid and formaldehyde en route to formation of CH_3OH through a series of one-electron reductions analogous to the PCET reduction of CO_2 examined. However, the first reduction step from pyridinium to pyridinyl radical was still calculated to be ~1 V more negative than the experimental observation. They attributed the difference to surface adsorption of pyridinyl radical, which could stabilize it relative to its being solvated.

Ertem *et al.* also investigated this system with their focus on both the platinum electrode surface, specifically Pt(111), and the function role of pyridinium during aqueous electrochemical reduction of CO_2 .[328] They found that CO_2 might be reduced by H atoms bound to the Pt surface that were transferred to CO_2 in a proton-coupled hydride transfer (PCHT) mechanism activated by pyridinium (Scheme 3). The surface-bound H atoms consumed by CO_2 reduction were then replenished by the one-electron reduction of pyridinium through the proton-coupled electron transfer, PCET. Hence, in this proposed mechanism, the pyridinium's role is essential to provide a high concentration of Brønsted acid in close proximity to CO_2 and the Pt surface, much higher than the concentration of free protons. In this proposed mechanism, the first step, is a purely proton-based reduction of the acidic pyridinium proton. Interestingly, the redox potential calculation correlated quite well with the experimental observation from cyclic voltammetry, -0.58 V vs. SCE.

Scheme 3. Mechanism proposed by Ertem *et al*. for the pyridinium-catalyzed reduction of CO_2 , implicating a Pt-H intermediate. Reprinted with permission from ref. [328]. Copyright 2013 American Chemical Society.

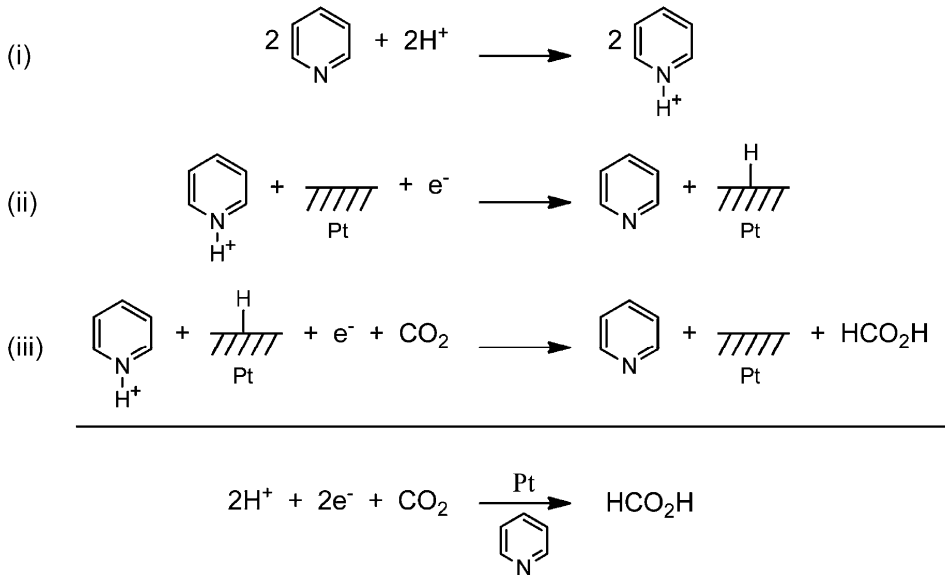

The role of pyridinium as electrocatalyst for CO_2 reduction was recently experimentally re-investigated by Yan *et al.*,[321] particularly focusing on the controversy between calculations and experimental observation of the redox potential of the first electrochemical step. They concluded that the quasi-reversible cyclic voltammetric waves observed at −0.58 V vs. SCE at a Pt electrode corresponded to reduction of pyridinium to a platinum hydride based on the observation that the redox potentials of pyridinium and its derivatives were independent of the energy states of their respective π^* orbitals, but were dependent exclusively on the acidity (pK_a) of the pyridinium species. This observation is corroborated with the redox potentials on Pt of more than 20 weak acids of varying structures: pyridinium derivatives, imidazolium and its derivatives, as well as aromatic and nonaromatic acids such as amines, phenols, and carboxylic acids. The reduction of the pyridinium proton to a surface hydride, which can also be described as inner-sphere reduction of pyridinium to form a surface hydride, rather than the formation of a π-based radical product, was consistent with the theoretical insights of Batista and his coworkers. Shortly after Bocarsly and colleagues reported on the pK_a dependence of $E_{1/2}$, Savéant *et al.* also concluded similar weak acid-based reduction results from a detailed cyclic voltammetric investigation.[329] However, they also reported that the Faradaic efficiency for methanol formation with pyridinium and a platinum working electrode on preparative-scale electrolysis was only in a range of 0.1% to 2.2%, significantly lower than Barton's original result of 22% under the same electrochemical conditions. Nonetheless, more recently, Portenkirchner *et al.* reported a Faradaic yield of 14 ± 1.5% for methanol formation in a similar system at a platinum electrode in the presence of pyridinium.[330] In this report, they explored methanol production by the direct comparison of protonated pyridazine and pyridine for their capabilities towards CO_2 reduction. Cyclic voltammetry studies as well as bulk controlled-potential electrolysis experiments were

performed. They concluded that methanol was detected as the main CO_2 reduction product in all cases, and these results essentially support the original reports by Bocarsly and coworkers.

Besides the aforementioned mechanistic investigations, other possible mechanisms or reaction pathways for pyridinium's role in electrocatalytic CO_2 reduction have also been proposed and quantum mechanically explored. Notably, Keith and Carter[324] and Lim *et al*.[327] separately investigated a dihydropyridine intermediate that was generated via a proton-coupled two-electron reduction from pyridinium. This dihydropyridine intermediate might be catalytically relevant due to the fact that dihydropyridine is the active moiety of the biological redox coenzyme nicotinamide adenine dinucleotide hydride (NADH). Keith and Carter investigated the redox potentials of species adsorbed on GaP photoelectrodes and reported that, on GaP surfaces, proton reduction or pyridinium reduction was energetically unfavorable even at very negative electrode potentials. However, it was thermodynamically favorable to convert a surface-bound pyridine into a 2 e^- reduced species such as dihydropyridine at less negative applied potentials. They also concluded that the transient 2 e^- reduced species, with a similar chemical moiety as NADH, holds reduction potentials that are similar to the thermodynamic redox potentials that would convert CO_2 to a variety of products. However, though the formation of the multi-electron reduced pyridinium species may be thermodynamically favorable, the process has a very high kinetic barrier. At the same time, Musgrave and coworkers elucidated a viable mechanism for pyridine-catalyzed reduction of CO_2 to methanol involving the kinetic investigation of dihydropyridine and including homogeneous catalytic steps (Scheme 4). They proposed a mechanism with alternating proton transfers and electron transfers (ET), namely PT–ET–PT–ET, for transforming pyridinium into dihydropyridine. The driving force for the reduction of CO_2 with dihydropyridine was attributed to the species' proclivity to regain aromaticity. They

predicted that the pyridinium/dihydropyridine redox couple was kinetically and thermodynamically competent in catalytically effecting hydride and proton transfers (the latter often mediated by an aqueous proton relay chain) to CO_2 and its two succeeding intermediates, namely, formic acid and formaldehyde, to ultimately form CH_3OH. More recently, Marjolin and Keith found by calculation that pyridinium, imidazolium, and phenantrholinium have two-electron reduction potentials to hydrogenated species close to the redox potentials for *CO_2* .[331] The Pourbaix diagram triple points dividing the protonated, the deprotonated, and the 2 e^- + 2 H^+ reduced species were seen as conditions under which proton or hydride transfers to CO_2 would be facile. However, no experimental evidence has been produced to support a dihydropyridine intermediate on any electrode surface, and, in the case of a platinum electrode, the experimentally determined one-electron nature of the reaction precludes hydride transfer from a dihydropyridine intermediate to *CO_2* .[321,332]

Scheme 4. Reduction of CO_2 to methanol with pyridine via a 1,2-dihydropyridine intermediate species. Reproduced with permission from ref. [327]. Copyright 2014 American Chemical Society.

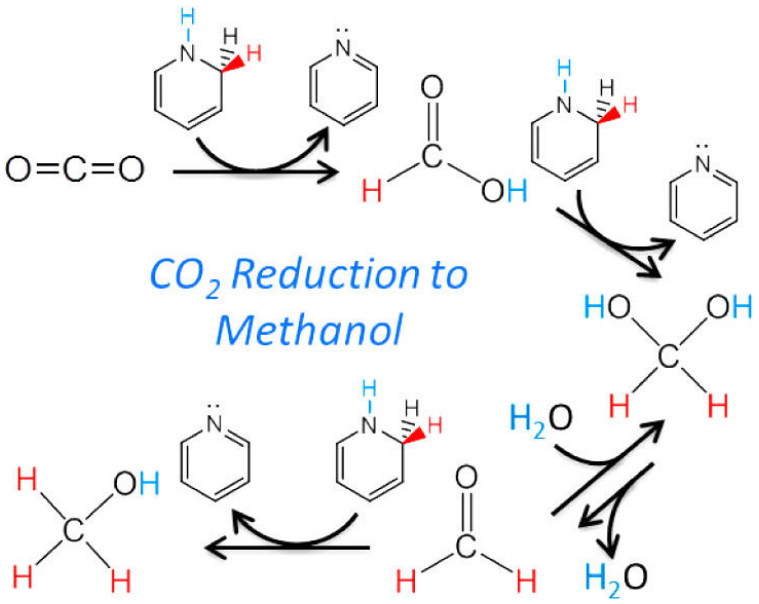

3. CO_2 REDUCTION ON POROUS MATERIALS

Materials such as metal-

organic frameworks (MOFs) and zeolites, while not semiconductors in the traditional sense, are still capable of performing photocatalytic reactions.[49] Such porous materials possess high surface-to-volume ratios, tunable porosities, and engineerable dimensionalities. MOFs and zeolites typically contain pores of sizes suitable for capturing small molecules, such as carbon dioxide and water, in the cavities.[333,334] Incorporating catalytic CO_2 reduction sites into these materials creates a favorable structure in which CO_2 can effectively adsorb, diffuse, and react in the porous framework.

3.1. Metal-Organic Frameworks for CO_2 Reduction

Metal-organic frameworks, frequently called MOFs, are crystalline coordination polymers with metal ion vertices joined by rigid organic ligands that serve as struts.[333] By changing the organic linkers, various properties, including pore size, electronics, and catalytic capabilities, can be adjusted, allowing a wide scope of possible MOFs. Several different MOFs have already been shown to reduce CO_2 photocatalytically.

Liu *et al*. grew zeolitic imidazolate framework 8 (ZIF-8, composed of $Zn(mIm)_2$ units; mIm = methyl imidazole) on the surface of Zn_2GeO_4 nanorods for use as CO_2 photoreduction catalysts (Figure 16).[236] The dissolved CO_2 adsorption on the hybrid catalyst was 3.8 times higher than that of the unmodified semiconductor nanorods. Compared to the parent Zn_2GeO_4, the hybrid catalyst showed improvement in the amount of methanol produced under illumination, increasing from 0.14 μmol g^{-1} h^{-1} to 0.22 μmol g^{-1} h^{-1}. This improvement was attributed to the ability of the ZIF-8 to adsorb dissolved CO_2 and the increased light absorption of the hybrid system, as shown by UV-Vis . 1% Pt loading of the hybrid material led to an even higher yield of methanol, due to improved electron-hole separation at the interface.

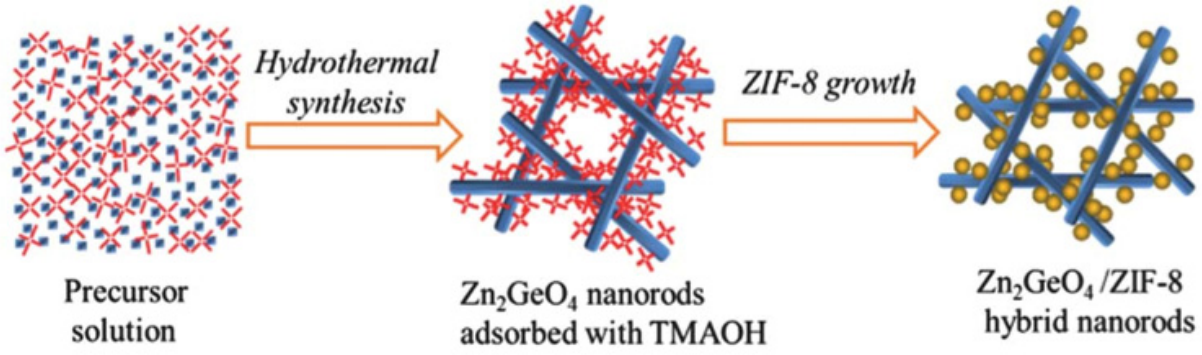

Figure 16. Schematic of ZIF-8 loading onto Zn_2GeO_4 nanorods. Reproduced from ref. [236] with permission from The Royal Society of Chemistry, copyright 2013.

Li *et al*. reported the use of three copper(II) ZIFs that are capable of CO_2 reduction under irradiation with visible light.[335] The frameworks, originally reported by Masciocchi *et al*., included an orthorhombic crystal structure, a monoclinic crystal structure, and a third framework whose crystal structure was unknown. The band gaps of these frameworks were 2.49, 2.70, and 2.81 eV, respectively (Figure 17). BET analysis indicated that the framework with the unresolved crystal structure had the highest surface area and the monoclinic one had the lowest. The orthorhombic phase had the highest activity for reduction to methanol; initially the monoclinic framework outperformed the unresolved structure, but after 4 hours of irradiation, the latter proved to be the better catalyst. The authors mainly attributed the high success of the orthorhombic framework to its lower bandgap, but note that the success of all three catalysts may be influenced by the similarity of the Cu_4N cluster featured in the zeolite to the known Cu_3N semiconductor. They suggest that the C=N band in the imidazole ring may also have similar functionality to the C=N band in C_3N_4 conductive polymers.

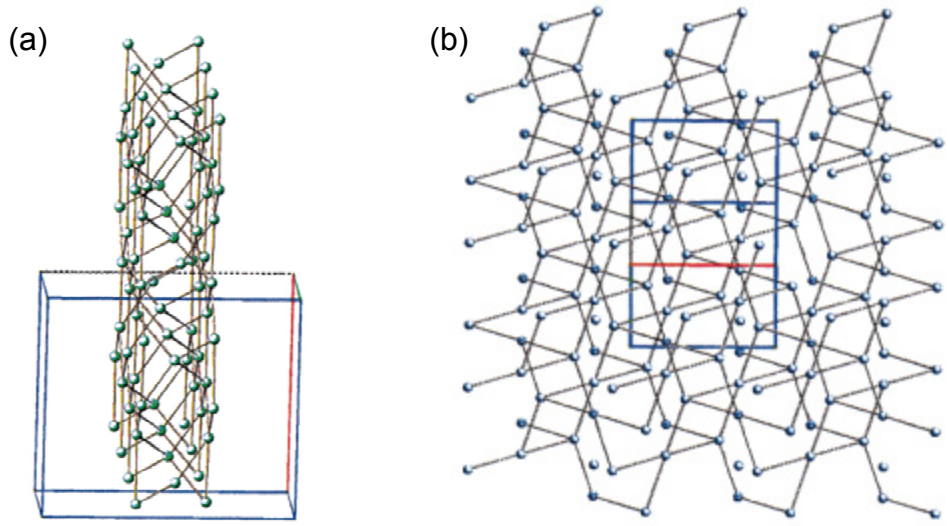

Figure 17. (a) Orthorhombic copper(II) ZIF and (b) Monoclinic copper(II) ZIF. Reproduced with permission from ref. [336]. Copyright 2001 American Chemical Society.

Other ZIFs have also been found to be catalytically active for the reduction of CO_2 . For example, Wang *et al.* used a cobalt-containing benzimidazolate MOF for the capture and photocatalytic reduction of CO_2 to CO.[337] This framework, Co-ZIF9 was found to be stable at temperatures less than 500 °C. In this study, $[Ru(bpy)_3]Cl_2 \cdot 6H_2O$ (bpy = 2,2'-bipyridine) was used as a photosensitizer. Triethanolamine was used as a sacrificial reductant. As with the ZIFs used by Li,[335] the conditions of the reaction were mild (room temperature, PCO_2 = 1 atm). Yields of 84 μmol h^{-1} for CO and 60 μmol h^{-1} for H_2 were observed, for a quantum yield of 1.48% under 420 nm irradiation. Although H_2 is generally viewed as an unwanted side-reaction, it was noted that product mixture of this reaction resembles syngas. No reaction occurred in the absence of either visible light, the photosensitizer, or CO_2 , and the CO yield dropped by a factor of 35 when the ZIF was removed from the system. A catalytic turnover number of 450 in 2.5 hours was reported.

Fu *et al*. reports an amine-functionalized Ti-centered metal organic framework, NH_2-MIL-125(Ti), that reduces CO_2 under visible light.[338] This MOF, with the formula $Ti_8O_8(OH)_4(bdc\text{-}NH_2)_6$ (bdc = benzene-1,4-dicarboxylate), has dangling NH_2 groups, that are free from coordination. Adsorption isotherms show that the amine functionalization increases the CO_2 uptake compared to the parent MOF. CO_2 photoreduction by NH_2-MIL-125(Ti) in acetonitrile with sacrificial TEOA led to the production of formate, which was not observed under irradiation of the parent MOF with visible light (420-800 nm). UV irradiation (365 nm) showed that both the amine-functionalized and parent MOFs reduce CO_2 to formate, with slightly higher activity associated with the amine-functionalized MOF. A color change upon irradiation in the presence of various gases (CO_2 , O_2, N_2) suggests that light is absorbed into a ligand to metal charge transfer state, creating a long-lived charge separation excited state. The Ti^{4+} is reduced to Ti^{3+} in the excited state, which then interacts with the incoming CO_2 to produce formate.

Sun and coworkers examined the effect of noble metal doping on the NH2-MIL-125(Ti) reported by Fu.[339] With the separate additions of gold and platinum nanostructures, it was found that visible light irradiation of the MOF in the presence of CO_2 and TEOA yields both formate and hydrogen. The Pt-enhanced MOF yielded the most formate, with the Au-enhanced MOF producing less than the parent MOF. Although the parent MOF as-synthesized contains Ti^{4+}, Ti^{3+} is suggested to be the active species for CO_2 reduction. The decrease in formate production when gold is added is explained by the Au acting as an electron trap, thereby hindering the formation of the active species. However, with Pt doping, photogenerated H_2 is dissociated across the Pt. The H atoms produced by this dissociation can interact with oxygen in the Ti-O cluster. In doing so, electrons are donated to the Ti, providing another pathway to the active Ti^{3+} species. This is believed to be the source of increased formate production in the Pt-doped MOF.

Wang *et al*. studied three Fe-based MOF materials and their amino substituted forms for CO_2 photocatalytic reduction.[340] One of the MOFs, MIL-101(Fe) demonstrated the highest catalytic activity for production of formate in both the amine-functionalized and bare forms, due to its coordinatively-unsaturated iron center. Amine functionalization further enhanced catalytic activity for all three MOFs.

Sun *et al*. reported CO_2 reduction by visible light in the presence of a MOF denoted as NH_2-UiO-66(Zr).[341] The parent MOF, UiO-66(Zr) (formula $Zr_6O_4(OH)_4(CO_2)_{12}$) has a slightly larger BET surface area than the amino-functionalized MOF, indicating that the amino groups block the micropores. However, the amino-functionalized MOF shows higher CO_2 adsorption capability than the parent MOF. Using sacrificial TEOA, visible light irradiation of CO_2 in the presence of the catalyst was found to produce formate. The parent MOF was not found to be photocatalytic for CO_2 reduction. ESR experiments suggest that irradiation causes an electron transfer from the organic ligands to the Zr-O clusters, only in the aminated MOF. The corresponding Zr^{3+} ESR signal was quenched upon introduction of CO_2 , implying it plays a role in the photocatalytic reduction. Photoluminescence studies revealed an electron transfer from the organic linker to the Zr-oxo cluster. The MOF was further modified to include 2,5-diaminoterephthalic acid into its framework, along with the 2-aminoterephthalate (ATA) linkers already present. This modification showed enhanced light absorption in the visible region, as well as enhanced adsorption of CO_2 . Irradiation with wavelengths greater than 515 nm yielded 7.28 μmol of formate in the presence of the mixed-linker MOF, while the MOF with only ATA linkers did not produce formate in this region.

Wang *et al.* successfully doped the UiO-67 MOF ($Zr_6O_4(OH)_4(bpdc)_6$), bpdc = *para*-biphenyldicarboxylate) with the rhenium-based CO_2 reduction catalyst ($Re^{I}(CO)_3(dcbpy)Cl$,

dcbpy = 2,2'-bypridine-5,5'-dicarboxylic acid).[342] It was shown that CO_2 reduction to CO occurs when > 300 nm wavelength light (from a filtered 450 W Xe-lamp) is shined upon a reaction vial containing acetonitrile, *CO_2* , the doped MOF, and trimethylamine as a sacrificial reductant. No CO was observed in the absence of either the Re-based cocatalyst, *CO_2* , or light. The turnover number (TON) of the modified MOF for the production of CO is approximately 5.0 over the course of 6 hours. This TON a factor of two larger than the TON observed for the rhenium catalyst in the absence of the UiO-67 scaffold. The increased catalytic ability is attributed to the stabilization of $Re^{I}(CO)_3$(dcbpy)Cl in the presence of the MOF. However, the Re-carbonyl moieties photodissociated from the dcbpy ligand in the MOF, resulting in a loss of activity over time.

Li *et al*. reports the use of an iridium-based coordination polymer as a heterogeneous photocatalyst for CO_2 reduction to formate under visible light.[343] The photoactive component of the polymer is the $[Ir(ppy)_2(dcbpy)]^-$ (dcbpy = 4,4'-dicarboxylic acid-2,2'-bipyridine) unit. This unit contains both a photosensitizer to increase light harvesting and an effective catalytic active site. The coordination polymer converts CO_2 to formate with a quantum yield of 1.2% under 475 nm light in acetonitrile with triethanolamine as a sacrificial electron donor. The catalyst was found stable for a period of hours, and was able to be used for five 6-hour runs with consistent results. Comparison of the polymer as a heterogeneous catalyst and the isolated photoactive unit as a homogeneous catalyst demonstrated that the photoactive unit was able to produce formate, but was photodegraded in the process. A mechanism was proposed, whereby the $[Ir(ppy)_2(dcbpy)]^-$ unit is excited by incoming light. The excited complex accepts an electron from the TEOA, and two neighboring photoreduced $[Ir(ppy)_2(dcbpy)]^-$ units donate electrons to *CO_2* , reducing it to formate. Cyclic voltammetry was used to determine that the Ir moiety is

thermodynamically capable of reducing CO_2 , and the proximity of the pyridine units from neighboring dcpby ligands in this framework adds to the feasibility of two consecutive single-electron transfers.

Liu *et al*. demonstrated the use of a Cu porphyrin-based MOF for CO_2 capture and reduction.[55] The MOF was prepared with and without Cu in the porphyrin ring, to assess the effect that Cu has on the CO_2 . The catalysts were irradiated under visible light, as dispersions in CO_2 -purged water with a small amount of triethylamine. The predominant product is methanol, with a rate approximately 7 times higher when the Cu is included. Nitrogen adsorption/desorption shows that the inclusion of Cu lowers the internal surface area of the MOF, however, CO_2 adsorption/desorption shows a large enhancement with this inclusion. The adsorption of CO_2 into the Cu-containing MOF is irreversible, meaning that desorption is incomplete; it is suggested that this is due to a chemical interaction of CO_2 with the MOF, rather than just a physical one. This chemisorption was confirmed by FTIR in both end-on and C-coordination modes.

Li *et al*. reports the integration of TiO_2 onto a Cu-based MOF, HKUST-1 ($[Cu_3(TMA)_2(H_2O)_3]_n$, TMA=benzene-1,3,5-tricarboxylate), that is known for its ability to store CO_2 .[344] The resultant MOF had a core-shell structure, with a porous anatase TiO_2 shell. The MOFs retain HKUST-1s ability to capture CO_2 , although the BET surface area decreased due to the low surface area of the TiO_2. UV irradiation in the presence of CO_2 yielded five times more methane than bare anatase, and the selectivity for methane over other products increased. Ultrafast spectroscopy confirmed that the hybrid material improved the efficiency of electron-hole separation over the individual materials, allowing for activation of the CO_2 that adsorbs into the MOF.

3.2. Zeolites

Zeolites are aluminosilicate minerals that occur naturally, though numerous others have been synthesized in order to obtain more homogeneous and tailored materials. Zeolites, like MOFs, typically have high porosity and high adsorption capacities for gases.[334] In addition, they can carry out photocatalytic reduction of CO_2 , though ultraviolet light is often necessary. Much of the research on CO_2 reduction on zeolites has been performed by Anpo and coworkers, typically with the inclusion of TiO_2.[78,112,116,345–356]

Ikeue *et al*. reported the use of hydroxylated and fluorinated Ti-β zeolites as CO_2 photoreduction catalysts.[354] These zeolites, first reported by Blasco *et al.*, incorporate Ti into an aluminum-free zeolite beta framework (Figure 18).[357] The hydroxylated zeolites, denoted Ti-β(OH), exhibited hydrophilic behavior, while the fluorinated zeolites, Ti-β(F), were hydrophobic. UV irradiation of the catalysts with a 100 W Hg lamp ($\lambda > 250$ nm) in the presence of CO_2 and water led to the formation of methane and methanol, with trace amounts of CO, ethylene, and oxygen. Ti-β(OH) strongly outperforms the Ti-β(F), although the fluorinated zeolite shows a higher ratio of methanol to methane. Due to its hydrophobic nature, the Ti-β(F) interacts much less with the water, leading to its higher selectivity for CH_3OH and its lower overall product yield. Photoluminescence studies were performed to gain insight into the mechanistic differences between the two catalysts. Ti-β(OH) exhibited a higher photoluminescence yield, suggesting a higher concentration of the charge-transfer excited state $[Ti^{3+}\text{-}O^{-}]^{*}$. The photoluminescence lifetime of Ti-β(OH) dropped from 173 μs to 147 μs with exposure to CO_2 and H_2O, whereas the lifetime for Ti-β(F) dropped only from 159 μs to 150 μs. This quenching indicates the interaction of CO_2 and H_2O with the excited charge-transfer state, and the difference in lifetimes can be attributed to the differences in hydrophilicity.

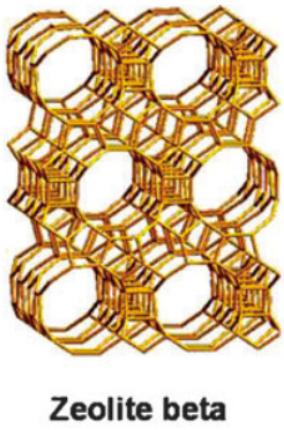

Figure 18. Structure of zeolite beta. Reproduced from ref. [358] with permission from the PCCP Owner Societies, copyright 2008.

Guan and coworkers investigated a hybrid system consisting of $Pt/K_2Ti_6O_{13}$ and a Fe-based catalyst loaded on a dealuminated Y-type zeolite (Fe-Cu-DAY).[249] Under UV irradiation, the Fe-Cu-DAY alone showed no catalytic activity for CO_2 reduction. The $Pt/K_2Ti_6O_{13}$ was confirmed to produce H_2, methane, formic acid, and formaldehyde under the same conditions. Using visible light, only H_2 and methane were observed. Use of the hybrid catalyst under UV/Vis irradiation at room temperature showed decreased activity for product formation, compared to the $Pt/K_2Ti_6O_{13}$. Using concentrated sunlight at temperatures exceeding 500 K, the catalyst system was charged with 202 kPa CO_2 and 4.0 mL water. Under these conditions, enhanced activity toward the production of formic acid, methanol, and ethanol was observed. The increase in activity is attributed both to the increase in photoelectrons for the Pt-loaded semiconductor, and in the increase in temperature across the entire system.

Ikeue *et al*. prepared porous self-standing Ti-containing silica thin films with different mesostructures for use as CO_2 reduction photocatalysts.[359] A hexagonally-structured film with 25 nm pores (Ti-PS(25)) was found by UV-Vis to have two distinct Ti environments and was selective for methane under UV irradiation in the presence of CO_2 . A cubic-structured film (Ti-

PS(c)) showed higher selectivity for the production of methanol, with methane as the minor product. The highest photocatalytic activity was observed for a hexagonal film with 50 nm pores (Ti-PS(50)), which was selective for methane production, with methanol as the minor product. In powdered form, Ti-PS(50) showed lower photocatalytic activity, but still outperformed the other catalysts. This drop in activity is attributed to light scattering by the particles, and demonstrates the advantage of using transparent thin films for photocatalytic reactions. Differences in product distributions are attributed to the concentration of surface hydroxides, with lower surface hydroxide concentrations being linked to increased methanol selectivity.

TS-1 is a zeolite that contains the TiO_2 motif in its framework. Yamagata *et al*. demonstrated the use of TS-1 to catalyze CO_2 reduction to methane under UV irradiation.[360] The catalyst was first activated by irradiation with a mercury lamp in the presence of hydrogen gas, which served as the hydrogen source for the methane. The concentration of Ti and adsorbed carbon species was found to be of the same order of magnitude, suggesting that the Ti acts as the photocatalytic site.[281]

4. PHOTO-DRIVEN CO_2 REDUCTION ON METALLIC CATHODES

The previous sections of this review have focused on the reduction of carbon dioxide on both particle and electrode-based semiconductor surfaces under illumination. While this is by far the most commonly studied means of harnessing light energy for CO_2 reduction, numerous other methods and configurations have been investigated to capture sunlight and convert it to chemical energy.[361,362] Some of these techniques, including concentrated solar thermal CO_2 splitting and homogeneous photocatalysis, are reviewed elsewhere in this issue. However, closely related to photoelectrochemistry is the use of photovoltaic-CO_2 electrolyzer systems which employ metallic electrodes driven by a separate solid-state p-n junction photovoltaic array. A second

configuration that utilizes a metallic cathode is a photoelectrochemical cell based on an n-type photoanode.[11] These systems are classified as PV-biased electrosynthetic and photoelectrosynthetic cells, respectively.[362]

4.1. Energy Matching

The previous sections primarily dealt with the cathodic half-cell in the CO_2 reduction reaction; however, both half-cells must be considered in the photoanode- and photovoltaic-driven systems. An essential concern in the design of a complete electrolysis system is the relative energetics of both the electrodes and the redox-active species of interest. In the context of this review, the cathodic and anodic reactions are the reduction of CO_2 ($E^{0\prime}$ = -0.40 V vs. SHE to CH_3OH at pH 7) and the oxidation of H_2O ($E^{0\prime}$ = -0.82 V vs. SHE at pH 7), respectively, so the photogenerated potential must be sufficient to bracket the redox potentials of both of those reactions and account for the significant overpotentials for each.[4,361]

A single-junction cell, which contains only one photosensitive material, has a maximum photochemical efficiency of ~30% with the optimum band gap of E_g = ~1.3 eV for solar illumination.[363,364] However, larger band gap materials, which have somewhat lower maximum theoretical efficiencies, are required to effect the two desired reactions, especially since the maximum voltage is limited to be ~300 mV less than E_g/q, where q is the elemental charge.[365] Semiconductors with larger band gaps are better able to straddle the relevant redox potentials, but can absorb less of the solar spectrum at the surface of the earth.[366] An alternative method for generating the requisite photovoltage is connecting multiple cells in series. An increased number N of photoconverters does increase the maximum efficiency above 30%,[361] but the current density decreases as $1/N$ as more cells are connected.[367]

The major efficiency limitations in a light-driven electrochemical system are the slow reaction kinetics at the electrodes. The operating voltage, as mentioned before, must account for both the thermodynamic potentials as well as the overpotentials for the two reactions, which are typically ~0.4 V for water oxidation and frequently up to 1 V for CO_2 reduction, to yield sufficient current densities.[19,367]

Another limitation that must be considered is the coupling between the photoactive material and the other electrode(s). In a PV-biased electrosynthetic cell, the system must be operated close to the maximum power point of the PV device (the "knee" of the curve), otherwise the impedance mismatch significantly curtails the power available to run the electrochemical cell (Figure 19).[4] In a photoanode-driven photoelectrochemical cell with a metal cathode, coupling losses are relatively small since the semiconductor is typically connected to the metal by an ohmic contact.[367]

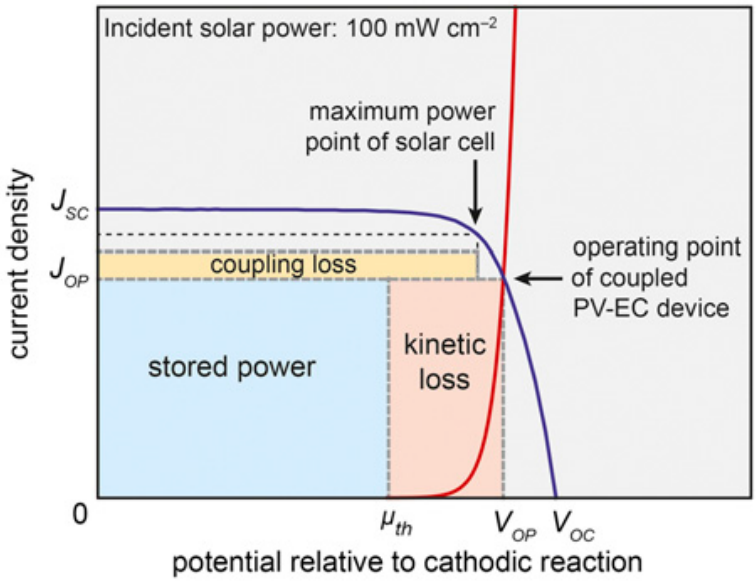

Figure 19. A general current density-voltage diagram for a coupled photovoltaic-electrochemical system. Reproduced from with permission from ref. [367]. Copyright 2013 The National Academy of Sciences.

4.2. Metal Cathodes

The electrochemical reduction of CO_2 on metal electrodes has been extensively studied by Hori, Lvov, and Hara, in both aqueous and non-aqueous systems and with different pressure schemes and cell designs (Figure 20).[11,19,295,368–371] The focus of this section will be on the most recent advances of metal-based electrochemical CO_2 reduction; not all metals that have CO_2 reduction capabilities are discussed here and the reader is directed to Hori's work in references 11 and 19 for a more thorough review of this topic. In aqueous solutions, where the discussion will be focused, the hydrogen evolution reaction (HER) has been the major competing reaction for CO_2 reduction. The metal electrodes are typically categorized by their primary product in solution: formic acid, carbon monoxide, or hydrogen. Copper, which makes a variety of hydrocarbons including products containing more than one carbon, holds a unique position in the reductive electrochemistry of CO_2 .

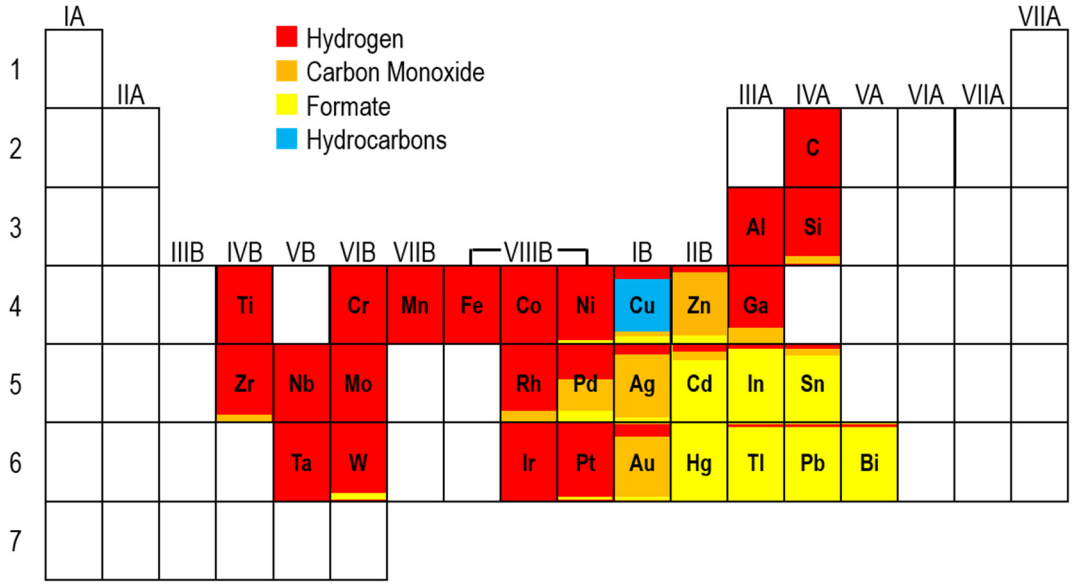

Figure 20. Periodic table depicting the primary reduction products in CO_2 -saturated aqueous electrolytes on metal and carbon electrodes. Based on data from Hori *et al.*[11]

4.2.1. Formic Acid-Producing Metals: Sn, In, Pb

Tin, lead, and indium surfaces oxidize in air, generating a passivating native oxide. Detweiler *et al.* found that an anodized oxide layer on indium increased the formate Faradaic efficiency and improved the electrode stability in the potential range -1.4 V to -1.8 V vs. SCE.[16] *In situ* IR spectroscopy suggested that the indium hydroxide formed on the surface was the catalytically active species that binds CO_2 and leads to formate production.

Kanan and coworkers have shown that a composite Sn/SnO_x material formed *in situ* greatly enhanced CO_2 reduction both in terms of current densities and Faradaic efficiencies, with CO and HCOOH accounting for 55% and 40% of the current, respectively. The preparation involves a -0.7 V vs. RHE deposition of Sn^{2+} on a Ti surface where SnO_x and Sn^0 are formed concurrently.[15] Wu *et al.* showed the dependence of the Faradaic efficiencies of CO and $HCOO^-$ on the thickness of the SnO_x layer, with the thin native oxide yielding the most formate.[372] This result contrasts with that on indium, on which a thicker oxide layer generated formate more selectively; however, the indium was anodized in aqueous solution whereas the tin was oxidized with a thermal treatment in air. Recently, a similar *in situ* IR study to that with indium was conducted on tin by Baruch *et al.*[21] As with indium, a surface carbonate was detected only under conditions at which CO_2 reduction took place, implicating it as the active species. However, evidence showed that the native Sn^{IV} oxide had to be reduced first to a Sn^{II} oxyhydroxide in order to bind and subsequently reduce CO_2 . Both the tin and indium systems require ~1.0 V overpotential under realistic operating conditions.[19,373]

In aqueous solutions, the electrochemical reduction of CO_2 on Pb electrodes also yields predominantly formate.[374] Using an electrochemical reactor with continuous electrolyte flow, Alvarez-Guerra *et al.* found that a high rate of formate production could be obtained (j ~ 10.5

mA cm^{-2}) with only a modest reduction in Faradaic efficiency to 57%.[375] A comparison study showed that tin can sustain high efficiencies at a faster electrolyte flow rate than lead.[376] At high CO_2 pressures, up to 60 atm, the Faradaic efficiencies for formic acid on both indium and lead have been observed to be 100% with current densities up to 200 mA cm^{-2}.[374] As with indium and tin, lead has also been shown to have a dependence on the surface oxide.[20] However, while in the previous cases the oxide promoted CO_2 reduction, the oxide-derived and untreated lead have similar carbon dioxide reduction activities, though the former greatly suppressed H_2 production and thus drastically increased the Faradaic efficiency for formate.

4.2.2. Carbon Monoxide-Producing Metals: Au, Ag, Pd

Au has been known to reduce CO_2 to CO electrochemically at high yield and selectivity, although typically overpotentials are fairly high.[11] Some recent Au studies focused on nanoscale tuning and forming alloys with other metals at the nanoscale. Chen *et al.* showed that Au nanoparticles formed *in situ* by electrochemically reducing a pre-formed thick and amorphous Au oxide can reduce CO_2 with only 140 mV overpotential (-0.25 V vs. RHE), and the electrode remained stable under electrolysis conditions for as long as 8 hours.[23] Using Au nanoparticles and nanowires, Zhu *et al.* have demonstrated that the edge sites of Au nanoparticles have the highest selectivity for CO formation.[377,378] Their 8 nm Au nanoparticles achieved 90% Faradaic efficiency at -0.67 V vs. RHE, better than nanoparticles of smaller size. This behavior was rationalized by pointing out that 8 nm nanoparticles had an ideal number of edge sites (which are highly catalytic for CO_2 reduction) while minimizing the number of corner sites (which are catalytic for H_2 formation). The Au nanowires, which had a much greater proportion of edge sites to corner sites, had a 94% Faradaic efficiency at -0.35 V vs. RHE, 320 mV less negative than with the nanoparticles. Kauffman *et al.* carried out a study on Au_{25} clusters that yielded the

electrochemical reduction of CO_2 at -1.0 V vs. RHE with ~100% Faradaic efficiency.[379] They also observed a reversible Au_{25}-CO_2 interaction similar to those seen in cluster oxidations, with a partial oxidation of the gold cluster by CO_2 and a shift in the $Au_{25}^{0/-1}$ redox wave, consistent with depletion of the Au_{25} HOMO.

Alloying Cu into Au nanoparticles was suggested to promote the formation of higher order reduced products. For example, one study demonstrated that $Cu_{63.9}Au_{36.1}$ particles yielded 15.9% methanol and 12% ethanol, much higher than the production on pure Cu electrodes, which are known to make ethanol at about 5% efficiency but do not form methanol at all.[380] Using a monolayer of uniform Au-Cu bimetallic nanoparticles with well-tuned compositions, Kim *et al.* showed that the nanoparticles' electronic and geometric properties acted cooperatively to determine the binding stabilities of CO_2 reduction intermediates, which, in turn, dictated reduction product distributions.[381] The predominant products were CO and H_2, though particles with more Cu also yielded formate and hydrocarbons. The proximity of Cu atoms, which have higher H-atom binding energies, to Au atoms increased the ability of the catalyst to hydrogenate CO_2 and led to more highly reduced species, including hydrocarbons.

Polycrystalline Ag is reported to reduce CO_2 with 81% selectivity to CO at a potential of -1.4 V vs. SHE.[11] Using an ionic liquid electrolyte containing the 1-ethyl-3-methylimidazolium cation, which dramatically reduced the overpotential to less than 0.2 V, Rosen *et al.* achieved a 96% CO Faradaic efficiency on a bulk Ag electrode. The ionic liquid was proposed to stabilize the intermediate $CO_2^{\bullet-}$ through complexation, which decreased the overpotential.[382] Nanostructures on the Ag surface may also help stabilize the radical intermediate. Lu and coworkers demonstrated a nanoporous Ag catalyst that could achieve three orders of magnitude larger CO partial current density with a smaller overpotential compared to a bulk Ag

electrode.[383] A silver nanoparticle size study by Salehi-Khojin *et al.* found that CO production efficiency increased as the Ag nanoparticle size decreased, to a maximum efficiency at 5 nm.[384]

A study by Januszewska *et al*. showed that CO_2 reduction activity can be tuned by the number of Pd layers co-deposited onto a Au substrate. The study used an overlaying Cu monolayer on the surface, while the catalytic activity is dependent on the supporting Pd inner layers.[385] Research by Furuya *et al.* exhibited that, if alloyed with Ru in a 1:1 ratio, Pd is capable of suppressing CO formation while giving a 90% Faradaic efficiency for formate formation at -1.1 V vs. NHE.[386]

The size-dependence of CO formation from CO_2 on Pd nanoparticles was recently investigated by Gao *et al.*[387] The smallest particles studied, 2.4 nm and 3.7 nm in diameter, had the highest partial current densities and Faradaic efficiencies, both of which dropped off as the size increased to 10.3 nm. Using DFT calculations, the authors suggested that, since the adsorption energies of intermediates COOH and CO increase from terrace to edge to corner sites, the smaller nanoparticles, which have the greatest proportion of edge and corner sites, have the highest activity.

4.2.3. Copper

Copper electrodes have been found to yield a rich CO_2 reduction chemistry, including highly reduced species such as methanol and methane, as well as multicarbon products such as ethylene, ethanol, and n-propanol.[11,388,389] Recent studies by Kuhl *et al.* that incorporate large format copper electrodes in an advanced analytical design including inline GC as well as *ex situ* NMR have yielded a total of 16 distinct CO_2 reduction products, many of which had two or three carbons.[390] Extensive studies have been carried out to elucidate what oxidative states or surface structures are vital for CO_2 reduction on Cu.[22,391–394] Electrodeposited cuprous oxide has been

shown to have high selectivity for methanol formation with 38% Faradaic efficiency, much higher than air-oxidized and anodized copper electrodes.[393] The *in situ* reduction of Cu_2O, formed by annealing copper foil in air produced Cu nanostructures that catalyzed the formation of CO and formate, rather than the more reduced products typically seen on copper, stably and with high Faradaic efficiencies (40% for CO, 33% for formate at -0.5 V vs. RHE at pH 7.2). The initial thickness of the Cu_2O layer was reported to determine the electrode stability and product selectivity.[22] Further studies by Li showed that this same oxide-derived Cu can electrochemically reduce CO to ethanol, n-propanol, and acetate with a 57% total Faradaic efficiency in the potential range between -0.25 and -0.5 V vs. RHE.[391] The improved reduction properties of oxide-derived Cu were proposed to result from a large number of active sites at grain boundaries.[391] Studies by Kas *et al.* on oxide-derived Cu nanoparticles indicated that the initial Cu_2O crystal phase had little impact on the hydrocarbon selectivity, whereas the Cu_2O layer thickness and local pH changes played important roles.[394] Copper nanoparticles supported on glassy carbon selectively reduced CO_2 to methane with 4 times the current density as compared to copper foil and with an average of 80% Faradaic efficiency.[395] It was also reported that CO_2 reduction occurs through a different mechanism than that of bulk copper by analyzing Tafel slopes. Mixtures of copper oxide with ZnO and Al_2O_3 yielded methanol with almost 100% efficiency, much higher than alloys of Cu with other metals such as Ni, Pd, or Ru.[396] The source of this shift in Faradaic efficiency has not been elucidated.

4.2.4. Hydrogen-Producing Metals: Pt, Fe, Ni

In aqueous solution, platinum serves as an excellent water reduction catalyst. At potentials where CO_2 reduction is expected to take place,H_2 forms primarily due to the metal's very low hydrogen overpotential. Platinum does reduce CO_2 to CO and formate with very low Faradaic

efficiency; however, the strong chemisorption of CO to the Pt surface causes rapid poisoning.[11,397] Since surface hydrides form readily on pristine platinum surfaces, one recently proposed mechanism for formate production involved formation of Pt-H moieties, which could perform a hydride transfer to CO_2 to yield $HCOO^-$.[321,328,398]

Recently, Kuhl *et al.* found that Pt, Ni, and Fe, all of which have fairly low hydrogen overpotentials and yield almost exclusively H_2 in aqueous solution, were able to form methane as well, albeit in very small quantities and at incredibly low efficiencies.[399] In addition, Pt and Ni produced some methanol, though none was detected from reduction on Fe. These products were not previously recognized due to the miniscule amounts formed, which could only be detected using sensitive inline gas chromatography.

4.3. Photoanode-Driven Photoelectrochemical Cells

Employing an n-type semiconductor as the anode in a carbon dioxide reduction cell allows for an integrated photoelectrochemical cell, ideally without additional external bias, akin to those already discussed using p-type photocathodes. In this kind of cell, the photoanode absorbs a photon, yielding a conduction band electron that proceeds through the external circuit to the cathode and a hole that oxidizes a solution species (Figure 21). As in any photoelectrochemical cell, the semiconductor band gap must be sufficiently large to straddle both of the electrochemical redox potentials and any associated overpotentials. The use of a photoanode grants greater flexibility in the choice of cathode material, either metal or semiconductor, to select for the desired CO_2 reduction products. Since Z-scheme systems, with two photoexcited semiconductor electrodes were discussed previously in Section 2.5.2, the following section will focus on cells with metallic cathodes.

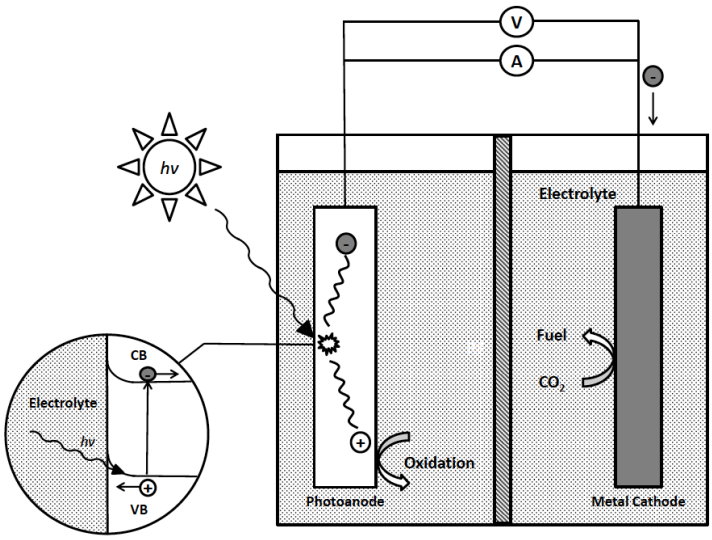

Figure 21. Photoanode-driven PEC, shown in a two-electrode configuration, with a metallic cathode, at which CO_2 reduction takes place, and a semiconductor photoanode.

The use of a photoanode to power the carbon dioxide reduction reaction has been investigated by several researchers, though considerably more study has been devoted to water splitting to hydrogen and oxygen.[32] Ogura and coworkers have done significant work on light-driven CO_2 reduction to methanol starting in the mid-1980s. Some of his initial work employed n-CdS (E_g = ~2.4 eV) as the photoanode,[400,401] though he later tested n-TiO_2 (E_g = 3.0 eV) as well.[401,402] In both cases, the cathode was platinum coated with a Prussian blue catalyst film, and the electrolyte was typically 0.1 M KCl containing 20 mM MeOH and either a pentacyanoferrate or chromate complex. The amount of formic acid and formaldehyde generated in these photochemical cells was negligible, and the sole product detected was methanol, which was confirmed by ^{13}C NMR. Methyl formate was implicated as an intermediate in the CO_2 reduction mechanism (Scheme 5).[401] Both of these systems had significant limitations on the anodic side of the cell. The n-CdS photoanode required a sacrificial reductant in order to prevent the photodegradation of the semiconductor; it did not actually effect water oxidation. The n-TiO_2

cell, though considerably more stable, was limited by the larger band gap of TiO_2, which allowed for poor overlap of the solar spectrum on Earth.

Scheme 5. Mechanism of reduction of CO_2 to methanol via methyl formate using Everitt's salt (ES), which is the reduced form of Prussian blue (PB), on a metal (M) cathode. Adapted with permission from ref. [401]. Copyright 1987 The Electrochemical Society.

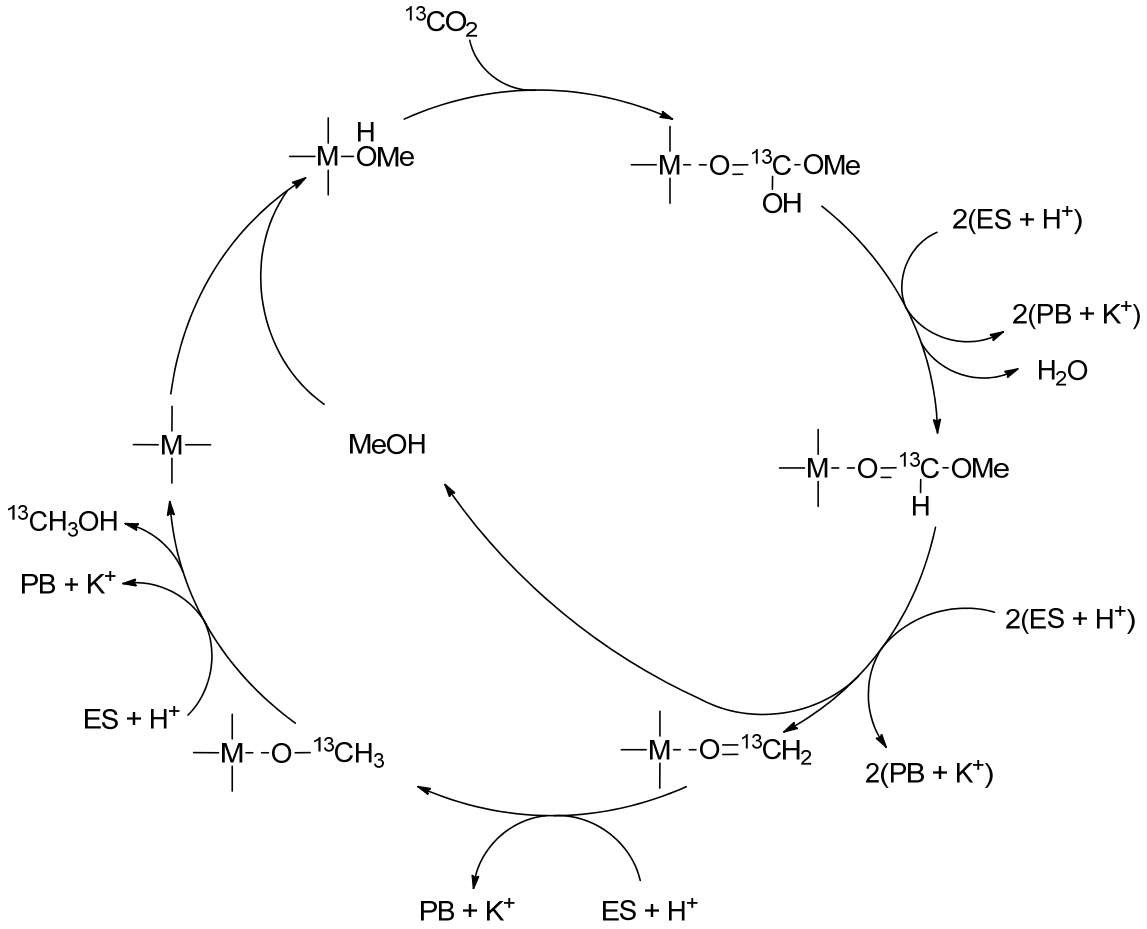

Other researchers have also employed n-TiO_2 as the photoanode. Izumi *et al*. utilized a monolithic electrode assembly formed by electrodepositing Cu onto a Ti foil that had been oxidized on one side, followed by electrodeposition of small amounts of Ag.[403] Photoelectrochemical reactions took place with the photoanode facing a solution of 0.25 M K_2SO_4 and the cathode in contact with 0.6 M $KHCO_3$; the only bias in this system was from the

pH gradient between the two half-cells. The electrodeposition of small amounts of Ag (atomic ratio of 9:1 Cu:Ag) decreased the yield of CH_4 and increased the yield of C_2H_4, indicating a cooperative effect that led to more C-C coupling than occurs on the pure metals. Ichikawa and Doi had a membrane-separated TiO_2 photoanode system, with ZnO on Cu as the cathode in 0.1 M $KHCO_3$.[404] The Faradaic efficiency was 20-40% for CH_4 under constant bias, but increased to over 40% when a pulse bias was applied. A Pt-modified rGO cathode loaded onto nickel foam was used with a Pt-modified TiO_2 nanotube photoanode to reduce CO_2 to a variety of products, including ethanol and acetic acid, under illumination. The rate of conversion of CO_2 was 1.5 $\mu mol\ cm^{-2}\ h^{-1}$ with a selectivity for liquid products of 99%.[405]

Centi and coworkers used a nanostructured n-TiO_2 film, supported on porous Ti, as their photocatalyst.[406,407] The anode was joined to the carbon cloth gas diffusion electrode (GDE) in a membrane electrode assembly (MEA) with a Nafion polymer electrolyte membrane (PEM). In preliminary tests, Pt nanoparticles on carbon were deposited onto the cathode GDE and proved successful in generating hydrogen under illumination. CO_2 reduction was conducted in the gas phase on Fe, Pt, Co, and Cu particles supported on multiwalled carbon nanotubes (MWCNTs). In addition to significant amounts of H_2 and CO, methanol and other multicarbon products, albeit in sub-micromolar quantities, were detected not just on the Cu particles, but the other three metals as well.[408] These findings are in marked contrast to the minimal activity of Co, Fe, and Pt towards CO_2 reduction in aqueous solution, in which all three preferentially reduce water to hydrogen.[11] However, the CO_2 reduction results were obtained not with the TiO_2 photoanode, but instead with an anodic half cell using a platinum counter electrode. Centi has yet to report the development of an integrated cell which performs the reduction of CO_2 on these catalysts while powered by an illuminated n-TiO_2 anode.

Deguchi and colleagues at Panasonic Corporation in 2012 announced a 0.2% energy conversion efficiency using an artificial light source to convert carbon dioxide to formate.[409] The system used an n-GaN photoanode (E_g=3.4 eV). According to the patent literature,[410–413] the n-GaN semiconductor was coated with Ni or Ti to protect the anode from photodegradation and more readily oxidize a 1 M NaOH anolyte. Other variations included a ~100 nm thick layer of n-$Al_{0.11}Ga_{0.89}N$ (E_g=3.7 eV) on top of the n-GaN; the authors theorized that the heterostructure between the two nitride semiconductors led to better charge separation and greater photocurrent.[412–414] The use of such high band gap materials required light of wavelengths less than 350 nm, a very small portion of the incident solar spectrum. The cathode in this system has not been revealed but any of the metallic systems already noted in this chapter could be used.[410,412] The catholyte, 0.1 M $KHCO_3$, was separated from the alkaline anolyte with a Nafion membrane. Interestingly, when n-TiO_2 served as the photoanode, no CO_2 reduction products formed, and only H_2 was evolved.[410] This lack of activity is likely due to the less negative position of the n-TiO_2 conduction band edge (-0.52 V vs. SHE[109]) relative to that of n-GaN (-0.89 V vs. SHE[415]).

4.4. Photovoltaic-Biased Electrochemical Cells

Powering the entire energy-intensive process of reducing carbon dioxide and oxidizing water with a single photoelectrode requires the semiconductor employed to have a wide band gap and correctly placed band edges, which limits both the materials that can be employed and the semiconductors ability to absorb at solar frequencies available on the earth. However, an alternative is to connect one or more photovoltaic junctions to a CO_2 electrolyzer that utilizes metal electrodes. A set of photovoltaic junctions which can have a band gap well-matched to the solar spectrum can then be connected in series (a PV array) to generate the voltage required to

carry out the desired reaction, while capturing a significant portion of the solar spectrum. With this type of setup, anodic and cathodic electrode materials which have lower water oxidation overpotentials and low CO_2 reduction overpotentials, respectively can be selected, independent of the photoactivity requirements of the system. That is, the electrolyzer and PV components may be optimized independently. As noted previously, the two constituent modules must be impedance matched at the maximum power point of the PV array to allow for maximum solar to chemical energy conversion efficiency.

Among the first to employ a solar cell-driven electrolyzer for CO_2 reduction were Ogura *et al*.[401,416,417] They employed the same cathodic system as in their photoanode-driven work, which involved a Prussian blue film mediator on a Pt electrode, a primary alcohol, and a homogeneous Fe or Cr complex. The photoanode was replaced with a platinum counter electrode, and the anolyte was nitrogen-saturated 0.1 M K_2SO_4. A variable resistor tuned the voltage delivered to the electrolyzer., The Faradaic efficiency for MeOH was at a maximum between 1.5 V and 2.0 V, and dropped off significantly at greater cell voltages, likely due to a large increase in water reduction.

Researchers at Det Norske Veritas (DNV) developed a flow cell electrolyzer with porous tin cathode catalysts.[418] The anodic half-cell contained a Pt-coated Nb anode in 1 M KOH. The primary product in the 2 M KCl catholyte was formate, with Faradaic efficiencies approaching 100%. Pure tin was found to degrade in performance over time, so alloys of tin were utilized to achieve greater longevity. Though there were no published peer-reviewed reports concerning the coupling of a PV device to this electrolyzer, a report from DNV indicated that a 600 cm^2 cell that can reduce 1 kg of CO_2 per day was incorporated into a trailer with a solar panel as a mobile

demonstration of their technology.[419] However, no indication as to the overall photoconversion efficiency was provided.

More recently, at the 2014 International Conference on Artificial Photosynthesis, Toshiba announced the development of a system that had a 1.5% overall efficiency for photo-induced CO_2 reduction. The company's press release indicates the use of a Si-based multijunction solar cell with a cobalt oxide water oxidation catalyst (WOC) in solution.[420] The cathode was nanostructured gold, producing CO as the primary product. The catholyte was 50% triethanolamine in water, saturated with CO_2 . Toshiba has also developed systems that contain quaternary ammonium ions bound to the surface of the gold through thiols and long alkyl linkers.[421] With these catalytic systems, other products besides CO are formed, including formic acid, formaldehyde, and methanol.

White and coworkers reported a net energy conversion efficiency of over 1.8% for a CO_2 to formate process using a commercial polycrystalline Si PV panel coupled to a three-cell flow electrolyzer stack employing an indium cathode and a commercial iridium oxide-based anode (Figure 22).[4] The anolyte was 1 M H_2SO_4, rather than the oft-used NaOH or KOH, to improve cell stability and avoid the requirement of continuous addition of base to the solution. $KHCO_3$ was used as the catholyte. Average Faradaic efficiencies for formate exceeded 50%, though more hydrogen was produced during periods of greater insolation. The impedance of the electrolyzer stack was not ideally matched to that of the PV array, causing the operating voltage and power to be significantly lower than the maximum output and leading to significant coupling losses. Had the two components of this system been more effectively coupled, total solar conversion efficiency could have exceeded 3%.

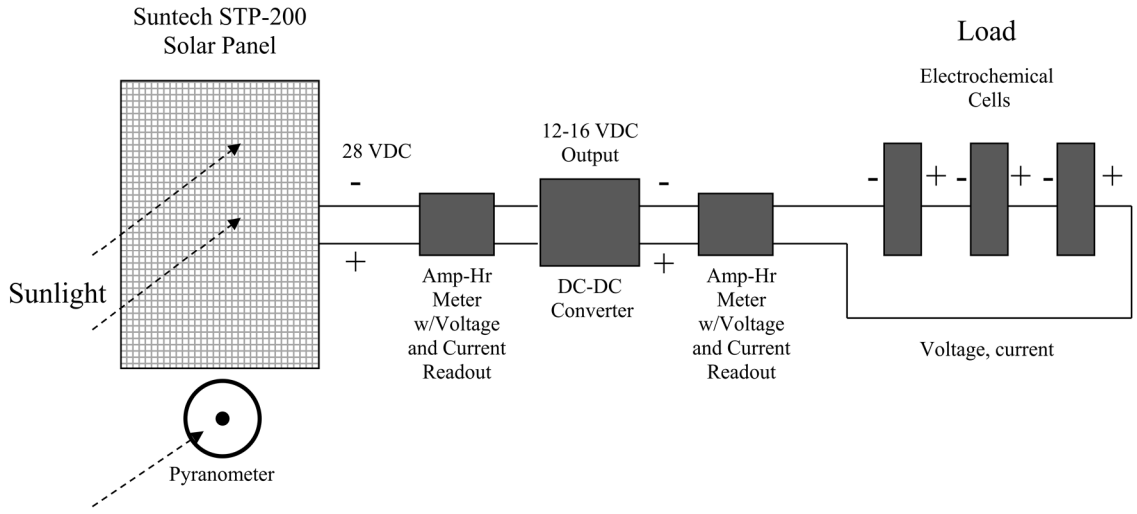

Figure 22. Electrical connections of the high conversion efficiency PV-biased electrolyzer described by White, *et al.* Reproduced from ref. [422] with permission from Elsevier, copyright 2014.

A monolithic device for CO_2 reduction with a CIGS ($Cu(In_xGa_{1-x})(S_ySe_{1-y})_2$) PV module was developed by Jeon *et al.*[423] The PV was coated onto conductive glass with a Co_3O_4 WOC on the opposite side. Nanostructured gold was used as the cathode to reduce CO_2 to CO in 0.5 M $KHCO_3$ with 91.2% Faradaic efficiency at an average photocurrent of 7.32 mA and cell voltage of 2.33 V. The overall solar to fuel efficiency was 4.23%, a marked increase over previous systems.

Torella *et al*. created a bioelectrochemical cell with a CoPi WOC anode and NiMoZn cathode, the latter of which generated hydrogen for use by the genetically engineered bacteria *Ralstonia eutropha*, *Re*2133-pEG12.[424] The bacteria produce, in addition to biomass, isopropanol, for which there was a maximum reported bioelectrochemical efficiency of 3.9%. Though the authors never connected a PV to their system, they claim that they would be able to achieve a solar to isopropanol yield of 0.7% if a 18% efficient PV device were utilized.

5. SUMMARY AND OUTLOOK

A wide variety of semiconductor systems have proven capable of harnessing near-ultraviolet and visible light and using that energy to drive the reduction of carbon dioxide through photocatalysis or photoelectrochemistry. The improved production of solar fuels is an essential component of the renewable energy portfolio of the future, enabling intermittent power sources to become more prevalent by storing excess energy with fewer losses and thus greater recoverability.

While early research in this field employed suspensions of simple semiconductor materials in aqueous solution, recent developments have focused on various doping and nanostructuring techniques, combinations of multiple semiconductors, and the addition of heterogeneous or homogeneous catalysts and sensitizers. The use of nanomaterials in particular has led to improved charge separation and to enhanced catalysis. Metals, both directly in contact with the light absorber and in a separate but electrically connected electrolysis cell, serve as electron sinks and catalysts, and they sometimes even enable CO_2 reduction on semiconductors whose own surfaces have excessively high overpotentials.

Many of the semiconductors described in this review are oxides, with TiO_2 receiving the bulk of scrutiny in this regard. Often these materials have band gaps approaching 3 eV; this hinders the absorption of a large proportion of the solar spectrum available at the earth's surface and diminishes the insolation to current efficiency. The efficiency of smaller band gap (~1.3 eV) semiconductors is still capped at the Shockley-Queiesser limit of ~30%.[363] Therefore, multijunction cells may be necessary to capture the majority of the solar spectrum, overcome the SQ limit, maintain long-term stability under illumination, and still straddle the CO_2 reduction and H_2O oxidation potentials. While some efforts have already been made to find working

combinations of semiconductors (Section 2.5), much of the domain of pairs (or even multiples) has yet to be explored.

Some of the innovations recently taken up in photocatalysis, such as photosensitization, were first studied for use in photovoltaics. Another such innovation, the use of organic semiconductors (OSCs), has, to our knowledge, not yet been employed in CO_2 reduction catalysis. While organic photovoltaics are still less efficient than silicon,[425] the use of these semiconductors in catalysis may prove to be particularly interesting due to their mutability. The vast scope of synthetic methods available permits tuning of the electronics,[426] but functional groups could also be appended to bind and reduce CO_2 more effectively.

As diverse as these studies have been, the vast majority of CO_2 -reduced products are single-carbon species such as methane, methanol, carbon monoxide, and formic acid. Some multicarbon products, primarily light hydrocarbons, have been reported to form, though they are generated almost exclusively at metallic copper and typically in low yields. While the established Fischer-Tropsch process is capable of taking solar-generated CO and H_2 to liquids, an important advance in catalysis would be the development of materials that can make carbon-carbon bonds and thus, higher-order hydrocarbons and alcohols at ambient conditions directly from CO_2 , water, and light.

AUTHOR INFORMATION

Corresponding Author

*E-mail: bocarsly@princeton.edu (A.B.B.)

Author Contributions

The manuscript was written through contributions of all authors. MFB, JEPIII, JLW, and ABB edited the manuscript, and JLW compiled it. All authors have given approval to the final version of the manuscript.

ACKNOWLEDGMENTS

We acknowledge the financial support provided by the United States Department of Energy Office of Basic Energy Sciences through Grant DE-SC0002133 for the photoelectrochemical aspects of this paper and the financial supported provided by the United States National Science Foundation through grant CHE-1308652 for the electrochemical and molecular catalysis aspects of this paper.

ABBREVIATIONS

bpy	2,2'-bipyridine
CB	conduction band
CE	counter electrode
CODH	carbon monoxide dehydrogenase
cyclam	1,4,8,11-tetraazacyclotetradecane
DFT	density functional theory
DMF	N,N-dimethylformamide
EPR	electron paramagnetic resonance
ET	electron transfer
EXAFS	extended X-ray absorption fine structure
FDH	formate dehydrogenase
FTIR	Fourier transform infrared
GDE	gas diffusion electrode
GO	graphene oxide
HER	hydrogen evolution reaction
HOMO	highest occupied molecular orbital
IPCE	incident photon-to-current efficiency
LDH	layered double hydroxide
LHCII	light-harvesting complex II
MeCN	acetonitrile
MOF	metal-organic framework
MPc	metallophthalocyanine
MWCNT	multi-walled carbon nanotube
NADH	nicotinamide adenine dinucleotide hydride
NHE	normal hydrogen electrode
NP	nanoparticles

NR	nanorods
NT	nanotubes
OSC	organic semiconductor
PCET	proton-coupled electron transfer
PEC	photoelectrochemical cell
PT	proton transfer
PV	photovoltaic
QD	quantum dot
QRE	quasi-reference electrode
RE	reference electrode
rGO	reduced graphene oxide
RHE	reversible hydrogen electrode
SCE	saturated calomel electrode
SHE	standard hydrogen electrode
TBAF	tetrabutylammonium tetrafluoroborate
TBAP	tetrabutylammonium perchlorate
TEAP	tetraethylammonium perchlorate
TEOA	tetraethanolamine
TMA^+	tetramethylammonium ion
TMACl	tetramethylammonium chloride
TNT	titania nanotubes
TON	turnover number
UV	ultraviolet
VB	valence band
WE	working electrode
WOC	water oxidation catalyst
ZIF	zeolitic imidazolate framework

SYMBOLS

c	speed of light
C_R	concentration of reduced species
C_O	concentration of oxidized species
$E^{0'}$	formal reduction potential
E_R^0	standard reduction potential of a half reaction
E_{rxn}^0	standard reduction potential of an electrochemical reaction
E_{ad}	energy of adsorption
E_F	Fermi energy
E_g	band gap of a semiconductor
E_{NHE}	electrochemical potential vs. NHE
E_R	redox potential of electrolyte
E_{RHE}	electrochemical potential vs. RHE
E_S	energy of surface states
E_{VB}	reduction potential of the valence band edge of a semiconductor
F	Faraday's constant

h	Plank's constant
i_{cat}	catalytic current
i_{mp}	current obtained at the maximum power point for a photovoltaic
i_{SC}	short-circuit current
j	current density
j_{ph}	photocurrent density
n	number of electrons transferred in an electrochemical step
${}_nE_{decomp}$	reduction potential of a cathodic decomposition reaction
${}_nE_F*$	quasi Fermi-level of electrons in the conduction band
${}_pE_{decomp}$	reduction potential of an anodic decomposition reaction
${}_pE_F*$	quasi-Fermi levels of electrons in the valence band
pK_a	logarithmic acid dissociation constant
P_{mono}	power intensity of a light source
q	elementary charge
$Q_{product}$	amount of charge that went into producing the desired product
Q_{total}	total charge passed in an electrochemical reaction
V_{mp}	voltage obtained at the maximum power point for a photovoltaic
V_{OC}	open-circuit voltage
ΔG_f^0	standard Gibbs energy of formation
$\Delta G^{0'}$	formal Gibbs energy
$\Delta G^{\ddagger}$	Gibbs energy of activation
ΔG_{rxn}^0	standard Gibbs energy of a reaction
$\Delta G_{electrolyte}$	free energy of the electrolyte
ΔG_{semi}	Gibbs energy of an electron
η	overpotential
λ	wavelength
ξ	Faradaic efficiency
ϕ_M	work function of a metal
ϕ_S	work function of a semiconductor

REFERENCES

(1) Fujishima, A.; Honda, K. Electrochemical Photolysis of Water at a Semiconductor Electrode. *Nature* **1972**, *238* (5358), 37–38.

(2) Becquerel, E. Recherches Sur Les Effets de La Radiation Chimique de La Lumière Solaire, Au Moyen Des Courants électriques. *Comptes Rendus Hebd. Séances Acad. Sci.* **1839**, *9*, 145–149.

(3) O'Regan, B.; Grätzel, M. A Low-Cost, High-Efficiency Solar Cell Based on Dye-Sensitized Colloidal TiO_2 Films. *Nature* **1991**, *353* (6346), 737–740.

(4) White, J. L.; Herb, J. T.; Kaczur, J. J.; Majsztrik, P. W.; Bocarsly, A. B. Photons to Formate: Efficient Electrochemical Solar Energy Conversion via Reduction of Carbon Dioxide. *J. CO_2 Util.* **2014**, *7*, 1–5.

(5) Biello, D. Reverse Combustion: Can CO_2 Be Turned Back into Fuel? *Scientific American*. September 23, 2010.

(6) Bard, A. J.; Faulkner, L. R. *Electrochemical Methods: Fundamentals and Applications*, 2nd ed.; John Wiley & Sons, Inc., 2001.

(7) *CRC Handbook of Chemistry and Physics*, 95th ed.; CRC Press, 2014.

(8) Surdhar, P. S.; Mezyk, S. P.; Armstrong, D. A. Reduction Potential of the Carboxyl Radical Anion in Aqueous Solutions. *J. Phys. Chem.* **1989**, *93* (8), 3360–3363.

(9) Qiao, J.; Liu, Y.; Hong, F.; Zhang, J. A Review of Catalysts for the Electroreduction of Carbon Dioxide to Produce Low-Carbon Fuels. *Chem. Soc. Rev.* **2013**, *43* (2), 631–675.

(10) Appel, A. M.; Helm, M. L. Determining the Overpotential for a Molecular Electrocatalyst. *ACS Catal.* **2014**, *4* (2), 630–633.

(11) Hori, Y. Electrochemical CO_2 Reduction on Metal Electrodes. In *Modern Aspects of Electrochemistry*; Vayenas, C. G., White, R. E., Gamboa-Aldeco, M. E., Eds.; 2008; pp 89–189.

(12) Lamy, E.; Nadjo, L.; Savéant, J. M. Standard Potential and Kinetic Parameters of the Electrochemical Reduction of Carbon Dioxide in Dimethylformamide. *Chem. Interfacial Electrochem.* **1977**, *78*, 403–407.

(13) Schwarz, H. A.; Dodson, R. W. Reduction Potentials of CO_2 - and the Alcohol Radicals. *J. Phys. Chem.* **1989**, *93* (1), 409–414.

(14) Komatsu, S. Electrochemical Reduction of CO_2 at Sb and Bi Electrodes in $KHCO_3$ Solution. *Denki Kagaku* **1995**, *63* (3), 217.

(15) Chen, Y.; Kanan, M. W. Tin Oxide Dependence of the CO_2 Reduction Efficiency on Tin Electrodes and Enhanced Activity for Tin/tin Oxide Thin-Film Catalysts. *J. Am. Chem. Soc.* **2012**, *134* (4), 1986–1989.

(16) Detweiler, Z. M.; White, J. L.; Bernasek, S. L.; Bocarsly, A. B. Anodized Indium Metal Electrodes for Enhanced Carbon Dioxide Reduction in Aqueous Electrolyte. *Langmuir* **2014**, *30* (25), 7593–7600.

(17) Barton, E. E.; Rampulla, D. M.; Bocarsly, A. B. Selective Solar-Driven Reduction of CO_2 to Methanol Using a Catalyzed P-GaP Based Photoelectrochemical Cell. *J. Am. Chem. Soc.* **2008**, *130*, 6342–6344.

(18) Ling, Y.; Wang, G.; Wheeler, D. A.; Zhang, J. Z.; Li, Y. Sn-Doped Hematite Nanostructures for Photoelectrochemical Water Splitting. *Nano Lett.* **2011**, *11* (5), 2119–2125.

(19) Hori, Y.; Wakebe, H.; Tsukamoto, T.; Koga, O. Electrocatalytic Process of CO Selectivity in Electrochemical Reduction of CO_2 at Metal Electrodes in Aqueous Media. *Electrochimica Acta* **1994**, *39*, 1833–1839.
(20) Lee, C. H.; Kanan, M. W. Controlling H+ vs CO_2 Reduction Selectivity on Pb Electrodes. *ACS Catal.* **2014**, *5* (1), 465–469.
(21) Baruch, M. F.; Pander, J.; White, J. L.; Bocarsly, A. B. Mechanistic Insights into the Reduction of CO_2 on Tin Electrodes Using In Situ ATR-IR Spectroscopy. *ACS Catal.* **2015**.
(22) Li, C. W.; Kanan, M. W. CO_2 Reduction at Low Overpotential on Cu Electrodes Resulting from the Reduction of Thick Cu_2O Films. *J. Am. Chem. Soc.* **2012**, *134* (17), 7231–7234.
(23) Chen, Y.; Li, C. W.; Kanan, M. W. Aqueous CO_2 Reduction at Very Low Overpotential on Oxide-Derived Au Nanoparticles. *J. Am. Chem. Soc.* **2012**, *134* (49), 19969–19972.
(24) Huynh, M. H. V.; Meyer, T. J. Proton-Coupled Electron Transfer. *Chem. Rev.* **2007**, *107* (11), 5004–5064.
(25) Costentin, C.; Robert, M.; Savéant, J.-M. Catalysis of the Electrochemical Reduction of Carbon Dioxide. *Chem. Soc. Rev.* **2013**, *42* (6), 2423–2436.
(26) Halmann, M. Photoelectrochemical Reduction of Aqueous Carbon Dioxide on P-Type Gallium Phosphide in Liquid Junction Solar Cells. *Nature* **1978**, *275* (5676), 115–116.
(27) Russell, P. G.; Kovac, N.; Srinivasan, S.; Steinberg, M. The Electrochemical Reduction of Carbon Dioxide, Formic Acid, and Formaldehyde. *J. Electrochem. Soc.* **1977**, *124* (9), 1329–1338.
(28) Bocarsly, A. B.; Tachikawa, H.; Faulkner, L. R. Photonic Electrochemistry. In *Laboratory Techniques in Electroanalytical Chemistry, Second Edition, Revised and Expanded*; Kissinger, P. T., Heineman, W. R., Eds.; CRC Press, 1996.
(29) Rajeshwar, K.; Ibanez, J. G. *Environmental Electrochemistry: Fundamentals and Applications in Pollution Sensors and Abatement*; Academic Press, 1997.
(30) Berger, L. I. *Semiconductor Materials*; CRC Press, 1996.
(31) Wang, J.; Tafen, D. N.; Lewis, J. P.; Hong, Z.; Manivannan, A.; Zhi, M.; Li, M.; Wu, N. Origin of Photocatalytic Activity of Nitrogen-Doped TiO_2 Nanobelts. *J. Am. Chem. Soc.* **2009**, *131* (34), 12290–12297.
(32) Li, J.; Wu, N. Semiconductor-Based Photocatalysts and Photoelectrochemical Cells for Solar Fuel Generation: A Review. *Catal. Sci. Technol.* **2014**.
(33) Meng, F.; Hong, Z.; Arndt, J.; Li, M.; Zhi, M.; Yang, F.; Wu, N. Visible Light Photocatalytic Activity of Nitrogen-Doped $La_2Ti_2O_7$ Nanosheets Originating from Band Gap Narrowing. *Nano Res.* **2012**, *5* (3), 213–221.
(34) van de Krol, R.; Grätzel, M. *Photoelectrochemical Hydrogen Production*; Springer Science & Business Media, 2011.
(35) Nozik, A. J. Photoelectrochemical Cells. *Philos. Trans. R. Soc. Lond. Ser. Math. Phys. Sci.* **1980**, *295* (1414), 453–470.
(36) Wang, Wei-Ning; Soulis, Johnathon; Yang, Y. Jeffrey; Biswas, Pratim. Comparison of CO_2 Photoreduction Systems: A Review. *Aerosol Air Qual. Res.* **2014**.
(37) Lewis, N. S. Mechanistic Studies of Light-Induced Charge Separation at Semiconductor/liquid Interfaces. *Acc. Chem. Res.* **1990**, *23* (6), 176–183.
(38) Castellano, R. *Solar Panel Processing*; Archives contemporaines, 2010.
(39) Chen, Z.; Dinh, H.; Miller, E. *Photoelectrochemical Water Splitting: Standards, Experimental Methods, and Protocols*; Springer Science & Business Media, 2013.

(40) Hamann, T. W.; Lewis, N. S. Control of the Stability, Electron-Transfer Kinetics, and pH-Dependent Energetics of Si/H_2O Interfaces through Methyl Termination of Si(111) Surfaces. *J. Phys. Chem. B* **2006**, *110* (45), 22291–22294.
(41) Gerischer, H. The Role of Semiconductor Structure and Surface Properties in Photoelectrochemical Processes. *J. Electroanal. Chem. Interfacial Electrochem.* **1983**, *150* (1–2), 553–569.
(42) Sze, S. M.; Ng, K. K. *Physics of Semiconductor Devices*, 3 edition.; Wiley-Interscience: Hoboken, N.J, 2006.
(43) Grovenor, C. R. M. Grain Boundaries in Semiconductors. *J. Phys. C Solid State Phys.* **1985**, *18* (21), 4079.
(44) Lenahan, P. M.; Schubert, W. K. Effects of Light and Modulation Frequency on Spin-Dependent Trapping at Silicon Grain Boundaries. *Phys. Rev. B* **1984**, *30* (3), 1544–1546.
(45) Kelly, J. J.; Memming, R. The Influence of Surface Recombination and Trapping on the Cathodic Photocurrent at p-Type III-V Electrodes. *J. Electrochem. Soc.* **1982**, *129* (4), 730–738.
(46) Peter, L. M.; Li, J.; Peat, R. Surface Recombination at Semiconductor Electrodes: Part I. Transient and Steady-State Photocurrents. *J. Electroanal. Chem. Interfacial Electrochem.* **1984**, *165* (1–2), 29–40.
(47) Nishida, M. A Theoretical Treatment of Charge Transfer via Surface States at a Semiconductor-electrolyte Interface: Analysis of the Water Photoelectrolysis Process. *J. Appl. Phys.* **1980**, *51* (3), 1669–1675.
(48) Indrakanti, V. P.; Schobert, H. H.; Kubicki, J. D. Quantum Mechanical Modeling of CO_2 Interactions with Irradiated Stoichiometric and Oxygen-Deficient Anatase TiO_2 Surfaces: Implications for the Photocatalytic Reduction of CO_2. *Energy Fuels* **2009**, *23* (10), 5247–5256.
(49) Tu, W.; Zhou, Y.; Zou, Z. Photocatalytic Conversion of CO_2 into Renewable Hydrocarbon Fuels: State-of-the-Art Accomplishment, Challenges, and Prospects. *Adv. Mater.* **2014**, *26* (27), 4607–4626.
(50) Yamanaka, K.; Sato, S.; Iwaki, M.; Kajino, T.; Morikawa, T. Photoinduced Electron Transfer from Nitrogen-Doped Tantalum Oxide to Adsorbed Ruthenium Complex. *J. Phys. Chem. C* **2011**, *115* (37), 18348–18353.
(51) Kumar, B.; Smieja, J. M.; Sasayama, A. F.; Kubiak, C. P. Tunable, Light-Assisted Co-Generation of CO and H_2 from CO_2 and H_2O by Re(bipy-tbu)$(CO)_3Cl$ and P-Si in Non-Aqueous Medium. *Chem. Commun.* **2011**, *48* (2), 272–274.
(52) Kou, Y.; Nakatani, S.; Sunagawa, G.; Tachikawa, Y.; Masui, D.; Shimada, T.; Takagi, S.; Tryk, D. A.; Nabetani, Y.; Tachibana, H.; et al. Visible Light-Induced Reduction of Carbon Dioxide Sensitized by a Porphyrin–rhenium Dyad Metal Complex on P-Type Semiconducting NiO as the Reduction Terminal End of an Artificial Photosynthetic System. *J. Catal.* **2014**, *310*, 57–66.
(53) Sato, S.; Arai, T.; Morikawa, T.; Uemura, K.; Suzuki, T. M.; Tanaka, H.; Kajino, T. Selective CO_2 Conversion to Formate Conjugated with H_2O Oxidation Utilizing Semiconductor/Complex Hybrid Photocatalysts. *J. Am. Chem. Soc.* **2011**, *133* (39), 15240–15243.
(54) Alenezi, K.; Ibrahim, S. K.; Li, P.; Pickett, C. J. Solar Fuels: Photoelectrosynthesis of CO from CO_2 at P-Type Si Using Fe Porphyrin Electrocatalysts. *Chem. – Eur. J.* **2013**, *19* (40), 13522–13527.

(55) Liu, Y.; Yang, Y.; Sun, Q.; Wang, Z.; Huang, B.; Dai, Y.; Qin, X.; Zhang, X. Chemical Adsorption Enhanced CO_2 Capture and Photoreduction over a Copper Porphyrin Based Metal Organic Framework. *ACS Appl. Mater. Interfaces* **2013**, *5* (15), 7654–7658.
(56) Yu, M.; Long, Y.-Z.; Sun, B.; Fan, Z. Recent Advances in Solar Cells Based on One-Dimensional Nanostructure Arrays. *Nanoscale* **2012**, *4* (9), 2783.
(57) Yoffe, A. D. Semiconductor Quantum Dots and Related Systems: Electronic, Optical, Luminescence and Related Properties of Low Dimensional Systems. *Adv. Phys.* **2001**, *50* (1), 1–208.
(58) Yoffe, A. D. Low-Dimensional Systems: Quantum Size Effects and Electronic Properties of Semiconductor Microcrystallites (zero-Dimensional Systems) and Some Quasi-Two-Dimensional Systems. *Adv. Phys.* **1993**, *42* (2), 173–262.
(59) Wang, C.; Thompson, R. L.; Baltrus, J.; Matranga, C. Visible Light Photoreduction of CO_2 Using CdSe/Pt/TiO_2 Heterostructured Catalysts. *J. Phys. Chem. Lett.* **2010**, *1* (1), 48–53.
(60) Yu, J.; Low, J.; Xiao, W.; Zhou, P.; Jaroniec, M. Enhanced Photocatalytic CO_2-Reduction Activity of Anatase TiO_2 by Coexposed {001} and {101} Facets. *J. Am. Chem. Soc.* **2014**, *136* (25), 8839–8842.
(61) Osterloh, F. E. Inorganic Nanostructures for Photoelectrochemical and Photocatalytic Water Splitting. *Chem. Soc. Rev.* **2013**, *42* (6), 2294–2320.
(62) Muskens, O. L.; Rivas, J. G.; Algra, R. E.; Bakkers, E. P. A. M.; Lagendijk, A. Design of Light Scattering in Nanowire Materials for Photovoltaic Applications. *Nano Lett.* **2008**, *8* (9), 2638–2642.
(63) Spurgeon, J. M.; Atwater, H. A.; Lewis, N. S. A Comparison Between the Behavior of Nanorod Array and Planar Cd(Se, Te) Photoelectrodes. *J. Phys. Chem. C* **2008**, *112* (15), 6186–6193.
(64) Baba, T. Slow Light in Photonic Crystals. *Nat. Photonics* **2008**, *2* (8), 465–473.
(65) Lokhande, C. D.; Pawar, S. H. Electrochemical Photovoltaic Cells for Solar Energy Conversion. *Mater. Chem. Phys.* **1984**, *11* (3), 201–277.
(66) Gerischer, H. On the Stability of Semiconductor Electrodes against Photodecomposition. *J. Electroanal. Chem. Interfacial Electrochem.* **1977**, *82* (1–2), 133–143.
(67) Gerischer, H. Photodecomposition of Semiconductors Thermodynamics, Kinetics and Application to Solar Cells. *Faraday Discuss. Chem. Soc.* **1980**, *70*, 137.
(68) Gerischer, H.; Gobrecht, J. On the Power-Characteristics of Electrochemical Solar Cells. *Berichte Bunsenges. Für Phys. Chem.* **1976**, *80* (4), 327–330.
(69) Rubin, H.-D.; Humphrey, B. D.; Bocarsly, A. B. Role of Surface Reactions in the Stabilization of N-CdS-Based Photoelectrochemical Cells. *Nature* **1984**, *308* (5957), 339–341.
(70) Park, S.-M.; Barber, M. E. Thermodynamic Stabilities of Semiconductor Electrodes. *J. Electroanal. Chem. Interfacial Electrochem.* **1979**, *99* (1), 67–75.
(71) Fan, F. R. F.; Bard, A. J. Semiconductor Electrodes. 24. Behavior of Photoelectrochemical Cells Based on P-Type Gallium Arsenide in Aqueous Solutions. *J. Am. Chem. Soc.* **1980**, *102* (11), 3677–3683.
(72) Halmann, M. Photochemical Fixation of Carbon Dioxide. In *Energy resources through photochemistry and catalysis*; Michael Grätzel, Ed.; Academic Press, 1983; pp 507–534.

(73) Jeyalakshmi, V.; Mahalakshmy, R.; Krishnamurthy, K. R.; Viswanathan, B. Photocatalytic Reduction of Carbon Dioxide by Water: A Step towards Sustainable Fuels and Chemicals. *Mater. Sci. Forum* **2012**, *734*, 1–62.
(74) Ikeda, S.; Kaname, I. The Photoelectrochemical Reduction of Carbon Dioxide as a Model of Artificial Photosynthesis. *Int. J. Sol. Energy* **1994**, *19* (1), 181–189.
(75) Ravindranathan Thampi, K.; McEvoy, A. J.; Grätzel, M. Photon Assisted Reduction of CO_2. In *Carbon dioxide chemistry : environmental issues*; Pradier, J. P., Pradier, C.-M., Eds.; Woodhead Publishing, 1994; pp 375–387.
(76) Roy, S. C.; Varghese, O. K.; Paulose, M.; Grimes, C. A. Toward Solar Fuels: Photocatalytic Conversion of Carbon Dioxide to Hydrocarbons. *ACS Nano* **2010**, *4* (3), 1259–1278.
(77) Kumar, B.; Llorente, M.; Froehlich, J.; Dang, T.; Sathrum, A.; Kubiak, C. P. Photochemical and Photoelectrochemical Reduction of CO_2. *Annu. Rev. Phys. Chem.* **2012**, *63* (1), 541–569.
(78) Anpo, M. Photocatalytic Reduction of CO_2 with H_2O on Highly Dispersed Ti-Oxide Catalysts as a Model of Artificial Photosynthesis. *J.* CO_2 *Util.* **2013**, *1*, 8–17.
(79) Liu, C.; Dasgupta, N. P.; Yang, P. Semiconductor Nanowires for Artificial Photosynthesis. *Chem. Mater.* **2014**, *26* (1), 415–422.
(80) Rongé, J.; Bosserez, T.; Martel, D.; Nervi, C.; Boarino, L.; Taulelle, F.; Decher, G.; Bordiga, S.; Martens, J. A. Monolithic Cells for Solar Fuels. *Chem. Soc. Rev.* **2014**, *43* (23), 7963–7981.
(81) Grätzel, M. Photoelectrochemical Cells. *Nature* **2001**, *414* (6861), 338–344.
(82) Habisreutinger, S. N.; Schmidt-Mende, L.; Stolarczyk, J. K. Photocatalytic Reduction of CO_2 on TiO_2 and Other Semiconductors. *Angew. Chem. Int. Ed.* **2013**, *52* (29), 7372–7408.
(83) Taniguchi, I.; Aurian-Blajeni, B.; Bockris, J. O. The Reduction of Carbon Dioxide at Illuminated P-Type Semiconductor Electrodes in Nonaqueous Media. *Electrochimica Acta* **1984**, *29* (7), 923–932.
(84) Junfu, L.; Baozhu, C. Photoelectrochemical Reduction of Carbon Dioxide on a P+/p-Si Photocathode in Aqueous Electrolyte. *J. Electroanal. Chem.* **1992**, *324* (1–2), 191–200.
(85) Hirota, K.; Tryk, D. A.; Yamamoto, T.; Hashimoto, K.; Okawa, M.; Fujishima, A. Photoelectrochemical Reduction of CO_2 in a High-Pressure CO_2 + Methanol Medium at P-Type Semiconductor Electrodes. *J. Phys. Chem. B* **1998**, *102* (49), 9834–9843.
(86) Aurian-Blajeni, B.; Taniguchi, I.; Bockris, J. O. Photoelectrochemical Reduction of Carbon Dioxide Using Polyaniline-Coated Silicon. *J. Electroanal. Chem. Interfacial Electrochem.* **1983**, *149* (1–2), 291–293.
(87) Hinogami, R.; Nakamura, Y.; Yae, S.; Nakato, Y. Modification of Semiconductor Surface with Ultrafine Metal Particles for Efficient Photoelectrochemical Reduction of Carbon Dioxide. *Appl. Surf. Sci.* **1997**, *121–122*, 301–304.
(88) Hinogami, R.; Nakamura, Y.; Yae, S.; Nakato, Y. An Approach to Ideal Semiconductor Electrodes for Efficient Photoelectrochemical Reduction of Carbon Dioxide by Modification with Small Metal Particles. *J. Phys. Chem. B* **1998**, *102* (6), 974–980.
(89) Ono, H.; Yokosuka, A.; Tasiro, T.; Morisaki, H.; Yugo, S. Characterization of Diamond-Coated Si Electrodes for Photoelectrochemical Reduction of CO_2, *New Diam. Front. Carbon Technol.* **2002**, *12*, 141–144.

(90) Gondal, M. A.; Ali, M. A.; Dastageer, M. A.; Chang, X. CO_2 Conversion into Methanol Using Granular Silicon Carbide (α6H-SiC): A Comparative Evaluation of 355 Nm Laser and Xenon Mercury Broad Band Radiation Sources. *Catal. Lett.* **2013**, *143* (1), 108–117.
(91) Cook, R. L.; MacDuff, R. C.; Sammells, A. F. Photoelectrochemical Carbon Dioxide Reduction to Hydrocarbons at Ambient Temperature and Pressure. *J. Electrochem. Soc.* **1988**, *135* (12), 3069–3070.
(92) Dzhabiev, T. S.; Tarasov, B. B.; Uskov, A. M. Photocatalytic Reduction of Carbon Dioxide in Aqueous Semiconductor Suspensions. *Catal. Today* **1992**, *13* (4), 695–696.
(93) Zhang, P.; Hou, X. L.; Mi, J. L.; Jiang, Q.; Aslan, H.; Dong, M. D. Curvature Effect of SiC Nanotubes and Sheets for CO_2 Capture and Reduction. *RSC Adv.* **2014**, *4* (90), 48994–48999.
(94) Taniguchi, Y.; Yoneyama, H.; Tamura, H. Photoelectrochemical Reduction of Carbon Dioxide at P-Type Gallium Phosphide Electrodes in the Presence of Crown Ether. *Bull. Chem. Soc. Jpn.* **1982**, *55* (7), 2034–2039.
(95) Aurian-Blajeni, B.; Halmann, M.; Manassen, J. Electrochemical Measurement on the Photoelectrochemical Reduction of Aqueous Carbon Dioxide on P-Gallium Phosphide and P-Gallium Arsenide Semiconductor Electrodes. *Sol. Energy Mater.* **1983**, *8* (4), 425–440.
(96) Ito, K.; Ikeda, S.; Yoshida, M.; Ohta, S.; Iida, T. On the Reduction Products of Carbon Dioxide at a P-Type Gallium Phosphide Photocathode in Aqueous Electrolytes. *Bull. Chem. Soc. Jpn.* **1984**, *57* (2), 583–584.
(97) Noda, H.; Yamamoto, A.; Ikeda, S.; Maeda, M.; Ito, K. Influence of Light Intensity on Photoe1ectroreduction of CO_2 at a p-GaP Photocathode. *Chem. Lett.* **1990**, *19* (9), 1757–1760.
(98) Ikeda, S.; Yamamoto, A.; Noda, H.; Maeda, M.; Ito, K. Influence of Surface Treatment of the P-GaP Photocathode on the Photoelectrochemical Reduction of Carbon Dioxide. *Bull. Chem. Soc. Jpn.* **1993**, *66* (9), 2473–2477.
(99) Flaisher, H.; Tenne, R.; Halmann, M. Photoelectrochemical Reduction of Carbon Dioxide in Aqueous Solutions on P-GaP Electrodes: An A.c. Impedance Study with Phase-Sensitive Detection. *J. Electroanal. Chem.* **1996**, *402* (1–2), 97–105.
(100) Guruswamy, V.; Bockris, J. O. The Photo-Electrochemical Production of C-C Bonds from Carbon Dioxide. *Int. J. Energy Res.* **1979**, *3* (4), 397–399.
(101) Muñoz-García, A. B.; Carter, E. A. Non-Innocent Dissociation of H_2O on GaP(110): Implications for Electrochemical Reduction of CO_2. *J. Am. Chem. Soc.* **2012**, *134* (33), 13600–13603.
(102) Keith, J. A.; Muñoz-García, A. B.; Lessio, M.; Carter, E. A. Cluster Models for Studying CO_2 Reduction on Semiconductor Photoelectrodes. *Top. Catal.* **2014**, *58* (1), 46–56.
(103) Kronawitter, C. X.; Lessio, M.; Zhao, P.; Riplinger, C.; Boscoboinik, A.; Starr, D. E.; Sutter, P.; Carter, E. A.; Koel, B. E. Observation of Surface-Bound Negatively Charged Hydride and Hydroxide on GaP(110) in H_2O Environments. *J. Phys. Chem. C* **2015**, *119* (31), 17762–17772.
(104) Kaneco, S.; Katsumata, H.; Suzuki, T.; Ohta, K. Photoelectrochemical Reduction of Carbon Dioxide at P-Type Gallium Arsenide and P-Type Indium Phosphide Electrodes in Methanol. *Chem. Eng. J.* **2006**, *116* (3), 227–231.
(105) Yoneyama, H.; Sugimura, K.; Kuwabata, S. Effects of Electrolytes on the Photoelectrochemical Reduction of Carbon Dioxide at Illuminated P-Type Cadmium

Telluride and P-Type Indium Phosphide Electrodes in Aqueous Solutions. *J. Electroanal. Chem. Interfacial Electrochem.* **1988**, *249* (1–2), 143–153.
(106) Hirota, K.; Tryk, D. A.; Hashimoto, K.; Okawa, M.; Fujishima, A. Photoelectrochemical Reduction of CO_2 at High Current Densities at p-InP Electrodes. *J. Electrochem. Soc.* **1998**, *145* (5), L82–L84.
(107) Kaneco, S.; Katsumata, H.; Suzuki, T.; Ohta, K. Photoelectrocatalytic Reduction of CO_2 in LiOH/methanol at Metal-Modified P-InP Electrodes. *Appl. Catal. B Environ.* **2006**, *64* (1–2), 139–145.
(108) Kaneco, S.; Ueno, Y.; Katsumata, H.; Suzuki, T.; Ohta, K. Photoelectrochemical Reduction of CO_2 at P-InP Electrode in Copper Particle-Suspended Methanol. *Chem. Eng. J.* **2009**, *148* (1), 57–62.
(109) Fujishima, A.; Rao, T. N.; Tryk, D. A. Titanium Dioxide Photocatalysis. *J. Photochem. Photobiol. C Photochem. Rev.* **2000**, *1* (1), 1–21.
(110) Konstantinou, I. K.; Albanis, T. A. TiO_2-Assisted Photocatalytic Degradation of Azo Dyes in Aqueous Solution: Kinetic and Mechanistic Investigations: A Review. *Appl. Catal. B Environ.* **2004**, *49* (1), 1–14.
(111) Aurian-Blajeni, B.; Halmann, M.; Manassen, J. Photoreduction of Carbon Dioxide and Water into Formaldehyde and Methanol on Semiconductor Materials. *Sol. Energy* **1980**, *25* (2), 165–170.
(112) Anpo, M.; Takeuchi, M. The Design and Development of Highly Reactive Titanium Oxide Photocatalysts Operating under Visible Light Irradiation. *J. Catal.* **2003**, *216* (1–2), 505–516.
(113) Usubharatana, P.; McMartin, D.; Veawab, A.; Tontiwachwuthikul, P. Photocatalytic Process for CO_2 Emission Reduction from Industrial Flue Gas Streams. *Ind. Eng. Chem. Res.* **2006**, *45* (8), 2558–2568.
(114) Kitano, M.; Matsuoka, M.; Ueshima, M.; Anpo, M. Recent Developments in Titanium Oxide-Based Photocatalysts. *Appl. Catal. Gen.* **2007**, *325* (1), 1–14.
(115) Dey, G. R. Chemical Reduction of CO_2 to Different Products during Photo Catalytic Reaction on TiO_2 under Diverse Conditions: An Overview. *J. Nat. Gas Chem.* **2007**, *16* (3), 217–226.
(116) Indrakanti, V. P.; Kubicki, J. D.; Schobert, H. H. Photoinduced Activation of CO_2 on Ti-Based Heterogeneous Catalysts: Current State, Chemical Physics-Based Insights and Outlook. *Energy Environ. Sci.* **2009**, *2* (7), 745–758.
(117) He, H.; Liu, C.; Dubois, K. D.; Jin, T.; Louis, M. E.; Li, G. Enhanced Charge Separation in Nanostructured TiO_2 Materials for Photocatalytic and Photovoltaic Applications. *Ind. Eng. Chem. Res.* **2012**, *51* (37), 11841–11849.
(118) Schwartzenberg, K. C.; Gray, K. A. Nanostructured Titania: The Current and Future Promise of Titania Nanotubes. *Catal. Sci. Technol.* **2012**, *2* (8), 1617–1624.
(119) Mori, K.; Yamashita, H.; Anpo, M. Photocatalytic Reduction of CO_2 with H_2O on Various Titanium Oxide Photocatalysts. *RSC Adv.* **2012**, *2* (8), 3165–3172.
(120) Dhakshinamoorthy, A.; Navalon, S.; Corma, A.; Garcia, H. Photocatalytic CO_2 Reduction by TiO_2 and Related Titanium Containing Solids. *Energy Environ. Sci.* **2012**, *5* (11), 9217–9233.
(121) Izumi, Y. Recent Advances in the Photocatalytic Conversion of Carbon Dioxide to Fuels with Water And/or Hydrogen Using Solar Energy and beyond. *Coord. Chem. Rev.* **2013**, *257* (1), 171–186.

(122) Corma, A.; Garcia, H. Photocatalytic Reduction of CO_2 for Fuel Production: Possibilities and Challenges. *J. Catal.* **2013**, *308*, 168–175.
(123) Ma, Y.; Wang, X.; Jia, Y.; Chen, X.; Han, H.; Li, C. Titanium Dioxide-Based Nanomaterials for Photocatalytic Fuel Generations. *Chem. Rev.* **2014**, *114* (19), 9987–10043.
(124) Fuku, K.; Mori, K.; Yamashita, H. Reductive Conversion of Carbon Dioxide Using Various Photocatalyst Materials. In *Transformation and Utilization of Carbon Dioxide*; Bhanage, B. M., Arai, M., Eds.; Green Chemistry and Sustainable Technology; Springer Berlin Heidelberg, 2014; pp 225–244.
(125) Zhou, Q.; Fang, Z.; Li, J.; Wang, M. Applications of CO_2 Nanotube Arrays in Environmental and Energy Fields: A Review. *Microporous Mesoporous Mater.* **2015**, *202*, 22–35.
(126) Yamashita, H.; Nishiguchi, H.; Kamada, N.; Anpo, M.; Teraoka, Y.; Hatano, H.; Ehara, S.; Kikui, K.; Palmisano, L.; Sclafani, A.; et al. Photocatalytic Reduction of CO_2 with H_2O on TiO_2 and Cu/TiO_2 Catalysts. *Res. Chem. Intermed.* **1994**, *20* (8), 815–823.
(127) Anpo, M.; Yamashita, H.; Ichihashi, Y.; Ehara, S. Photocatalytic Reduction of CO_2 with H_2O on Various Titanium Oxide Catalysts. *J. Electroanal. Chem.* **1995**, *396*, 21–26.
(128) Chen, L.; Graham, M. E.; Li, G.; Gentner, D. R.; Dimitrijevic, N. M.; Gray, K. A. Photoreduction of CO_2 by TiO_2 Nanocomposites Synthesized through Reactive Direct Current Magnetron Sputter Deposition. *Thin Solid Films* **2009**, *517* (19), 5641–5645.
(129) Schulte, K. L.; DeSario, P. A.; Gray, K. A. Effect of Crystal Phase Composition on the Reductive and Oxidative Abilities of TiO_2 Nanotubes under UV and Visible Light. *Appl. Catal. B Environ.* **2010**, *97* (3–4), 354–360.
(130) Liu, L.; Zhao, H.; Andino, J. M.; Li, Y. Photocatalytic CO_2 Reduction with H_2O on TiO_2 Nanocrystals: Comparison of Anatase, Rutile, and Brookite Polymorphs and Exploration of Surface Chemistry. *ACS Catal.* **2012**, *2* (8), 1817–1828.
(131) Tseng, I.-H.; Chang, W.-C.; Wu, J. C. S. Photoreduction of CO_2 Using Sol–gel Derived Titania and Titania-Supported Copper Catalysts. *Appl. Catal. B Environ.* **2002**, *37* (1), 37–48.
(132) Hurum, D. C.; Agrios, A. G.; Gray, K. A.; Rajh, T.; Thurnauer, M. C. Explaining the Enhanced Photocatalytic Activity of Degussa P25 Mixed-Phase TiO_2 Using EPR. *J. Phys. Chem. B* **2003**, *107* (19), 4545–4549.
(133) Saladin, F.; Forss, L.; Kamber, I. Photosynthesis of CH4 at a TiO_2 Surface from Gaseous H_2O and CO_2. *J. Chem. Soc. Chem. Commun.* **1995**, No. 5, 533–534.
(134) Wang, P.-Q.; Bai, Y.; Liu, J.-Y.; Fan, Z.; Hu, Y.-Q. One-Pot Synthesis of Rutile TiO_2 Nanoparticle Modified Anatase TiO_2 Nanorods toward Enhanced Photocatalytic Reduction of CO_2 into Hydrocarbon Fuels. *Catal. Commun.* **2012**, *29*, 185–188.
(135) Wang, W.-N.; An, W.-J.; Ramalingam, B.; Mukherjee, S.; Niedzwiedzki, D. M.; Gangopadhyay, S.; Biswas, P. Size and Structure Matter: Enhanced CO_2 Photoreduction Efficiency by Size-Resolved Ultrafine Pt Nanoparticles on TiO_2 Single Crystals. *J. Am. Chem. Soc.* **2012**, *134* (27), 11276–11281.
(136) Liu, L. Understanding the Reaction Mechanism of Photocatalytic Reduction of CO_2 with H_2O on TiO_2-Based Photocatalysts: A Review. *Aerosol Air Qual. Res.* **2014**, *14* (2), 453–469.
(137) Rasko, J.; Solymosi, F. Infrared Spectroscopic Study of the Photoinduced Activation of CO_2 on TiO_2 and Rh/TiO_2 Catalysts. *J. Phys. Chem.* **1994**, *98* (29), 7147–7152.

(138) Dimitrijevic, N. M.; Vijayan, B. K.; Poluektov, O. G.; Rajh, T.; Gray, K. A.; He, H.; Zapol, P. Role of Water and Carbonates in Photocatalytic Transformation of CO_2 to CH4 on Titania. *J. Am. Chem. Soc.* **2011**, *133* (11), 3964–3971.
(139) Sathish, M.; Viswanathan, B.; Viswanath, R. P.; Gopinath, C. S. Synthesis, Characterization, Electronic Structure, and Photocatalytic Activity of Nitrogen-Doped TiO_2 Nanocatalyst. *Chem. Mater.* **2005**, *17* (25), 6349–6353.
(140) Varghese, O. K.; Paulose, M.; LaTempa, T. J.; Grimes, C. A. High-Rate Solar Photocatalytic Conversion of CO_2 and Water Vapor to Hydrocarbon Fuels. *Nano Lett.* **2009**, *9* (2), 731–737.
(141) Zhang, Q.; Li, Y.; Ackerman, E. A.; Gajdardziska-Josifovska, M.; Li, H. Visible Light Responsive Iodine-Doped TiO_2 for Photocatalytic Reduction of CO_2 to Fuels. *Appl. Catal. Gen.* **2011**, *400* (1–2), 195–202.
(142) Zhao, C.; Liu, L.; Zhang, Q.; Wang, J.; Li, Y. Photocatalytic Conversion of CO_2 and H_2O to Fuels by Nanostructured Ce–TiO_2 /SBA-15 Composites. *Catal. Sci. Technol.* **2012**, *2* (12), 2558–2568.
(143) Li, X.; Zhuang, Z.; Li, W.; Pan, H. Photocatalytic Reduction of CO_2 over Noble Metal-Loaded and Nitrogen-Doped Mesoporous TiO_2. *Appl. Catal. Gen.* **2012**, *429–430*, 31–38.
(144) Michalkiewicz, B.; Majewska, J.; Kądziołka, G.; Bubacz, K.; Mozia, S.; Morawski, A. W. Reduction of CO_2 by Adsorption and Reaction on Surface of TiO_2-Nitrogen Modified Photocatalyst. *J. CO_2 Util.* **2014**, *5*, 47–52.
(145) He, Z.; Wen, L.; Wang, D.; Xue, Y.; Lu, Q.; Wu, C.; Chen, J.; Song, S. Photocatalytic Reduction of CO_2 in Aqueous Solution on Surface-Fluorinated Anatase TiO_2 Nanosheets with Exposed {001} Facets. *Energy Fuels* **2014**, *28* (6), 3982–3993.
(146) Lee, C.-W.; Antoniou Kourounioti, R.; Wu, J. C. S.; Murchie, E.; Maroto-Valer, M.; Jensen, O. E.; Huang, C.-W.; Ruban, A. Photocatalytic Conversion of CO_2 to Hydrocarbons by Light-Harvesting Complex Assisted Rh-Doped TiO_2 Photocatalyst. *J. CO_2 Util.* **2014**, *5*, 33–40.
(147) Yang, C.-T.; Wood, B. C.; Bhethanabotla, V. R.; Joseph, B. CO_2 Adsorption on Anatase TiO_2(101) Surfaces in the Presence of Subnanometer Ag/Pt Clusters: Implications for CO_2 hotoreduction. *J. Phys. Chem. C* **2014**, *118* (45), 26236–26248.
(148) Lee, J.; Sorescu, D. C.; Deng, X. Electron-Induced Dissociation of CO_2 on TiO_2(110). *J. Am. Chem. Soc.* **2011**, *133* (26), 10066–10069.
(149) Inoue, T.; Fujishima, A.; Konishi, S.; Honda, K. Photoelectrocatalytic Reduction of Carbon Dioxide in Aqueous Suspensions of Semiconductor Powders. *Nature* **1979**, *277* (5698), 637–638.
(150) Halmann, M.; Ulman, M.; Aurian-Blajeni, B. Photochemical Solar Collector for the Photoassisted Reduction of Aqueous Carbon Dioxide. *Sol. Energy* **1983**, *31* (4), 429–431.
(151) Anpo, M.; Aikawa, N.; Kubokawa, Y.; Che, M.; Louis, C.; Giamello, E. Photoluminescence and Photocatalytic Activity of Highly Dispersed Titanium Oxide Anchored onto Porous Vycor Glass. *J. Phys. Chem.* **1985**, *89* (23), 5017–5021.
(152) Anpo, M.; Chiba, K. Photocatalytic Reduction of CO_2 on Anchored Titanium Oxide Catalysts. *J. Mol. Catal.* **1992**, *74* (1–3), 207–212.
(153) Yamashita, H.; Shiga, A.; Kawasaki, S.; Ichihashi, Y.; Ehara, S.; Anpo, M. Photocatalytic Synthesis of CH4 and CH3OH from CO_2 and H_2O on Highly Dispersed Active Titanium Oxide Catalysts. *Energy Convers. Manag.* **1995**, *36* (6–9), 617–620.

(154) Dey, G. R.; Belapurkar, A. D.; Kishore, K. Photo-Catalytic Reduction of Carbon Dioxide to Methane Using TiO_2 as Suspension in Water. *J. Photochem. Photobiol. Chem.* **2004**, *163* (3), 503–508.
(155) Kočí, K.; Obalová, L.; Matějová, L.; Plachá, D.; Lacný, Z.; Jirkovský, J.; Šolcová, O. Effect of TiO_2 Particle Size on the Photocatalytic Reduction of CO_2. *Appl. Catal. B Environ.* **2009**, *89* (3–4), 494–502.
(156) Lin, H.; Huang, C. P.; Li, W.; Ni, C.; Shah, S. I.; Tseng, Y.-H. Size Dependency of Nanocrystalline TiO_2 on Its Optical Property and Photocatalytic Reactivity Exemplified by 2-Chlorophenol. *Appl. Catal. B Environ.* **2006**, *68* (1–2), 1–11.
(157) Yamashita, H.; Kamada, N.; He, H.; Tanaka, K.; Ehara, S.; Anpo, M. Reduction of CO_2 with H_2O on TiO_2 (100) and TiO_2 (110) Single Crystals under UV-Irradiation. *Chem. Lett.* **1994**, *23* (5), 855–858.
(158) Pan, J.; Liu, G.; Lu, G. Q. (Max); Cheng, H.-M. On the True Photoreactivity Order of {001}, {010}, and {101} Facets of Anatase TiO_2 Crystals. *Angew. Chem. Int. Ed.* **2011**, *50* (9), 2133–2137.
(159) Xu, H.; Ouyang, S.; Li, P.; Kako, T.; Ye, J. High-Active Anatase TiO_2 Nanosheets Exposed with 95% {100} Facets Toward Efficient H2 Evolution and CO_2 Photoreduction. *ACS Appl. Mater. Interfaces* **2013**, *5* (4), 1348–1354.
(160) Vijayan, B.; Dimitrijevic, N. M.; Rajh, T.; Gray, K. Effect of Calcination Temperature on the Photocatalytic Reduction and Oxidation Processes of Hydrothermally Synthesized Titania Nanotubes. *J. Phys. Chem. C* **2010**, *114* (30), 12994–13002.
(161) Linsebigler, A. L.; Lu, G.; Yates, J. T. Photocatalysis on TiO_2 Surfaces: Principles, Mechanisms, and Selected Results. *Chem. Rev.* **1995**, *95* (3), 735–758.
(162) Tseng, I.-H.; Wu, J. C.-S. Chemical States of Metal-Loaded Titania in the Photoreduction of CO_2. *Catal. Today* **2004**, *97* (2–3), 113–119.
(163) Ganesh, I. Conversion of Carbon Dioxide into Methanol – a Potential Liquid Fuel: Fundamental Challenges and Opportunities (a Review). *Renew. Sustain. Energy Rev.* **2014**, *31*, 221–257.
(164) Hou, W.; Hung, W. H.; Pavaskar, P.; Goeppert, A.; Aykol, M.; Cronin, S. B. Photocatalytic Conversion of CO_2 to Hydrocarbon Fuels via Plasmon-Enhanced Absorption and Metallic Interband Transitions. *ACS Catal.* **2011**, *1* (8), 929–936.
(165) Xie, S.; Wang, Y.; Zhang, Q.; Deng, W.; Wang, Y. MgO- and Pt-Promoted TiO_2 as an Efficient Photocatalyst for the Preferential Reduction of Carbon Dioxide in the Presence of Water. *ACS Catal.* **2014**, *4* (10), 3644–3653.
(166) Hirano, K.; Inoue, K.; Yatsu, T. Photocatalysed Reduction of CO_2 in Aqueous TiO_2 Suspension Mixed with Copper Powder. *J. Photochem. Photobiol. Chem.* **1992**, *64* (2), 255–258.
(167) Adachi, K.; Ohta, K.; Mizuno, T. Photocatalytic Reduction of Carbon Dioxide to Hydrocarbon Using Copper-Loaded Titanium Dioxide. *Sol. Energy* **1994**, *53* (2), 187–190.
(168) Wu, J. C. S.; Lin, H.-M.; Lai, C.-L. Photo Reduction of CO_2 to Methanol Using Optical-Fiber Photoreactor. *Appl. Catal. Gen.* **2005**, *296* (2), 194–200.
(169) Tan, J. Z. Y.; Fernández, Y.; Liu, D.; Maroto-Valer, M.; Bian, J.; Zhang, X. Photoreduction of CO_2 Using Copper-Decorated TiO_2 Nanorod Films with Localized Surface Plasmon Behavior. *Chem. Phys. Lett.* **2012**, *531*, 149–154.

(170) Rani, S.; Bao, N.; Roy, S. C. Solar Spectrum Photocatalytic Conversion of CO_2 and Water Vapor Into Hydrocarbons Using TiO_2 Nanoparticle Membranes. *Appl. Surf. Sci.* **2014**, *289*, 203–208.
(171) Zhang, X.; Han, F.; Shi, B.; Farsinezhad, S.; Dechaine, G. P.; Shankar, K. Photocatalytic Conversion of Diluted CO_2 into Light Hydrocarbons Using Periodically Modulated Multiwalled Nanotube Arrays. *Angew. Chem. Int. Ed.* **2012**, *51* (51), 12732–12735.
(172) Zhai, Q.; Xie, S.; Fan, W.; Zhang, Q.; Wang, Y.; Deng, W.; Wang, Y. Photocatalytic Conversion of Carbon Dioxide with Water into Methane: Platinum and Copper(I) Oxide Co-Catalysts with a Core–Shell Structure. *Angew. Chem.* **2013**, *125* (22), 5888–5891.
(173) Neaţu, Ş.; Maciá-Agulló, J. A.; Concepción, P.; Garcia, H. Gold–Copper Nanoalloys Supported on TiO_2 as Photocatalysts for CO_2 Reduction by Water. *J. Am. Chem. Soc.* **2014**, *136* (45), 15969–15976.
(174) Zhang, Q.-H.; Han, W.-D.; Hong, Y.-J.; Yu, J.-G. Photocatalytic Reduction of CO_2 with H_2O on Pt-Loaded TiO_2 Catalyst. *Catal. Today* **2009**, *148* (3–4), 335–340.
(175) Feng, X.; Sloppy, J. D.; LaTempa, T. J.; Paulose, M.; Komarneni, S.; Bao, N.; Grimes, C. A. Synthesis and Deposition of Ultrafine Pt Nanoparticles within High Aspect Ratio TiO_2 Nanotube Arrays: Application to the Photocatalytic Reduction of Carbon Dioxide. *J. Mater. Chem.* **2011**, *21* (35), 13429–13433.
(176) Wang, Y.; Lai, Q.; Zhang, F.; Shen, X.; Fan, M.; He, Y.; Ren, S. High Efficiency Photocatalytic Conversion of CO_2 with H_2O over Pt/TiO_2 Nanoparticles. *RSC Adv.* **2014**, *4* (84), 44442–44451.
(177) Yui, T.; Kan, A.; Saitoh, C.; Koike, K.; Ibusuki, T.; Ishitani, O. Photochemical Reduction of CO_2 Using TiO_2 : Effects of Organic Adsorbates on TiO_2 and Deposition of Pd onto TiO_2. *ACS Appl. Mater. Interfaces* **2011**, *3* (7), 2594–2600.
(178) Sasirekha, N.; Basha, S. J. S.; Shanthi, K. Photocatalytic Performance of Ru Doped Anatase Mounted on Silica for Reduction of Carbon Dioxide. *Appl. Catal. B Environ.* **2006**, *62* (1–2), 169–180.
(179) Tahir, M.; Amin, N. S. Indium-Doped TiO_2 Nanoparticles for Photocatalytic CO_2 Reduction with H_2O Vapors to CH4. *Appl. Catal. B Environ.* **2015**, *162*, 98–109.
(180) Xia, X.-H.; Jia, Z.-J.; Yu, Y.; Liang, Y.; Wang, Z.; Ma, L.-L. Preparation of Multi-Walled Carbon Nanotube Supported TiO_2 and Its Photocatalytic Activity in the Reduction of CO_2 with H_2O. *Carbon* **2007**, *45* (4), 717–721.
(181) Liang, Y. T.; Vijayan, B. K.; Gray, K. A.; Hersam, M. C. Minimizing Graphene Defects Enhances Titania Nanocomposite-Based Photocatalytic Reduction of CO_2 for Improved Solar Fuel Production. *Nano Lett.* **2011**, *11* (7), 2865–2870.
(182) Asahi, R.; Morikawa, T.; Irie, H.; Ohwaki, T. Nitrogen-Doped Titanium Dioxide as Visible-Light-Sensitive Photocatalyst: Designs, Developments, and Prospects. *Chem. Rev.* **2014**, *114* (19), 9824–9852.
(183) Bubacz, K.; Choina, J.; Dolat, D.; Borowiak-Paleń, E.; Moszyński, D.; Morawski, A. W. Studies on Nitrogen Modified TiO_2 Photocatalyst Prepared in Different Conditions. *Mater. Res. Bull.* **2010**, *45* (9), 1085–1091.
(184) Lu, D.; Zhang, M.; Zhang, Z.; Li, Q.; Wang, X.; Yang, J. Self-Organized Vanadium and Nitrogen Co-Doped Titania Nanotube Arrays with Enhanced Photocatalytic Reduction of CO_2 into CH_4. *Nanoscale Res. Lett.* **2014**, *9* (1), 272.

(185) Xiong, Z.; Zhao, Y.; Zhang, J.; Zheng, C. Efficient Photocatalytic Reduction of CO_2 into Liquid Products over Cerium Doped Titania Nanoparticles Synthesized by a Sol–gel Auto-Ignited Method. *Fuel Process. Technol.* **2015**.
(186) Grätzel, M. Dye-Sensitized Solar Cells. *J. Photochem. Photobiol. C Photochem. Rev.* **2003**, *4* (2), 145–153.
(187) Finkelstein-Shapiro, D.; Petrosko, S. H.; Dimitrijevic, N. M.; Gosztola, D.; Gray, K. A.; Rajh, T.; Tarakeshwar, P.; Mujica, V. CO_2 Preactivation in Photoinduced Reduction via Surface Functionalization of TiO_2 Nanoparticles. *J. Phys. Chem. Lett.* **2013**, *4* (3), 475–479.
(188) Nguyen, T.-V.; Wu, J. C. S.; Chiou, C.-H. Photoreduction of CO_2 over Ruthenium Dye-Sensitized TiO_2-Based Catalysts under Concentrated Natural Sunlight. *Catal. Commun.* **2008**, *9* (10), 2073–2076.
(189) Ozcan, O.; Yukruk, F.; Akkaya, E. U.; Uner, D. Dye Sensitized Artificial Photosynthesis in the Gas Phase over Thin and Thick TiO_2 Films under UV and Visible Light Irradiation. *Appl. Catal. B Environ.* **2007**, *71* (3–4), 291–297.
(190) Ozcan, O.; Yukruk, F.; Akkaya, E. U.; Uner, D. Dye Sensitized CO_2 Reduction over Pure and Platinized TiO_2. *Top. Catal.* **2007**, *44* (4), 523–528.
(191) Liu, S.; Zhao, Z.; Wang, Z. Photocatalytic Reduction of Carbon Dioxide Using Sol–gel Derived Titania-Supported CoPc Catalysts. *Photochem. Photobiol. Sci.* **2007**, *6* (6), 695–700.
(192) Zhao, Z.-H.; Fan, J.-M.; Wang, Z.-Z. Photo-Catalytic CO_2 Reduction Using Sol–gel Derived Titania-Supported Zinc-Phthalocyanine. *J. Clean. Prod.* **2007**, *15* (18), 1894–1897.
(193) Zhao, Z.; Fan, J.; Xie, M.; Wang, Z. Photo-Catalytic Reduction of Carbon Dioxide with in-Situ Synthesized CoPc/TiO_2 under Visible Light Irradiation. *J. Clean. Prod.* **2009**, *17* (11), 1025–1029.
(194) Jin, T.; Liu, C.; Li, G. Photocatalytic CO_2 Reduction Using a Molecular Cobalt Complex Deposited on TiO_2 Nanoparticles. *Chem. Commun.* **2014**, *50* (47), 6221–6224.
(195) Neri, G.; Walsh, J. J.; Wilson, C.; Reynal, A.; Lim, J. Y. C.; Li, X.; White, A. J. P.; Long, N. J.; Durrant, J. R.; Cowan, A. J. A Functionalised Nickel Cyclam Catalyst for CO_2 Reduction: Electrocatalysis, Semiconductor Surface Immobilisation and Light-Driven Electron Transfer. *Phys. Chem. Chem. Phys.* **2015**, *17* (3), 1562–1566.
(196) Cecchet, F.; Alebbi, M.; Bignozzi, C. A.; Paolucci, F. Efficiency Enhancement of the Electrocatalytic Reduction of CO_2: Fac-[Re(v-bpy)(CO)3Cl] Electropolymerized onto Mesoporous TiO Electrodes. *Inorganica Chim. Acta* **2006**, *359* (12), 3871–3874.
(197) Anfuso, C. L.; Snoeberger, R. C.; Ricks, A. M.; Liu, W.; Xiao, D.; Batista, V. S.; Lian, T. Covalent Attachment of a Rhenium Bipyridyl CO_2 Reduction Catalyst to Rutile TiO_2. *J. Am. Chem. Soc.* **2011**, *133* (18), 6922–6925.
(198) Anfuso, C. L.; Xiao, D.; Ricks, A. M.; Negre, C. F. A.; Batista, V. S.; Lian, T. Orientation of a Series of *CO_2* Reduction Catalysts on Single Crystal TiO_2 Probed by Phase-Sensitive Vibrational Sum Frequency Generation Spectroscopy (PS-VSFG). *J. Phys. Chem. C* **2012**, *116* (45), 24107–24114.
(199) Woolerton, T. W.; Sheard, S.; Reisner, E.; Pierce, E.; Ragsdale, S. W.; Armstrong, F. A. Efficient and Clean Photoreduction of CO_2 to CO by Enzyme-Modified TiO_2 Nanoparticles Using Visible Light. *J. Am. Chem. Soc.* **2010**, *132* (7), 2132–2133.

(200) Woolerton, T. W.; Sheard, S.; Pierce, E.; Ragsdale, S. W.; Armstrong, F. A. CO_2 Photoreduction at Enzyme-Modified Metal Oxide Nanoparticles. *Energy Environ. Sci.* **2011**, *4* (7), 2393–2399.
(201) Beley, M.; Collin, J.-P.; Ruppert, R.; Sauvage, J.-P. Nickel(II)-Cyclam: An Extremely Selective Electrocatalyst for Reduction of CO_2 in Water. *J. Chem. Soc. Chem. Commun.* **1984**, No. 19, 1315–1316.
(202) Beley, M.; Collin, J. P.; Ruppert, R.; Sauvage, J. P. Electrocatalytic Reduction of Carbon Dioxide by Nickel cyclam2+ in Water: Study of the Factors Affecting the Efficiency and the Selectivity of the Process. *J. Am. Chem. Soc.* **1986**, *108* (24), 7461–7467.
(203) Froehlich, J. D.; Kubiak, C. P. Homogeneous CO_2 Reduction by Ni(cyclam) at a Glassy Carbon Electrode. *Inorg. Chem.* **2012**, *51* (7), 3932–3934.
(204) Smieja, J. M.; Kubiak, C. P. Re(bipy-tBu)(CO)3Cl−improved Catalytic Activity for Reduction of Carbon Dioxide: IR-Spectroelectrochemical and Mechanistic Studies. *Inorg. Chem.* **2010**, *49* (20), 9283–9289.
(205) Benson, E. E.; Sampson, M. D.; Grice, K. A.; Smieja, J. M.; Froehlich, J. D.; Friebel, D.; Keith, J. A.; Carter, E. A.; Nilsson, A.; Kubiak, C. P. The Electronic States of Rhenium Bipyridyl Electrocatalysts for CO_2 Reduction as Revealed by X-Ray Absorption Spectroscopy and Computational Quantum Chemistry. *Angew. Chem. Int. Ed.* **2013**, *52* (18), 4841–4844.
(206) Grice, K. A.; Gu, N. X.; Sampson, M. D.; Kubiak, C. P. Carbon Monoxide Release Catalysed by Electron Transfer: Electrochemical and Spectroscopic Investigations of [Re(bpy-R)$(CO)_4$](OTf) Complexes Relevant to CO_2 Reduction. *Dalton Trans.* **2013**, *42* (23), 8498–8503.
(207) Sampson, M. D.; Froehlich, J. D.; Smieja, J. M.; Benson, E. E.; Sharp, I. D.; Kubiak, C. P. Direct Observation of the Reduction of Carbon Dioxide by Rhenium Bipyridine Catalysts. *Energy Environ. Sci.* **2013**, *6* (12), 3748–3755.
(208) Chabolla, S. A.; Dellamary, E. A.; Machan, C. W.; Tezcan, F. A.; Kubiak, C. P. Combined Steric and Electronic Effects of Positional Substitution on Dimethyl-Bipyridine rhenium(I)tricarbonyl Electrocatalysts for the Reduction of CO_2. *Inorganica Chim. Acta* **2014**, *422*, 109–113.
(209) Riplinger, C.; Sampson, M. D.; Ritzmann, A. M.; Kubiak, C. P.; Carter, E. A. Mechanistic Contrasts between Manganese and Rhenium Bipyridine Electrocatalysts for the Reduction of Carbon Dioxide. *J. Am. Chem. Soc.* **2014**, *136* (46), 16285–16298.
(210) Handoko, A. D.; Tang, J. Controllable Proton and CO_2 Photoreduction over Cu2O with Various Morphologies. *Int. J. Hydrog. Energy* **2013**, *38* (29), 13017–13022.
(211) Tennakone, K.; Jayatissa, A. H.; Punchihewa, S. Selective Photoreduction of Carbon Dioxide to Methanol with Hydrous Cuprous Oxide. *J. Photochem. Photobiol. Chem.* **1989**, *49* (3), 369–375.
(212) Ba, X.; Yan, L.-L.; Huang, S.; Yu, J.; Xia, X.-J.; Yu, Y. New Way for CO_2 Reduction under Visible Light by a Combination of a Cu Electrode and Semiconductor Thin Film: Cu_2O Conduction Type and Morphology Effect. *J. Phys. Chem. C* **2014**, *118* (42), 24467–24478.
(213) Chen, X.; Zhou, Y.; Liu, Q.; Li, Z.; Liu, J.; Zou, Z. Ultrathin, Single-Crystal WO_3 Nanosheets by Two-Dimensional Oriented Attachment toward Enhanced Photocatalystic Reduction of CO_2 into Hydrocarbon Fuels under Visible Light. *ACS Appl. Mater. Interfaces* **2012**, *4* (7), 3372–3377.

(214) Shown, I.; Hsu, H.-C.; Chang, Y.-C.; Lin, C.-H.; Roy, P. K.; Ganguly, A.; Wang, C.-H.; Chang, J.-K.; Wu, C.-I.; Chen, L.-C.; et al. Highly Efficient Visible Light Photocatalytic Reduction of CO_2 to Hydrocarbon Fuels by Cu-Nanoparticle Decorated Graphene Oxide. *Nano Lett.* **2014**, *14* (11), 6097–6103.
(215) Yahaya, A. H.; Gondal, M. A.; Hameed, A. Selective Laser Enhanced Photocatalytic Conversion of CO_2 into Methanol. *Chem. Phys. Lett.* **2004**, *400* (1–3), 206–212.
(216) Bachmeier, A.; Hall, S.; Ragsdale, S. W.; Armstrong, F. A. Selective Visible-Light-Driven CO_2 Reduction on a P-Type Dye-Sensitized NiO Photocathode. *J. Am. Chem. Soc.* **2014**, *136* (39), 13518–13521.
(217) Wan, L.; Wang, X.; Yan, S.; Yu, H.; Li, Z.; Zou, Z. ZnO Plates Synthesized from the Ammonium Zinc Nitrate Hydroxide Precursor. *CrystEngComm* **2012**, *14* (1), 154.
(218) Sato, S.; Morikawa, T.; Saeki, S.; Kajino, T.; Motohiro, T. Visible-Light-Induced Selective CO_2 Reduction Utilizing a Ruthenium Complex Electrocatalyst Linked to a P-Type Nitrogen-Doped Ta2O5 Semiconductor. *Angew. Chem. Int. Ed.* **2010**, *49* (30), 5101–5105.
(219) Suzuki, T. M.; Nakamura, T.; Saeki, S.; Matsuoka, Y.; Tanaka, H.; Yano, K.; Kajino, T.; Morikawa, T. Visible Light-Sensitive Mesoporous N-Doped Ta2O5 Spheres: Synthesis and Photocatalytic Activity for Hydrogen Evolution and CO_2 Reduction. *J. Mater. Chem.* **2012**, *22* (47), 24584–24590.
(220) Akimov, A. V.; Jinnouchi, R.; Shirai, S.; Asahi, R.; Prezhdo, O. V. Theoretical Insights into the Impact of Ru Catalyst Anchors on the Efficiency of Photocatalytic CO_2 Reduction on Ta_2O_5. *J. Phys. Chem. B* **2014**.
(221) Liu, C.; Dubois, K. D.; Louis, M. E.; Vorushilov, A. S.; Li, G. Photocatalytic CO_2 Reduction and Surface Immobilization of a Tricarbonyl Re(I) Compound Modified with Amide Groups. *ACS Catal.* **2013**, *3* (4), 655–662.
(222) Kohno, Y.; Ishikawa, H.; Tanaka, T.; Funabiki, T.; Yoshida, S. Photoreduction of Carbon Dioxide by Hydrogen over Magnesium Oxide. *Phys. Chem. Chem. Phys.* **2001**, *3* (6), 1108–1113.
(223) Yamamoto, M.; Yoshida, T.; Yamamoto, N.; Yoshida, H.; Yagi, S. In-Situ FT-IR Study on the Mechanism of CO_2 Reduction with Water over Metal (Ag or Au) Loaded Ga_2O_3 Photocatalysts. *E-J. Surf. Sci. Nanotechnol.* **2014**, *12*, 299–303.
(224) Park, H.; Choi, J. H.; Choi, K. M.; Lee, D. K.; Kang, J. K. Highly Porous Gallium Oxide with a High CO_2 Affinity for the Photocatalytic Conversion of Carbon Dioxide into Methane. *J. Mater. Chem.* **2012**, *22* (12), 5304–5307.
(225) Hoch, L. B.; Wood, T. E.; O'Brien, P. G.; Liao, K.; Reyes, L. M.; Mims, C. A.; Ozin, G. A. The Rational Design of a Single-Component Photocatalyst for Gas-Phase CO_2 Reduction Using Both UV and Visible Light. *Adv. Sci.* **2014**, *1* (1).
(226) Lo, C.-C.; Hung, C.-H.; Yuan, C.-S.; Wu, J.-F. Photoreduction of Carbon Dioxide with H2 and H_2O over TiO_2 and ZrO_2 in a Circulated Photocatalytic Reactor. *Sol. Energy Mater. Sol. Cells* **2007**, *91* (19), 1765–1774.
(227) Kohno, Y.; Tanaka, T.; Funabiki, T.; Yoshida, S. Photoreduction of Carbon Dioxide with Hydrogen over ZrO_2. *Chem. Commun.* **1997**, No. 9, 841–842.
(228) Sayama, K.; Arakawa, H. Photocatalytic Decomposition of Water and Photocatalytic Reduction of Carbon Dioxide over Zirconia Catalyst. *J. Phys. Chem.* **1993**, *97* (3), 531–533.

(229) Kohno, Y.; Tanaka, T.; Funabiki, T.; Yoshida, S. Photoreduction of CO_2 with H2 over ZrO2. A Study on Interaction of Hydrogen with Photoexcited CO_2 *Phys. Chem. Chem. Phys.* **2000**, *2* (11), 2635–2639.
(230) Liu, Y.; Huang, B.; Dai, Y.; Zhang, X.; Qin, X.; Jiang, M.; Whangbo, M.-H. Selective Ethanol Formation from Photocatalytic Reduction of Carbon Dioxide in Water with BiVO4 Photocatalyst. *Catal. Commun.* **2009**, *11* (3), 210–213.
(231) Mao, J.; Peng, T.; Zhang, X.; Li, K.; Zan, L. Selective Methanol Production from Photocatalytic Reduction of CO_2 on BiVO4 under Visible Light Irradiation. *Catal. Commun.* **2012**, *28*, 38–41.
(232) Lekse, J. W.; Underwood, M. K.; Lewis, J. P.; Matranga, C. Synthesis, Characterization, Electronic Structure, and Photocatalytic Behavior of CuGaO2 and CuGa1–xFexO2 (x = 0.05, 0.10, 0.15, 0.20) Delafossites. *J. Phys. Chem. C* **2011**, *116* (2), 1865–1872.
(233) Gu, J.; Wuttig, A.; Krizan, J. W.; Hu, Y.; Detweiler, Z. M.; Cava, R. J.; Bocarsly, A. B. Mg-Doped CuFeO2 Photocathodes for Photoelectrochemical Reduction of Carbon Dioxide. *J. Phys. Chem. C* **2013**, *117* (24), 12415–12422.
(234) Matsumoto, Y.; Obata, M.; Hombo, J. Photocatalytic Reduction of Carbon Dioxide on P-Type CaFe2O4 Powder. *J. Phys. Chem.* **1994**, *98* (11), 2950–2951.
(235) Liu, Q.; Zhou, Y.; Kou, J.; Chen, X.; Tian, Z.; Gao, J.; Yan, S.; Zou, Z. High-Yield Synthesis of Ultralong and Ultrathin Zn2GeO4 Nanoribbons toward Improved Photocatalytic Reduction of CO_2 into Renewable Hydrocarbon Fuel. *J. Am. Chem. Soc.* **2010**, *132* (41), 14385–14387.
(236) Liu, Q.; Low, Z.-X.; Li, L.; Razmjou, A.; Wang, K.; Yao, J.; Wang, H. ZIF-8/Zn2GeO4 Nanorods with an Enhanced CO_2 Adsorption Property in an Aqueous Medium for Photocatalytic Synthesis of Liquid Fuel. *J. Mater. Chem. A* **2013**, *1* (38), 11563–11569.
(237) Shi, H.; Wang, T.; Chen, J.; Zhu, C.; Ye, J.; Zou, Z. Photoreduction of Carbon Dioxide Over NaNbO3 Nanostructured Photocatalysts. *Catal. Lett.* **2011**, *141* (4), 525–530.
(238) Li, X.; Li, W.; Zhuang, Z.; Zhong, Y.; Li, Q.; Wang, L. Photocatalytic Reduction of Carbon Dioxide to Methane over SiO2-Pillared HNb_3O_8. *J. Phys. Chem. C* **2012**, *116* (30), 16047–16053.
(239) Li, X.; Pan, H.; Li, W.; Zhuang, Z. Photocatalytic Reduction of CO_2 to Methane over HNb3O8 Nanobelts. *Appl. Catal. Gen.* **2012**, *413–414*, 103–108.
(240) Lee, D.-S.; Chen, H.-J.; Chen, Y.-W. Photocatalytic Reduction of Carbon Dioxide with Water Using $InNbO_4$ Catalyst with NiO and Co_3O_4 Cocatalysts. *J. Phys. Chem. Solids* **2012**, *73* (5), 661–669.
(241) Pan, P.-W.; Chen, Y.-W. Photocatalytic Reduction of Carbon Dioxide on NiO/$InTaO_4$ under Visible Light Irradiation. *Catal. Commun.* **2007**, *8* (10), 1546–1549.
(242) Chen, H.-C.; Chou, H.-C.; Wu, J. C. S.; Lin, H.-Y. Sol-Gel Prepared $InTaO_4$ and Its Photocatalytic Characteristics. *J. Mater. Res.* **2008**, *23* (05), 1364–1370.
(243) Tsai, C.-W.; Chen, H. M.; Liu, R.-S.; Asakura, K.; Chan, T.-S. Ni@NiO Core–Shell Structure-Modified Nitrogen-Doped InTaO4 for Solar-Driven Highly Efficient CO_2 Reduction to Methanol. *J. Phys. Chem. C* **2011**, *115* (20), 10180–10186.
(244) Li, K.; Handoko, A. D.; Khraisheh, M.; Tang, J. Photocatalytic Reduction of CO_2 and Protons Using Water as an Electron Donor over Potassium Tantalate Nanoflakes. *Nanoscale* **2014**, *6* (16), 9767–9773.

(245) Chen, X.; Wang, J.; Huang, C.; Zhang, S.; Zhang, H.; Li, Z.; Zou, Z. Barium Zirconate: A New Photocatalyst for Converting CO_2 into Hydrocarbons under UV Irradiation. *Catal. Sci. Technol.* **2014**.
(246) Ulman, M.; Tinnemans, A. H. A.; Mackor, A.; Aurian-Blajeni, B.; Halmann, M. Photoreduction of Carbon Dioxide to Formic Acid, Formaldehyde, Methanol, Acetaldehyde and Ethanol Using Aqueous Suspensions of Strontium Titanate with Transition Metal Additives. *Int. J. Sol. Energy* **1982**, *1* (3), 213–222.
(247) Xie, K.; Umezawa, N.; Zhang, N.; Reunchan, P.; Zhang, Y.; Ye, J. Self-Doped $SrTiO_{3-\delta}$ Photocatalyst with Enhanced Activity for Artificial Photosynthesis under Visible Light. *Energy Environ. Sci.* **2011**, *4* (10), 4211–4219.
(248) Guan, G.; Kida, T.; Harada, T.; Isayama, M.; Yoshida, A. Photoreduction of Carbon Dioxide with Water over K2Ti6O13 Photocatalyst Combined with Cu/ZnO Catalyst under Concentrated Sunlight. *Appl. Catal. Gen.* **2003**, *249* (1), 11–18.
(249) Guan, G.; Kida, T.; Yoshida, A. Reduction of Carbon Dioxide with Water under Concentrated Sunlight Using Photocatalyst Combined with Fe-Based Catalyst. *Appl. Catal. B Environ.* **2003**, *41* (4), 387–396.
(250) Iizuka, K.; Wato, T.; Miseki, Y.; Saito, K.; Kudo, A. Photocatalytic Reduction of Carbon Dioxide over Ag Cocatalyst-Loaded ALa4Ti4O15 (A = Ca, Sr, and Ba) Using Water as a Reducing Reagent. *J. Am. Chem. Soc.* **2011**, *133* (51), 20863–20868.
(251) Takayama, T.; Tanabe, K.; Saito, K.; Iwase, A.; Kudo, A. The $KCaSrTa_5O_{15}$ Photocatalyst with Tungsten Bronze Structure for Water Splitting and CO_2 Reduction. *Phys. Chem. Chem. Phys.* **2014**, *16* (44), 24417–24422.
(252) Kim, W.; Yuan, G.; McClure, B. A.; Frei, H. Light Induced Carbon Dioxide Reduction by Water at Binuclear ZrO Co(II) Unit Coupled to Ir Oxide Nanocluster Catalyst. *J. Am. Chem. Soc.* **2014**, *136* (31), 11034–11042.
(253) Ahmed, N.; Shibata, Y.; Taniguchi, T.; Izumi, Y. Photocatalytic Conversion of Carbon Dioxide into Methanol Using zinc–copper–M(III) (M = Aluminum, Gallium) Layered Double Hydroxides. *J. Catal.* **2011**, *279* (1), 123–135.
(254) Teramura, K.; Iguchi, S.; Mizuno, Y.; Shishido, T.; Tanaka, T. Photocatalytic Conversion of CO_2 in Water over Layered Double Hydroxides. *Angew. Chem. Int. Ed.* **2012**, *51* (32), 8008–8011.
(255) Ahmed, N.; Morikawa, M.; Izumi, Y. Photocatalytic Conversion of Carbon Dioxide into Methanol Using Optimized Layered Double Hydroxide Catalysts. *Catal. Today* **2012**, *185* (1), 263–269.
(256) Aurian-Blajeni, B.; Ahsan Habib, M.; Taniguchi, I.; Bockris, J. O. The Study of Adsorbed Species during the Photoassisted Reduction of Carbon Dioxide at a P-CdTe Electrode. *J. Electroanal. Chem. Interfacial Electrochem.* **1983**, *157* (2), 399–404.
(257) Taniguchi, I.; Aurian-Blajeni, B.; Bockris, J. O. Photo-Aided Reduction of Carbon Dioxide to Carbon Monoxide. *J. Electroanal. Chem. Interfacial Electrochem.* **1983**, *157* (1), 179–182.
(258) Taniguchi, I.; Aurian-Blajeni, B.; Bockris, J. O. The Mediation of the Photoelectrochemical Reduction of Carbon Dioxide by Ammonium Ions. *J. Electroanal. Chem. Interfacial Electrochem.* **1984**, *161* (2), 385–388.
(259) Bockris, J. O.; Wass, J. C. On the Photoelectrocatalytic Reduction of Carbon Dioxide. *Mater. Chem. Phys.* **1989**, *22*, 249–280.

(260) Eggins, B. R.; Irvine, J. T. S.; Murphy, E. P.; Grimshaw, J. Formation of Two-Carbon Acids from Carbon Dioxide by Photoreduction on Cadmium Sulphide. *J. Chem. Soc. Chem. Commun.* **1988**, No. 16, 1123–1124.
(261) Eggins, B. R.; Robertson, P. K. J.; Murphy, E. P.; Woods, E.; Irvine, J. T. S. Factors Affecting the Photoelectrochemical Fixation of Carbon Dioxide with Semiconductor Colloids. *J. Photochem. Photobiol. Chem.* **1998**, *118* (1), 31–40.
(262) Berto, T. C.; Zhang, L.; Hamers, R. J.; Berry, J. F. Electrolyte Dependence of CO_2 Electroreduction: Tetraalkylammonium Ions Are Not Electrocatalysts. *ACS Catal.* **2015**, *5* (2), 703–707.
(263) Kisch, H.; Twardzik, G. Heterogeneous Photocatalysis, IX. Zinc Sulfide Catalyzed Photoreduction of Carbon Dioxide. *Chem. Ber.* **1991**, *124* (5), 1161–1162.
(264) Kanemoto, M.; Hosokawa, H.; Wada, Y.; Murakoshi, K.; Yanagida, S.; Sakata, T.; Mori, H.; Ishikawa, M.; Kobayashi, H. Semiconductor Photocatalysis. Part 20.—Role of Surface in the Photoreduction of Carbon Dioxide Catalysed by Colloidal ZnS Nanocrystallites in Organic Solvent. *J. Chem. Soc. Faraday Trans.* **1996**, *92* (13), 2401–2411.
(265) Fujiwara, H.; Hosokawa, H.; Murakoshi, K.; Wada, Y.; Yanagida, S. Surface Characteristics of ZnS Nanocrystallites Relating to Their Photocatalysis for CO_2 Reduction1. *Langmuir* **1998**, *14* (18), 5154–5159.
(266) Jang, J.-W.; Cho, S.; Magesh, G.; Jang, Y. J.; Kim, J. Y.; Kim, W. Y.; Seo, J. K.; Kim, S.; Lee, K.-H.; Lee, J. S. Aqueous-Solution Route to Zinc Telluride Films for Application to CO_2 Reduction. *Angew. Chem. Int. Ed.* **2014**, *53* (23), 5852–5857.
(267) Cabrera, C. R.; Abruña, H. D. Electrocatalysis of CO_2 Reduction at Surface Modified Metallic and Semiconducting Electrodes. *J. Electroanal. Chem. Interfacial Electrochem.* **1986**, *209* (1), 101–107.
(268) Jaramillo, T. F.; Jørgensen, K. P.; Bonde, J.; Nielsen, J. H.; Horch, S.; Chorkendorff, I. Identification of Active Edge Sites for Electrochemical H2 Evolution from MoS2 Nanocatalysts. *Science* **2007**, *317* (5834), 100–102.
(269) Chan, K.; Tsai, C.; Hansen, H. A.; Nørskov, J. K. Molybdenum Sulfides and Selenides as Possible Electrocatalysts for CO_2 Reduction. *ChemCatChem* **2014**, *6* (7), 1899–1905.
(270) Aliwi, S. M.; Aushana, A. M.; Al-Jubori, K. F. Photoelectrolytic Reduction of Carbon Dioxide in Aqueous Suspension of Metal Sulfide Powders. *J. Sol. Energy Res.* **1988**, *6* (1), 57–69.
(271) Zeng, G.; Qiu, J.; Li, Z.; Pavaskar, P.; Cronin, S. B. CO_2 Reduction to Methanol on TiO_2 -Passivated GaP Photocatalysts. *ACS Catal.* **2014**, *4* (10), 3512–3516.
(272) Li, H.; Lei, Y.; Huang, Y.; Fang, Y.; Xu, Y.; Zhu, L.; Li, X. Photocatalytic Reduction of Carbon Dioxide to Methanol by Cu_2O/SiC Nanocrystallite under Visible Light Irradiation. *J. Nat. Gas Chem.* **2011**, *20* (2), 145–150.
(273) Li, X.; Chen, J.; Li, H.; Li, J.; Xu, Y.; Liu, Y.; Zhou, J. Photoreduction of CO_2 to Methanol over Bi2S3/CdS Photocatalyst under Visible Light Irradiation. *J. Nat. Gas Chem.* **2011**, *20* (4), 413–417.
(274) Ahmad Beigi, A.; Fatemi, S.; Salehi, Z. Synthesis of Nanocomposite CdS/TiO_2 and Investigation of Its Photocatalytic Activity for CO_2 Reduction to CO and CH_4 under Visible Light Irradiation. *J.* CO_2 *Util.* **2014**, *7*, 23–29.
(275) Li, P.; Zhang, J.; Wang, H.; Jing, H.; Xu, J.; Sui, X.; Hu, H.; Yin, H. The Photoelectric Catalytic Reduction of CO_2 to Methanol on CdSeTe NSs/TiO_2 NTs. *Catal. Sci. Technol.* **2014**, *4* (4), 1070–1077.

(276) Li, X.; Liu, H.; Luo, D.; Li, J.; Huang, Y.; Li, H.; Fang, Y.; Xu, Y.; Zhu, L. Adsorption of CO_2 on Heterostructure $CdS(Bi_2S_3)/TiO_2$ Nanotube Photocatalysts and Their Photocatalytic Activities in the Reduction of CO_2 to Methanol under Visible Light Irradiation. *Chem. Eng. J.* **2012**, *180*, 151–158.
(277) Wang, C.; Thompson, R. L.; Ohodnicki, P.; Baltrus, J.; Matranga, C. Size-Dependent Photocatalytic Reduction of CO_2 with PbS Quantum Dot Sensitized TiO_2 Heterostructured Photocatalysts. *J. Mater. Chem.* **2011**, *21* (35), 13452–13457.
(278) Park, H.; Ou, H.-H.; Colussi, A. J.; Hoffmann, M. R. Artificial Photosynthesis of C1–C3 Hydrocarbons from Water and CO_2 on Titanate Nanotubes Decorated with Nanoparticle Elemental Copper and CdS Quantum Dots. *J. Phys. Chem. A* **2015**.
(279) Abou Asi, M.; He, C.; Su, M.; Xia, D.; Lin, L.; Deng, H.; Xiong, Y.; Qiu, R.; Li, X. Photocatalytic Reduction of CO_2 to Hydrocarbons Using $AgBr/TiO_2$ Nanocomposites under Visible Light. *Catal. Today* **2011**, *175* (1), 256–263.
(280) Li, P.; Sui, X.; Xu, J.; Jing, H.; Wu, C.; Peng, H.; Lu, J.; Yin, H. Worm-like InP/TiO_2 NTs Heterojunction with Unmatched Energy Band Photo-Enhanced Electrocatalytic Reduction of CO_2 to Methanol. *Chem. Eng. J.* **2014**, *247*, 25–32.
(281) Tan, L.-L.; Ong, W.-J.; Chai, S.-P.; Mohamed, A. R. Reduced Graphene Oxide-TiO_2 Nanocomposite as a Promising Visible-Light-Active Photocatalyst for the Conversion of Carbon Dioxide. *Nanoscale Res. Lett.* **2013**, *8* (1), 465.
(282) Bi, F.; Ehsan, M. F.; Liu, W.; He, T. Visible-Light Photocatalytic Conversion of Carbon Dioxide into Methane Using Cu_2O/TiO_2 Hollow Nanospheres. *Chin. J. Chem.* **2015**, *33* (1), 112–118.
(283) Slamet; Nasution, Hosna W.; Purnama, Ezza; Riyani, Kapti; Gunlazuardi, Jarnuzi. Effect of Copper Species in a Photocatalytic Synthesis of Methanol from Carbon Dioxide over Copper-Doped Titania Catalysts. *World Appl. Sci. J.* **2009**, *6* (1), 112–122.
(284) Arai, T.; Sato, S.; Kajino, T.; Morikawa, T. Solar CO_2 Reduction Using H_2O by a Semiconductor/metal-Complex Hybrid Photocatalyst: Enhanced Efficiency and Demonstration of a Wireless System Using $SrTiO_3$ Photoanodes. *Energy Environ. Sci.* **2013**, *6* (4), 1274–1282.
(285) Liu, Y.; Ji, G.; Dastageer, M. A.; Zhu, L.; Wang, J.; Zhang, B.; Chang, X.; Gondal, M. A. Highly-Active Direct Z-Scheme Si/TiO_2 Photocatalyst for Boosted CO_2 Reduction into Value-Added Methanol. *RSC Adv.* **2014**, *4* (100), 56961–56969.
(286) Ohno, T.; Murakami, N.; Koyanagi, T.; Yang, Y. Photocatalytic Reduction of CO_2 over a Hybrid Photocatalyst Composed of WO_3 and Graphitic Carbon Nitride ($g\text{-}C_3N_4$) under Visible Light. *J. CO_2 Util.* **2014**, *6*, 17–25.
(287) Sekizawa, K.; Maeda, K.; Domen, K.; Koike, K.; Ishitani, O. Artificial Z-Scheme Constructed with a Supramolecular Metal Complex and Semiconductor for the Photocatalytic Reduction of CO_2. *J. Am. Chem. Soc.* **2013**, *135* (12), 4596–4599.
(288) Zhou, Y.; Zou, Z.; Li, P.; Li, H.; Wang, X. Y.; Xiao, M.; Xu, Q. F.; Meng, X. All Solid-State Z-Scheme System Arrays of $Fe_2V_4O_{13}$/RGO/CdS for Visible Light-Driving Photocatalytic CO_2 Reduction into Renewable Hydrocarbon Fuel. *Chem. Commun.* **2014**.
(289) Yan, S.; Yu, H.; Wang, N.; Li, Z.; Zou, Z. Efficient Conversion of CO_2 and H_2O into Hydrocarbon Fuel over $ZnAl_2O_4$-Modified Mesoporous ZnGaNO under Visible Light Irradiation. *Chem. Commun.* **2012**, *48* (7), 1048–1050.

(290) Yan, S.; Wang, J.; Gao, H.; Wang, N.; Yu, H.; Li, Z.; Zhou, Y.; Zou, Z. Zinc Gallogermanate Solid Solution: A Novel Photocatalyst for Efficiently Converting CO_2 into Solar Fuels. *Adv. Funct. Mater.* **2013**, *23* (14), 1839–1845.
(291) Zhang, N.; Ouyang, S.; Kako, T.; Ye, J. Mesoporous Zinc Germanium Oxynitride for CO_2 Photoreduction under Visible Light. *Chem. Commun.* **2012**, *48* (9), 1269–1271.
(292) Liu, J.-Y.; Garg, B.; Ling, Y.-C. $Cu_xAg_yIn_zZn_kSm$ Solid Solutions Customized with RuO_2 or $Rh_{1.32}Cr_{0.66}O_3$ Co-Catalyst Display Visible Light-Driven Catalytic Activity for CO_2 Reduction to CH_3OH. *Green Chem.* **2011**, *13* (8), 2029–2031.
(293) Frese, K. W.; Canfield, D. Reduction of CO_2 on n-GaAs Electrodes and Selective Methanol Synthesis. *J. Electrochem. Soc.* **1984**, *131* (11), 2518–2522.
(294) Zafrir, M.; Ulman, M.; Zuckerman, Y.; Halmann, M. Photoelectrochemical Reduction of Carbon Dioxide to Formic Acid, Formaldehyde and Methanol on p-Gallium Arsenide in an Aqueous V(II)-V(III) Chloride Redox System. *J. Electroanal. Chem. Interfacial Electrochem.* **1983**, *159* (2), 373–389.
(295) Hara, K.; Kudo, A.; Sakata, T. Electrochemical Reduction of Carbon Dioxide under High Pressure on Various Electrodes in an Aqueous Electrolyte. *J. Electroanal. Chem.* **1995**, *391* (1–2), 141–147.
(296) Tinnemans, A.; Koster, T.; Thewissen, D.; Mackor, A. Tetraaza-macrocyclic Cobalt(II) and Nickel(II) Complexes as Electron-transfer Agents in the Photo (electro) Chemical and Electrochemical Reduction of Carbon Dioxide. *Recl. Trav. Chim. Pays-Bas* **1984**, *103* (10), 288–295.
(297) Gu, J.; Yan, Y.; Krizan, J. W.; Gibson, Q. D.; Detweiler, Z. M.; Cava, R. J.; Bocarsly, A. B. P-Type $CuRhO_2$ as a Self-Healing Photoelectrode for Water Reduction under Visible Light. *J. Am. Chem. Soc.* **2014**, *136* (3), 830–833.
(298) Bradley, M.; Tysak, T. P-Type Silicon Based Photoelectrochemical Cells for Optical Energy Conversion: Electrochemistry of Tetra-Azomacrocyclic Metal Complexes at Illuminated. *J. Electroanal. Chem. Interfacial Electrochem.* **1982**, *135* (1), 153–157.
(299) Bard, A. J.; Bocarsly, A. B.; Fan, F. R. F.; Walton, E. G.; Wrighton, M. S. The Concept of Fermi Level Pinning at Semiconductor/liquid Junctions. Consequences for Energy Conversion Efficiency and Selection of Useful Solution Redox Couples in Solar Devices. *J. Am. Chem. Soc.* **1980**, *102* (11), 3671–3677.
(300) Bocarsly, A. B.; Bookbinder, D. C.; Dominey, R. N.; Lewis, N. S.; Wrighton, M. S. Photoreduction at Illuminated p-Type Semiconducting Silicon Photoelectrodes. Evidence for Fermi Level Pinning. *J. Am. Chem. Soc.* **1980**, *102* (11), 3683–3688.
(301) Bradley, M. G.; Tysak, T.; Graves, D. J.; Viachiopoulos, N. A. Electrocatalytic Reduction of Carbon Dioxide at Illuminated p-Type Silicon Semiconduccting Electrodes. *J Chem Soc Chem Commun* **1983**, No. 7, 349–350.
(302) Kumar, B.; Smieja, J. M.; Kubiak, C. P. Photoreduction of CO_2 on P-Type Silicon Using Re (bipy-Bu)$(CO)_3Cl$: Photovoltages Exceeding 600 mV for the Selective Reduction of CO_2 to CO. *J. Phys. Chem. C* **2010**, *114* (33), 14220–14223.
(303) Beley, M.; Collin, J.-P.; Sauvage, J.-P.; Petit, J.-P.; Chartier, P. Photoassisted Electro-Reduction of CO_2 on P-GaAs in the Presence of Ni cyclam2+. *J. Electroanal. Chem. Interfacial Electrochem.* **1986**, *206* (1–2), 333–339.
(304) Petit, J.-P.; Chartier, P.; Beley, M.; Sauvage, J.-P. Selective Photoelectrochemical Reduction of CO_2 to CO in an Aqueous Medium on P-GaP, Mediated by Ni Cyclam. *New J. Chem.* **1987**, *11* (11-12), 751–752.

(305) Petit, J.-P.; Chartier, P.; Beley, M.; Deville, J.-P. Molecular Catalysts in Photoelectrochemical Cells: Study of an Efficient System for the Selective Photoelectroreduction of CO_2: P-GaP or P-GaAs/Ni(cyclam)$^{2+}$, Aqueous Medium. *J. Electroanal. Chem. Interfacial Electrochem.* **1989**, *269* (2), 267–281.
(306) Reda, T.; Plugge, C. M.; Abram, N. J.; Hirst, J. Reversible Interconversion of Carbon Dioxide and Formate by an Electroactive Enzyme. *Proc. Natl. Acad. Sci.* **2008**, *105* (31), 10654–10658.
(307) Burgess, B. K.; Lowe, D. J. Mechanism of Molybdenum Nitrogenase. *Chem. Rev.* **1996**, *96* (7), 2983–3012.
(308) Dobbek, H. Structural Aspects of Mononuclear Mo/W-Enzymes. *Coord. Chem. Rev.* **2011**, *255* (9), 1104–1116.
(309) Jormakka, M.; Törnroth, S.; Byrne, B.; Iwata, S. Molecular Basis of Proton Motive Force Generation: Structure of Formate Dehydrogenase-N. *Science* **2002**, *295* (5561), 1863–1868.
(310) Romão, M. J. Molybdenum and Tungsten Enzymes: A Crystallographic and Mechanistic Overview. *Dalton Trans.* **2009**, No. 21, 4053–4068.
(311) Yan, Y.; Chandrasekaran, P.; Mague, J. T.; DeBeer, S.; Sproules, S.; Donahue, J. P. Redox-Controlled Interconversion between Trigonal Prismatic and Octahedral Geometries in a Monodithiolene Tetracarbonyl Complex of Tungsten. *Inorg. Chem.* **2011**, *51*(1), 346–361.
(312) Yan, Y.; Keating, C.; Chandrasekaran, P.; Jayarathne, U.; Mague, J. T.; DeBeer, S.; Lancaster, K. M.; Sproules, S.; Rubtsov, I. V.; Donahue, J. P. Ancillary Ligand Effects upon Dithiolene Redox Noninnocence in Tungsten Bis(dithiolene) Complexes. *Inorg. Chem.* **2013**, *52* (11), 6743–6751.
(313) Parkinson, B. A.; Weaver, P. F. Photoelectrochemical Pumping of Enzymatic CO_2 Reduction. *Nature* **1984**, *309* (5964), 148–149.
(314) Chaudhary, Y. S.; Woolerton, T. W.; Allen, C. S.; Warner, J. H.; Pierce, E.; Ragsdale, S. W.; Armstrong, F. A. Visible Light-Driven CO_2 Reduction by Enzyme Coupled CdS Nanocrystals. *Chem. Commun.* **2011**, *48* (1), 58–60.
(315) Kuwabata, S.; Nishida, K.; Tsuda, R.; Inoue, H.; Yoneyama, H. Photochemical Reduction of Carbon Dioxide to Methanol Using ZnS Microcrystallite as a Photocatalyst in the Presence of Methanol Dehydrogenase. *J. Electrochem. Soc.* **1994**, *141* (6), 1498–1503.
(316) Yuan, J.; Zheng, L.; Hao, C. Role of Pyridine in Photoelectrochemical Reduction of CO_2 to Methanol at a CuInS2 Thin Film Electrode. *RSC Adv.* **2014**, *4* (74), 39435–39438.
(317) Jeon, J. H.; Mareeswaran, P. M.; Choi, C. H.; Woo, S. I. Synergism between CdTe Semiconductor and Pyridine – Photoenhanced Electrocatalysis for CO_2 Reduction to Formic Acid. *RSC Adv.* **2013**, *4* (6), 3016–3019.
(318) Tacconi, N. R. de; Chanmanee, W.; Dennis, B. H.; MacDonnell, F. M.; Boston, D. J.; Rajeshwar, K. Electrocatalytic Reduction of Carbon Dioxide Using Pt/C-TiO_2 Nanocomposite Cathode. *Electrochem. Solid-State Lett.* **2011**, *15* (1), B5–B8.
(319) Bocarsly, A. B.; Gibson, Q. D.; Morris, A. J.; L'Esperance, R. P.; Detweiler, Z. M.; Lakkaraju, P. S.; Zeitler, E. L.; Shaw, T. W. Comparative Study of Imidazole and Pyridine Catalyzed Reduction of Carbon Dioxide at Illuminated Iron Pyrite Electrodes. *ACS Catal.* **2012**, *2* (8), 1684–1692.
(320) Barton Cole, E.; Lakkaraju, P. S.; Rampulla, D. M.; Morris, A. J.; Abelev, E.; Bocarsly, A. B. Using a One-Electron Shuttle for the Multielectron Reduction of CO_2 to Methanol:

Kinetic, Mechanistic, and Structural Insights. *J. Am. Chem. Soc.* **2010**, *132* (33), 11539–11551.
(321) Yan, Y.; Zeitler, E. L.; Gu, J.; Hu, Y.; Bocarsly, A. B. Electrochemistry of Aqueous Pyridinium: Exploration of a Key Aspect of Electrocatalytic Reduction of CO_2 to Methanol. *J. Am. Chem. Soc.* **2013**, *135* (38), 14020–14023.
(322) Keith, J. A.; Carter, E. A. Theoretical Insights into Pyridinium-Based Photoelectrocatalytic Reduction of CO_2 *J. Am. Chem. Soc.* **2012**, *134* (18), 7580–7583.
(323) Keith, J. A.; Carter, E. A. Quantum Chemical Benchmarking, Validation, and Prediction of Acidity Constants for Substituted Pyridinium Ions and Pyridinyl Radicals. *J. Chem. Theory Comput.* **2012**, *8* (9), 3187–3206.
(324) Keith, J. A.; Carter, E. A. Theoretical Insights into Electrochemical CO_2 Reduction Mechanisms Catalyzed by Surface-Bound Nitrogen Heterocycles. *J. Phys. Chem. Lett.* **2013**, *4* (23), 4058–4063.
(325) Keith, J. A.; Carter, E. A. Electrochemical Reactivities of Pyridinium in Solution: Consequences for CO 2 Reduction Mechanisms. *Chem. Sci.* **2013**, *4* (4), 1490–1496.
(326) Lim, C.-H.; Holder, A. M.; Musgrave, C. B. Mechanism of Homogeneous Reduction of *CO_2* by Pyridine: Proton Relay in Aqueous Solvent and Aromatic Stabilization. *J. Am. Chem. Soc.* **2012**, *135* (1), 142–154.
(327) Lim, C.-H.; Holder, A. M.; Hynes, J. T.; Musgrave, C. B. Reduction of CO_2 to Methanol Catalyzed by a Biomimetic Organo-Hydride Produced from Pyridine. *J. Am. Chem. Soc.* **2014**, *136* (45), 16081–16095.
(328) Ertem, M. Z.; Konezny, S. J.; Araujo, C. M.; Batista, V. S. Functional Role of Pyridinium during Aqueous Electrochemical Reduction of CO_2 on Pt (111). *J. Phys. Chem. Lett.* **2013**, *4* (5), 745–748.
(329) Costentin, C.; Canales, J. C.; Haddou, B.; Savéant, J.-M. Electrochemistry of Acids on Platinum. Application to the Reduction of Carbon Dioxide in the Presence of Pyridinium Ion in Water. *J. Am. Chem. Soc.* **2013**, *135* (47), 17671–17674.
(330) Portenkirchner, E.; Enengl, C.; Enengl, S.; Hinterberger, G.; Schlager, S.; Apaydin, D.; Neugebauer, H.; Knör, G.; Sariciftci, N. S. A Comparison of Pyridazine and Pyridine as Electrocatalysts for the Reduction of Carbon Dioxide to Methanol. *ChemElectroChem* **2014**, *1* (9), 1543–1548.
(331) Marjolin, A.; Keith, J. A. Thermodynamic Descriptors for Molecules That Catalyze Efficient CO_2 Electroreductions. *ACS Catal.* **2015**, *5* (2), 1123–1130.
(332) Zeitler, E. L. Mechanism of Acid Reduction at Low and High Overpotential Metal Electrodes in the Presence and Absence of CO_2: Implications for CO_2 Reduction by N-Heterocycles. Ph.D., Princeton University: United States -- New Jersey, 2014.
(333) Rowsell, J. L. C.; Yaghi, O. M. Metal–organic Frameworks: A New Class of Porous Materials. *Microporous Mesoporous Mater.* **2004**, *73* (1–2), 3–14.
(334) Rhodes, C. J. Zeolites: Physical Aspects and Environmental Applications. *Annu. Rep. Sect. C Phys. Chem.* **2007**, *103* (0), 287–325.
(335) Li, J.; Luo, D.; Yang, C.; He, S.; Chen, S.; Lin, J.; Zhu, L.; Li, X. Copper(II) Imidazolate Frameworks as Highly Efficient Photocatalysts for Reduction of CO_2 into Methanol under Visible Light Irradiation. *J. Solid State Chem.* **2013**, *203*, 154–159.
(336) Masciocchi, N.; Bruni, S.; Cariati, E.; Cariati, F.; Galli, S.; Sironi, A. Extended Polymorphism in Copper(II) Imidazolate Polymers: A Spectroscopic and XRPD Structural Study. *Inorg. Chem.* **2001**, *40* (23), 5897–5905.

(337) Wang, S.; Yao, W.; Lin, J.; Ding, Z.; Wang, X. Cobalt Imidazolate Metal–Organic Frameworks Photosplit CO_2 under Mild Reaction Conditions. *Angew. Chem. Int. Ed.* **2014**, *53* (4), 1034–1038.
(338) Fu, Y.; Sun, D.; Chen, Y.; Huang, R.; Ding, Z.; Fu, X.; Li, Z. An Amine-Functionalized Titanium Metal–Organic Framework Photocatalyst with Visible-Light-Induced Activity for CO_2 Reduction. *Angew. Chem. Int. Ed.* **2012**, *51* (14), 3364–3367.
(339) Sun, D.; Liu, W.; Fu, Y.; Fang, Z.; Sun, F.; Fu, X.; Zhang, Y.; Li, Z. Noble Metals Can Have Different Effects on Photocatalysis Over Metal–Organic Frameworks (MOFs): A Case Study on M/NH2-MIL-125(Ti) (M=Pt and Au). *Chem. – Eur. J.* **2014**, *20* (16), 4780–4788.
(340) Wang, D.; Huang, R.; Liu, W.; Sun, D.; Li, Z. Fe-Based MOFs for Photocatalytic CO_2 Reduction: Role of Coordination Unsaturated Sites and Dual Excitation Pathways. *ACS Catal.* **2014**, 4254–4260.
(341) Sun, D.; Fu, Y.; Liu, W.; Ye, L.; Wang, D.; Yang, L.; Fu, X.; Li, Z. Studies on Photocatalytic CO_2 Reduction over NH2-Uio-66(Zr) and Its Derivatives: Towards a Better Understanding of Photocatalysis on Metal–Organic Frameworks. *Chem. – Eur. J.* **2013**, *19* (42), 14279–14285.
(342) Wang, C.; Xie, Z.; deKrafft, K. E.; Lin, W. Doping Metal–Organic Frameworks for Water Oxidation, Carbon Dioxide Reduction, and Organic Photocatalysis. *J. Am. Chem. Soc.* **2011**, *133* (34), 13445–13454.
(343) Li, L.; Zhang, S.; Xu, L.; Wang, J.; Shi, L.-X.; Chen, Z.-N.; Hong, M.; Luo, J. Effective Visible-Light Driven CO_2 Photoreduction via a Promising Bifunctional Iridium Coordination Polymer. *Chem. Sci.* **2014**, *5* (10), 3808–3813.
(344) Li, R.; Hu, J.; Deng, M.; Wang, H.; Wang, X.; Hu, Y.; Jiang, H.-L.; Jiang, J.; Zhang, Q.; Xie, Y.; et al. Integration of an Inorganic Semiconductor with a Metal–Organic Framework: A Platform for Enhanced Gaseous Photocatalytic Reactions. *Adv. Mater.* **2014**, *26* (28), 4783–4788.
(345) Anpo, M.; Nakaya, H.; Kodama, S.; Kubokawa, Y.; Domen, K.; Onishi, T. Photocatalysis over Binary Metal Oxides. Enhancement of the Photocatalytic Activity of Titanium Dioxide in Titanium-Silicon Oxides. *J. Phys. Chem.* **1986**, *90* (8), 1633–1636.
(346) Inoue, H.; Matsuyama, T.; Liu, B.-J.; Sakata, T.; Mori, H.; Yoneyama, H. Photocatalytic Activities for Carbon Dioxide Reduction of TiO_2 Microcrystals Prepared in SiO2 Matrices Using a Sol-Gel Method. *Chem. Lett.* **1994**, *23* (3), 653–656.
(347) Anpo, M.; Yamashita, H.; Ichihashi, Y.; Fujii, Y.; Honda, M. Photocatalytic Reduction of CO_2 with H_2O on Titanium Oxides Anchored within Micropores of Zeolites: Effects of the Structure of the Active Sites and the Addition of Pt. *J. Phys. Chem. B* **1997**, *101* (14), 2632–2636.
(348) Anpo, M.; Yamashita, H.; Ikeue, K.; Fujii, Y.; Ichihashi, Y.; Zhang, S. G.; Park, D. R.; Ehara, S.; Park, S.-E.; Chang, J.-S.; et al. Photocatalytic Reduction of CO_2 with H_2O on Titanium Oxides Anchored within Zeolites. In *Studies in Surface Science and Catalysis*; Inui, T., Anpo, M., Izui, K., Yanagida, S., Yamaguchi, T., Eds.; Advances in Chemical Conversions for Mitigating Carbon Dioxide Proceedings of the Fourth International Conference on Carbon Dioxide Utilization; Elsevier, 1998; Vol. 114, pp 177–182.
(349) Anpo, M.; Yamashita, H.; Ikeue, K.; Fujii, Y.; Zhang, S. G.; Ichihashi, Y.; Park, D. R.; Suzuki, Y.; Koyano, K.; Tatsumi, T. Photocatalytic Reduction of CO_2 with H_2O on Ti-

MCM-41 and Ti-MCM-48 Mesoporous Zeolite Catalysts. *Catal. Today* **1998**, *44* (1–4), 327–332.
(350) Yamashita, H.; Fujii, Y.; Ichihashi, Y.; Zhang, S. G.; Ikeue, K.; Park, D. R.; Koyano, K.; Tatsumi, T.; Anpo, M. Selective Formation of CH3OH in the Photocatalytic Reduction of CO_2 with H_2O on Titanium Oxides Highly Dispersed within Zeolites and Mesoporous Molecular Sieves. *Catal. Today* **1998**, *45* (1–4), 221–227.
(351) Yamashita, H.; Kawasaki, S.; Takeuchi, M.; Fujii, Y.; Ichihashi, Y.; Suzuki, Y.; Park, S.-E.; Chang, J.-S.; Yoo, J. W.; Anpo, M. Photocatalytic Reduction of CO_2 with H_2O on Ti/Si Binary Oxide Catalysts Prepared by the Sol-Gel Method. In *Studies in Surface Science and Catalysis*; Inui, T., Anpo, M., Izui, K., Yanagida, S., Yamaguchi, T., Eds.; Advances in Chemical Conversions for Mitigating Carbon Dioxide Proceedings of the Fourth International Conference on Carbon Dioxide Utilization; Elsevier, 1998; Vol. 114, pp 561–564.
(352) Ikeue, K.; Yamashita, H.; Anpo, M. Photocatalytic Reduction of CO_2 with H_2O on Titanium Oxides Prepared within the FSM-16 Mesoporous Zeolite. *Chem. Lett.* **1999**, *28* (11), 1135–1136.
(353) Ulagappan, N.; Frei, H. Mechanistic Study of CO_2 Photoreduction in Ti Silicalite Molecular Sieve by FT-IR Spectroscopy. *J. Phys. Chem. A* **2000**, *104* (33), 7834–7839.
(354) Ikeue, K.; Yamashita, H.; Anpo, M.; Takewaki, T. Photocatalytic Reduction of CO_2 with H_2O on Ti−β Zeolite Photocatalysts: Effect of the Hydrophobic and Hydrophilic Properties. *J. Phys. Chem. B* **2001**, *105* (35), 8350–8355.
(355) Yamashita, H.; Ikeue, K.; Takewaki, T.; Anpo, M. In Situ XAFS Studies on the Effects of the Hydrophobic–Hydrophilic Properties of Ti-Beta Zeolites in the Photocatalytic Reduction of CO_2 with H_2O. *Top. Catal.* **2002**, *18* (1-2), 95–100.
(356) Lin, W.; Han, H.; Frei, H. CO_2 Splitting by H_2O to CO and O_2 under UV Light in Ti MCM-41 Silicate Sieve. *J. Phys. Chem. B* **2004**, *108* (47), 18269–18273.
(357) Blasco, T.; Camblor, M. A.; Corma, A.; Esteve, P.; Martínez, A.; Prieto, C.; Valencia, S. Unseeded Synthesis of Al-Free Ti-β Zeolite in Fluoride Medium: A Hydrophobic Selective Oxidation Catalyst. *Chem. Commun.* **1996**, No. 20, 2367–2368.
(358) Aprile, C.; Corma, A.; Garcia, H. Enhancement of the Photocatalytic Activity of TiO_2 through Spatial Structuring and Particle Size Control: From Subnanometric to Submillimetric Length Scale. *Phys. Chem. Chem. Phys.* **2008**, *10* (6), 769–783.
(359) Ikeue, K.; Nozaki, S.; Ogawa, M.; Anpo, M. Photocatalytic Reduction of CO_2 with H_2O on Ti-Containing Porous Silica Thin Film Photocatalysts. *Catal. Lett.* **2002**, *80* (3-4), 111–114.
(360) Yamagata, S.; Nishijo, M.; Murao, N.; Ohta, S.; Mizoguchi, I. CO_2 Reduction to CH_4 with H_2 on Photoirradiated TS-1. *Zeolites* **1995**, *15* (6), 490–493.
(361) Bard, A. J.; Fox, M. A. Artificial Photosynthesis: Solar Splitting of Water to Hydrogen and Oxygen. *Acc. Chem. Res.* **1995**, *28* (3), 141–145.
(362) Nielander, A. C.; Shaner, M. R.; Papadantonakis, K. M.; Francis, S. A.; Lewis, N. S. A Taxonomy for Solar Fuels Generators. *Energy Environ. Sci.* **2014**, *8* (1), 16–25.
(363) Shockley, W.; Queisser, H. J. Detailed Balance Limit of Efficiency of P-n Junction Solar Cells. *J. Appl. Phys.* **1961**, *32* (3), 510–519.
(364) Archer, M. D.; Bolton, J. R. Requirements for Ideal Performance of Photochemical and Photovoltaic Solar Energy Converters. *J. Phys. Chem.* **1990**, *94* (21), 8028–8036.

(365) Henry, C. H. Limiting Efficiencies of Ideal Single and Multiple Energy Gap Terrestrial Solar Cells. *J. Appl. Phys.* **1980**, *51* (8), 4494–4500.
(366) Bird, R. E.; Hulstrom, R. L.; Lewis, L. J. Terrestrial Solar Spectral Data Sets. *Sol. Energy* **1983**, *30* (6), 563–573.
(367) Winkler, M. T.; Cox, C. R.; Nocera, D. G.; Buonassisi, T. Modeling Integrated Photovoltaic-Electrochemical Devices Using Steady-State Equivalent Circuits. *Proc. Natl. Acad. Sci.* **2013**, *110* (12), E1076–E1082.
(368) Lvov, S. N.; Beck, J. R.; LaBarbera, M. S. Electrochemical Reduction of CO_2 to Fuels. In *Carbon-Neutral Fuels and Energy Carriers*; Muradov, N. Z., Veziroglu, T. N., Eds.; CRC Press: New York, 2012; pp 363–400.
(369) Sánchez-Sánchez, C. M.; Montiel, V.; Tryk, D. A.; Aldaz, A.; Fujishima, A. Electrochemical Approaches to Alleviation of the Problem of Carbon Dioxide Accumulation. *Pure Appl. Chem.* **2001**, *73* (12), 1917–1927.
(370) Jitaru, M.; Lowy, D. A.; Toma, M.; Toma, B. C.; Oniciu, L. Electrochemical Reduction of Carbon Dioxide on Flat Metallic Cathodes. *J. Appl. Electrochem.* **1997**, *27* (45), 875–889.
(371) Li, W. Electrocatalytic Reduction of CO_2 to Small Organic Molecule Fuels on Metal Catalysts. In *Advances in* CO_2 *Conversion and Utilization*; Hu, Y. H., Ed.; American Chemical Society: Washington, DC, 2010; pp 55–76.
(372) Wu, J.; Risalvato, F. G.; Ma, S.; Zhou, X.-D. Electrochemical Reduction of Carbon Dioxide III. The Role of Oxide Layer Thickness on the Performance of Sn Electrode in a Full Electrochemical Cell. *J. Mater. Chem. A* **2014**, *2* (6), 1647–1651.
(373) Kapusta, S.; Hackerman, N. The Electroreduction of Carbon Dioxide and Formic Acid on Tin and Indium Electrodes. *J. Electrochem. Soc.* **1983**, *130* (3), 607–613.
(374) Todoroki, M.; Hara, K.; Kudo, A.; Sakata, T. Electrochemical Reduction of High Pressure CO_2 at Pb, Hg and In Electrodes in an Aqueous $KHCO_3$ Solution. *J. Electroanal. Chem.* **1995**, *394* (1-2), 199–203.
(375) Alvarez-Guerra, M.; Quintanilla, S.; Irabien, A. Conversion of Carbon Dioxide into Formate Using a Continuous Electrochemical Reduction Process in a Lead Cathode. *Chem. Eng. J.* **2012**, *207–208*, 278–284.
(376) Alvarez-Guerra, M.; Del Castillo, A.; Irabien, A. Continuous Electrochemical Reduction of Carbon Dioxide into Formate Using a Tin Cathode: Comparison with Lead Cathode. *Chem. Eng. Res. Des.* **2014**, *92* (4), 692–701.
(377) Zhu, W.; Zhang, Y.-J.; Zhang, H.; Lv, H.; Li, Q.; Michalsky, R.; Peterson, A. A.; Sun, S. Active and Selective Conversion of CO_2 to CO on Ultrathin Au Nanowires. *J. Am. Chem. Soc.* **2014**, *136* (46), 16132–16135.
(378) Zhu, W.; Michalsky, R.; Metin, Ö.; Lv, H.; Guo, S.; Wright, C. J.; Sun, X.; Peterson, A. A.; Sun, S. Monodisperse Au Nanoparticles for Selective Electrocatalytic Reduction of CO_2 to CO. *J. Am. Chem. Soc.* **2013**, *135* (45), 16833–16836.
(379) Kauffman, D. R.; Alfonso, D.; Matranga, C.; Qian, H.; Jin, R. Experimental and Computational Investigation of Au_{25} Clusters and CO_2: A Unique Interaction and Enhanced Electrocatalytic Activity. *J. Am. Chem. Soc.* **2012**, *134* (24), 10237–10243.
(380) Jia, F.; Yu, X.; Zhang, L. Enhanced Selectivity for the Electrochemical Reduction of CO_2 to Alcohols in Aqueous Solution with Nanostructured Cu–Au Alloy as Catalyst. *J. Power Sources* **2014**, *252*, 85–89.

(381) Kim, D.; Resasco, J.; Yu, Y.; Asiri, A. M.; Yang, P. Synergistic Geometric and Electronic Effects for Electrochemical Reduction of Carbon Dioxide Using Gold–copper Bimetallic Nanoparticles. *Nat. Commun.* **2014**, *5*.
(382) Rosen, B. A.; Salehi-Khojin, A.; Thorson, M. R.; Zhu, W.; Whipple, D. T.; Kenis, P. J. A.; Masel, R. I. Ionic Liquid-Mediated Selective Conversion of CO_2 to CO at Low Overpotentials. *Science* **2011**, *334*, 643–644.
(383) Lu, Q.; Rosen, J.; Zhou, Y.; Hutchings, G. S.; Kimmel, Y. C.; Chen, J. G.; Jiao, F. A Selective and Efficient Electrocatalyst for Carbon Dioxide Reduction. *Nat. Commun.* **2014**, *5*, 3242.
(384) Salehi-Khojin, A.; Jhong, H.-R. M.; Rosen, B. A.; Zhu, W.; Ma, S.; Kenis, P. J. A.; Masel, R. I. Nanoparticle Silver Catalysts That Show Enhanced Activity for Carbon Dioxide Electrolysis. *J. Phys. Chem. C* **2013**, *117* (4), 1627–1632.
(385) Januszewska, A.; Jurczakowski, R.; Kulesza, P. J. CO_2 Electroreduction at Bare and Cu-Decorated Pd Pseudomorphic Layers: Catalyst Tuning by Controlled and Indirect Supporting onto Au(111). *Langmuir* **2014**.
(386) Furuya, N.; Yamazaki, T.; Shibata, M. High Performance Ru-Pd Catalysts for CO_2 Reduction at Gas-Diffusion Electrodes. *J. Electroanal. Chem.* **1997**, *431*, 39–41.
(387) Gao, D.; Zhou, H.; Wang, J.; Miao, S.; Yang, F.; Wang, G.; Wang, J.; Bao, X. Size-Dependent Electrocatalytic Reduction of CO_2 over Pd Nanoparticles. *J. Am. Chem. Soc.* **2015**, *137* (13), 4288–4291.
(388) Cook, R. L.; MacDuff, R. C.; Sammells, A. F. Efficient High Rate Carbon Dioxide Reduction to Methane and Ethylene at in Situ Electrodeposited Copper Electrode. *J. Electrochem. Soc.* **1987**, *134* (9), 2375.
(389) Frese, K. W. Electrochemical Reduction of CO_2 at Intentionally Oxidized Copper Electrodes. *J. Electrochem. Soc.* **1991**, *138* (11), 3338–3344.
(390) Kuhl, K. P.; Cave, E. R.; Abram, D. N.; Jaramillo, T. F. New Insights into the Electrochemical Reduction of Carbon Dioxide on Metallic Copper Surfaces. *Energy Environ. Sci.* **2012**, *5* (5), 7050–7059.
(391) Li, C. W.; Ciston, J.; Kanan, M. W. Electroreduction of Carbon Monoxide to Liquid Fuel on Oxide-Derived Nanocrystalline Copper. *Nature* **2014**, *508* (7497), 504–507.
(392) Yano, J.; Morita, T.; Shimano, K.; Nagami, Y.; Yamasaki, S. Selective Ethylene Formation by Pulse-Mode Electrochemical Reduction of Carbon Dioxide Using Copper and Copper-Oxide Electrodes. *J. Solid State Electrochem.* **2007**, *11* (4), 554–557.
(393) Le, M.; Ren, M.; Zhang, Z.; Sprunger, P. T.; Kurtz, R. L.; Flake, J. C. Electrochemical Reduction of CO_2 to CH3OH at Copper Oxide Surfaces. *J. Electrochem. Soc.* **2011**, *158* (5), E45–E49.
(394) Kas, R.; Kortlever, R.; Milbrat, A.; Koper, M. T. M.; Mul, G.; Baltrusaitis, J. Electrochemical CO_2 Reduction on Cu2O-Derived Copper Nanoparticles: Controlling the Catalytic Selectivity of Hydrocarbons. *Phys. Chem. Chem. Phys.* **2014**, *16* (24), 12194.
(395) Manthiram, K.; Beberwyck, B. J.; Alivisatos, A. P. Enhanced Electrochemical Methanation of Carbon Dioxide with a Dispersible Nanoscale Copper Catalyst. *J. Am. Chem. Soc.* **2014**, *136* (38), 13319–13325.
(396) Kobayashi, T.; Takahashi, H. Novel CO_2 Electrochemical Reduction to Methanol for H2 Storage. *Energy Fuels* **2003**, *18* (1), 285–286.

(397) Vassiliev, Y. B.; Bagotzky, V. S.; Osetrova, N. V.; Mikhailova, A. A. Electroreduction of Carbon Dioxide: Part III. Adsorption and Reduction of CO_2 on Platinum. *J. Electroanal. Chem. Interfacial Electrochem.* **1985**, *189* (2), 311–324.
(398) Liao, K.; Askerka, M.; Zeitler, E. L.; Bocarsly, A. B.; Batista, V. S. Electrochemical Reduction of Aqueous Imidazolium on Pt(111) by Proton Coupled Electron Transfer. *Top. Catal.* **2014**, 1–7.
(399) Kuhl, K. P.; Hatsukade, T.; Cave, E. R.; Abram, D. N.; Kibsgaard, J.; Jaramillo, T. F. Electrocatalytic Conversion of Carbon Dioxide to Methane and Methanol on Transition Metal Surfaces. *J. Am. Chem. Soc.* **2014**, *136* (40), 14107–14113.
(400) Ogura, K.; Takagi, M. Electrocatalytic Reduction of Carbon Dioxide to Methanol: Part III. Use of an Electrochemical Photocell. *J. Electroanal. Chem.* **1986**, *201*, 359–365.
(401) Ogura, K. Catalytic Conversion of Carbon Monoxide and Carbon Dioxide into Methanol with Photocells. *J. Electrochem. Soc.* **1987**, *134* (11), 2749–2754.
(402) Ogura, K.; Uchida, H. Electrocatalytic Reduction of CO_2 to Methanol: Part VIII. Photoassisted Electrolysis and Electrochemical Photocell with n-TiO_2 Anode. *J. Electroanal. Chem.* **1987**, *220*, 333–337.
(403) Ohnishi, Y.; Izumi, I.; Morimoto, K. Selective CO_2 Reduction Using the Photochemical Diode of the System n-TiO_2 ,Ti,Cu-Ag. *Denki Kagaku* **1998**, *66* (6), 590–593.
(404) Ichikawa, S.; Doi, R. Hydrogen Production from Water and Conversion of Carbon Dioxide to Useful Chemicals by Room Temperature Photoelectrocatalysis. *Catal. Today* **1996**, *27* (1–2), 271–277.
(405) Cheng, J.; Zhang, M.; Wu, G.; Wang, X.; Zhou, J.; Cen, K. Optimizing CO_2 Reduction Conditions to Increase Carbon Atom Conversion Using a Pt-RGO||Pt-TNT Photoelectrochemical Cell. *Sol. Energy Mater. Sol. Cells* **2015**, *132*, 606–614.
(406) Ampelli, C.; Centi, G.; Passalacqua, R.; Perathoner, S. Synthesis of Solar Fuels by a Novel Photoelectrocatalytic Approach. *Energy Environ. Sci.* **2010**, *3* (3), 292–301.
(407) Ampelli, C.; Passalacqua, R.; Genovese, C.; Perathoner, S.; Centi, G. A Novel Photo-Electrochemical Approach for the Chemical Recycling of Carbon Dioxide to Fuels. *Chem. Eng. Trans.* **2011**, *25*, 683–688.
(408) Genovese, C.; Ampelli, C.; Perathoner, S.; Centi, G. Electrocatalytic Conversion of CO_2 on Carbon Nanotube-Based Electrodes for Producing Solar Fuels. *J. Catal.* **2013**, *308*, 237–249.
(409) Panasonic Corporation. *Press Release*; Panasonic Corporation: Osaka, Japan, 2012.
(410) Deguchi, M.; Yotsuhashi, S.; Yamada, Y. Method for Reducing Carbon Dioxide. US8414758 B2, April 9, 2013.
(411) Yotsuhashi, S.; Deguchi, M.; Yamada, Y. Method for Reducing Carbon Dioxide. US8696883 B2, April 15, 2014.
(412) Deguchi, M.; Yotsuhashi, S.; Yamada, Y.; Ohkawa, K. Method for Reducing Carbon Dioxide. US8709227 B2, April 29, 2014.
(413) Deguchi, M.; Yotsuhashi, S.; Yamada, Y.; Ohkawa, K. Method for Reducing Carbon Dioxide. US8709228 B2, April 29, 2014.
(414) Yotsuhashi, S.; Deguchi, M.; Hashiba, H.; Zenitani, Y.; Hinogami, R.; Yamada, Y.; Ohkawa, K. Enhanced CO_2 Reduction Capability in an AlGaN/GaN Photoelectrode. *Appl. Phys. Lett.* **2012**, *100* (24), 243904.

(415) Kocha, S. S.; Peterson, M. W.; Arent, D. J.; Redwing, J. M.; Tischler, M. A.; Turner, J. A. Electrochemical Investigation of the Gallium Nitride-Aqueous Electrolyte Interface. *J. Electrochem. Soc.* **1995**, *142* (12), L238–L240.
(416) Ogura, K.; Yoshida, I. Catalytic Conversion of CO and CO_2 into Methanol with a Solar Cell. *J. Mol. Catal.* **1986**, *34*, 309–311.
(417) Ogura, K.; Yoshida, I. Electrocatalytic Reduction of Carbon Dioxide to Methanol-VI. Use of a Solar Cell and Comparison with that of Carbon Monoxide. *Electrochimica Acta* **1987**, *32* (8), 1191–1195.
(418) Agarwal, A. S.; Zhai, Y.; Hill, D.; Sridhar, N. The Electrochemical Reduction of Carbon Dioxide to Formate/Formic Acid: Engineering and Economic Feasibility. *ChemSusChem* **2011**, *4* (9), 1301–1310.
(419) Sridhar, N.; Hill, D. *Carbon Dioxide Utilization: Electrochemical Conversion of* CO_2 *- Opportunities and Challenges*; Research and Innovation; Position Paper 07-2011; Det Norske Veritas, 2011.
(420) Toshiba Corporation. *Toshiba Develops World's Highest Efficiency Artificial Photosynthesis Technology for Generation of Fuel and Feedstock from Carbon Dioxide.*; Press Release; Toshiba Corporation: Tokyo, Japan, 2014.
(421) Tamura, Jun; Mikoshiba, Satoshi; Ono, Akihiko; Huang, Chingchun; Kudo, Yuki; Kitagawa, Ryota; Tsutsumi, Eishi; Sugano, Yoshitsune. Reduction Catalyst and Chemical Reactor. WO/2014/192891.
(422) White, J. L.; Herb, J. T.; Kaczur, J. J.; Majsztrik, P. W.; Bocarsly, A. B. Photons to Formate: Efficient Electrochemical Solar Energy Conversion via Reduction of Carbon Dioxide. *J. CO_2 Util.* **2014**, *7*, 1–5.
(423) Jeon, H. S.; Koh, J. H.; Park, S. J.; Jee, M. S.; Ko, D.-H.; Hwang, Y. J.; Min, B. K. A Monolithic and Standalone Solar-Fuel Device Having Comparable Efficiency to Photosynthesis in Nature. *J. Mater. Chem. A* **2015**, *3* (11), 5835–5842.
(424) Torella, J. P.; Gagliardi, C. J.; Chen, J. S.; Bediako, D. K.; Colón, B.; Way, J. C.; Silver, P. A.; Nocera, D. G. Efficient Solar-to-Fuels Production from a Hybrid Microbial–water-Splitting Catalyst System. *Proc. Natl. Acad. Sci.* **2015**, *112* (8), 2337–2342.
(425) Green, M. A.; Emery, K.; Hishikawa, Y.; Warta, W.; Dunlop, E. D. Solar Cell Efficiency Tables (Version 45). *Prog. Photovolt. Res. Appl.* **2015**, *23* (1), 1–9.
(426) Li, C.; Liu, M.; Pschirer, N. G.; Baumgarten, M.; Müllen, K. Polyphenylene-Based Materials for Organic Photovoltaics. *Chem. Rev.* **2010**, *110* (11), 6817–6855.

AUTHOR BIOGRAPHIES

James L. White, a native of Pennsylvania, earned his B.S. degree in chemistry with minors in biochemistry, mathematics, and economics from the University of Delaware in 2011, where he did undergraduate research on solid oxide fuel cell electrolytes with Prof. Joshua L. Hertz. He is currently in his fifth year of studying electrochemistry in the Department of Chemistry at Princeton University with Andrew B. Bocarsly. He has been studying CO_2 reduction on metal-based electrodes, direct ethanol fuel cells, Nafion membranes, and energy efficiency.

Maor F. Baruch received a B.S. in chemistry from the University of Massachusetts Lowell while conducting research under the supervision of Professor James E. Whitten. There, he studied the growth kinetics of nanoparticles and helped develop a handheld chemiresistor sensor array system for the detection of organic vapors. He is currently a fifth-year Ph. D. candidate at Princeton University working under Professor Andrew B. Bocarsly. His current research interests include the application of mass spectrometry and *in situ* ATR-IR spectroscopy to CO_2 reduction electrochemistry.

James E. Pander, III received Bachelor of Science degrees in chemistry and applied mathematics from Penn State University in 2012, and is currently a fourth-year graduate student in the Chemistry department at Princeton University working under Andrew Bocarsly. During his undergraduate studies, he worked on electrocatalyst development for use as chemically modified electrodes for the selective detection of gasotransmitter molecules. As a graduate student at Princeton, his research interests include the use of porphyrins to create chemically modified electrodes for electrocatalytic CO_2 reduction and studying the mechanism of CO_2 reduction on post-transition metal electrodes using a variety of *in situ* and *ex situ* spectroscopic techniques.

Yuan Hu received his B.S. degree in Chemistry from Nanjing University, and then he spent two years working with Dr. Charles Lake in Indiana University of Pennsylvania to complete his M.S. degree in Chemistry. After joining the Bocarsly Lab in 2010, Yuan focused his research on using photoelectrochemical approaches to generate renewable fuels, specifically designing and synthesizing novel semiconductors for solar-assisted H_2 evolution and CO_2 reduction.

Ivy C. Fortmeyer is a fifth year graduate student in the Princeton University Department of Chemistry, working under Andrew B. Bocarsly. She graduated from Columbia University with a B.A. in chemistry in 2011. Her current research focuses on the spectroscopic examination of a polymerization process in cyanide-bridged coordination polymers, and the subsequent gelation that occurs therein.

James Eujin Park received his B.A. in chemistry from Boston University in 2013. He is currently a Ph.D. candidate in Prof. Bocarsly's group at Princeton University. His research is mainly focused on the development of Cu-based oxide semiconductors for CO_2 reduction.

Tao Zhang graduated from Peking University in 2013 with a bachelor's degree in chemistry. Currently, he is a third-year graduate student at Princeton University, studying under Prof. Andrew B. Bocarsly. He is investigating the role of homogeneous catalysts for CO_2 reduction on semiconductors, both photoelectrochemically and spectroscopically.

Dr. Kuo Liao is a recent Ph.D. graduate from the Department of Chemistry at Princeton University, having worked under Prof. Andrew Bocarsly from 2010 to 2015. His research focused on mechanistic investigations of catalyzed CO_2 reduction on metal electrodes utilizing both electrochemical analytical methods and modeling. In 2010, he graduated with a B.S. degree with honors from Nanjing University School of Chemistry and Chemical Engineering.

Dr. Jing Gu obtained her B.S. at Wuhan University in 2006 and Ph.D. at Tulane University in 2011. She worked as a postdoctoral researcher in Professor Andrew Bocarsly's lab on novel semiconductor oxide material development for the solar conversion of carbon dioxide. She is currently a postdoctoral fellow at National Renewable Energy Lab, working on the development of novel interfaces between molecular catalysts and semiconductor materials.

Dr. Yong Yan received his B.S. degree in Department of Chemistry at Wuhan University (2006) and Ph.D. degree in Inorganic Chemistry from Tulane University, in New Orleans, Louisiana (2012). After that he has worked as a postdoctoral researcher in Princeton University under Prof. Andrew Bocarsly, where he has conducted renewable energy research primarily focusing on atmospheric carbon dioxide electrocatalytic and photoelectrochemical reductions in aqueous solutions to generate methanol and other fuels. Since 2014, Dr. Yan has been at the National Renewable Energy Laboratory (NREL) in Golden, Colorado as a postdoctoral researcher. His current interests include design and development of Mn oxide water oxidation catalysts, III-V semiconductor photocatalysts, and perovskite photoactive materials for solar fuels, particularly focusing on exploring catalysts' structure-function relationships.

Dr. Travis W. Shaw recently earned his Ph.D. from Princeton University after studying analogues of $Mn(bpy)(CO)_3Br$ catalysts for the electrochemical reduction of CO_2 as an National Science Foundation Graduate Research Fellow under Andrew B. Bocarsly. Previously, he had done research in organic synthesis with Prof. Dionicio R. Siegel at the University of Texas at Austin, from which he earned a B.S. in biochemistry.

Dr. Esta Abelev earned her B.S. degree in chemical engineering and Ph.D. in Materials Science and Engineering at Technion – Israel Institute of Technology. Her Ph.D. study was done in the

laboratory of Prof. Ein-Eli where she studied the electrochemical behavior of copper focusing on finding novel copper corrosion inhibitors for chemical-mechanical planarization applications. In 2007, she joined Prof. Steven L. Bernasek's group at Princeton University as a postdoctoral fellow and studied the effect of low concentrations of H_2S in aqueous solutions on iron corrosion by electrochemical and surface analysis. Later she worked in Intel Corp. and SRI International as a semiconductor process development engineer. In 2014, she joined Prof. Andrew B. Bocarsly's group where she works on development of new materials related to light energy conversion and the generation of solar fuels.

Dr. Andrew B. Bocarsly is a Professor of Chemistry at Princeton University and has served on the faculty there since 1980. Dr. Bocarsly earned his Ph.D. in chemistry at the Massachusetts Institute of Technology in 1980 with a dissertation on charge transfer processes in semiconductors. He has received an Alfred P. Sloan Fellowship, the Sigma Xi (Princeton Section) Science Educator Award, and the American Chemical Society-Exxon Solid State Chemistry award. He has mentored over 50 graduate students and postdoctoral associates, as well as numerous undergraduates. Dr. Bocarsly has published almost 200 journal articles and several book chapters, and he holds a number of patents. He is a co-founder and serves as President of the Scientific Advisory Board for Liquid Light, Inc., a New Jersey-based carbon dioxide reduction startup.

TOC graphic